THESIS FOR THE DEGREE OF DOCTOR OF PHILOSOPHY

Engineering central carbon metabolism with phosphoketolase pathways in *Saccharomyces cerevisiae*

JOHN HELLGREN

CHALMERS
UNIVERSITY OF TECHNOLOGY

Department of Biology and Biological Engineering

CHALMERS UNIVERSITY OF TECHNOLOGY

Gothenburg, Sweden 2021

Engineering central carbon metabolism with phosphoketolase pathways in *Saccharomyces cerevisiae*

JOHN HELLGREN
ISBN 978-91-7905-580-6

Doktorsavhandlingar vid Chalmers tekniska högskola
Ny serie nr 5047
ISSN 0346-718X

Department of Biology and Biological Engineering
Chalmers University of Technology
SE-412 96 Gothenburg
Sweden
Telephone + 46 (0)31-772 1000

Cover: Rewiring of metabolic pathways to acetyl-CoA with phosphoketolases. Yeast template from SwissBioPics (CC BY4.0 license).

Printed by Chalmers Reproservice
Gothenburg, Sweden 2021

Engineering central carbon metabolism with phosphoketolase pathways in *Saccharomyces cerevisiae*

John Hellgren
Department of Biology and Biological Engineering
Chalmers University of Technology

ABSTRACT

We need more efficient biocatalysts to make sustainable microbial production of chemicals and fuels more profitable before they can replace petroleum-based sources. Rewiring the metabolic pathways in the biocatalysts to avoid the loss of carbon as CO_2 can aid in improving product yields and thereby the profitability of the process. In this thesis, I investigated the use of phosphoketolase (PK) pathways in the yeast *Saccharomyces cerevisiae* to produce the precursor metabolite acetyl-CoA without loss of carbon as CO_2. Firstly, we investigated the effect of acetyl-phosphate (AcP) accumulation from the linear PK pathway when downstream product formation is limited. Accumulated AcP was degraded to acetate, which limited the benefit of the PK pathway. Furthermore, we investigated a combinatorial strategy to supply acetyl-CoA and NADPH for fatty acid (FA) production. We combined the PK strategy with overexpression of the transcription factor Stb5 to activate NADPH generating pathways. This strategy increased the FA titer in the glucose phase, but with a counteractive response that possibly arose from the lack of an effective NADPH sink.

Secondly, we expanded the linear PK pathway to a novel configuration of the cyclic non-oxidative glycolysis (NOG) that can recycle all the carbon from glucose into acetyl-CoA, thus potentially increasing product yields even further. We showed through kinetic modeling that the new configuration resolves potential bottlenecks in the previous configuration. We verified both *in vitro* and *in vivo* functionality of the cycle in *S. cerevisiae*. Furthermore, we demonstrated increased titers of an acetyl-CoA-derived product in the glucose phase compared to the linear PK pathway, indicating increased precursor supply from the cycle. Finally, we further characterized the *S. cerevisiae* strain with the cycle, using omics. Most notably, the cycle strain yielded respiro-fermentative growth in chemostat cultures with acetate as the main overflow metabolite. This points to a metabolic imbalance and extensive AcP degradation to acetate, which needs to be resolved before the cycle can be efficiently utilized. This thesis highlights the status of this novel NOG configuration and will aid in the further development of cell factories with high-yield production of acetyl-CoA-derived products.

Keywords: Carbon-conservation, GATHCYC, metabolic engineering, non-oxidative glycolysis, platform strain, precursor supply, proteomics, sustainability, transcriptomics

List of Publications

This thesis is based on the following publications and manuscripts:

Paper I: Bergman, A., **Hellgren, J**., Moritz, T., Siewers, V., Nielsen, J. & Chen, Y. Heterologous phosphoketolase expression redirects flux towards acetate, perturbs sugar phosphate pools and increases respiratory demand in *Saccharomyces cerevisiae*. *Microb Cell Fact* **18,** 25 (2019).

Paper II: Bergman, A., Vitay, D., **Hellgren, J**., Chen, Y., Nielsen, J. & Sievers, V. Effects of overexpression of *STB5* in *Saccharomyces cerevisiae* on fatty acid biosynthesis, physiology and transcriptome. *FEMS Yeast Res.* **19**, 27 (2019).

Paper III: **Hellgren, J**., Godina, A., Nielsen, J. & Siewers, V. Promiscuous phosphoketolase and metabolic rewiring enables novel non-oxidative glycolysis in yeast for high-yield production of acetyl-CoA derived products. *Metab. Eng.* **62**, 150–160 (2020).

Paper IV: **Hellgren, J**., Qi, Q., Nielsen, J. & Siewers, V. Proteome and transcriptome analysis of a yeast strain expressing a cyclic phosphoketolase pathway for improved acetyl-CoA supply. *Manuscript.*

Contribution summary

Paper I: Performed the RNAseq profiling and analysis, assisted in bioreactor fermentations, edited the manuscript

Paper II: Performed the RNAseq profiling and analysis, assisted in bioreactor fermentations, edited the manuscript

Paper III: Designed the study, performed all experiments, wrote the manuscript

Paper IV: Designed the study, performed all experiments, wrote the manuscript

Preface

This dissertation serves as partial fulfillment of the requirements to obtain the degree of Doctor of Philosophy at the Department of Biology and Biological Engineering at Chalmers University of Technology. The PhD research was carried out between September 2017 and December 2021 at the division of Systems and Synthetic Biology under the supervision of Verena Siewers. The project was co-supervised by Jens Nielsen, examined by Ivan Mijakovic, and funded by Energimyndigheten, The Swedish Research Council, and Chalmers Area of Advance Energy.

John Hellgren

December 2021

Table of Contents

There's always another secret

Brandon Sanderson, The Final Empire

1 Introduction

Sustainable microbial production of formerly petroleum-based fuels and chemicals is a key part of eliminating our dependency on fossil fuels and mitigating climate change [1]. However, there are high demands on cost-effective bio-based production to make this happen [2]. In the field of metabolic engineering, we aim to engineer the microbial biocatalyst to be able to efficiently convert sugars to fuels, chemicals and pharmaceuticals. Apart from reducing the dependency on fossil fuels, the utilization of biocatalysts allows the production of bioactive compounds not accessible through chemical synthesis. The biocatalyst can be genetically engineered to conduct multiple steps of a process by introducing traits from several organisms into one host. Production of many different industrially relevant products can stem from one precursor metabolite, making the construction of a platform biocatalyst with high production of that specific precursor metabolite attractive. However, microbial production also leads to the formation of CO_2. Implementing the use of carbon-conserving and carbon-fixating pathways in a biocatalyst to avoid this loss of carbon could make the process more commercially viable and reduce the impact on climate change [3].

1.1 Aims and significance

In this thesis, I evaluated the use of phosphoketolase pathways in the yeast *Saccharomyces cerevisiae* as a strategy for precursor metabolite supply without carbon loss as CO_2 in a platform strain with the end goal of improving product yields. Apart from evaluating existing strategies with the phosphoketolase pathway, I implemented and investigated a novel cyclic phosphoketolase pathway for the complete recycling of substrate to precursor metabolites. This work will aid in the development of *S. cerevisiae* as an attractive production host, potentially allowing a more cost-effective production of industrially relevant products in the future, making sustainable production with biocatalyst preferable to using petroleum-based sources.

Chapter 2 of this thesis begins with introducing *S. cerevisiae* as a production host, along with an overview of the central carbon metabolism, the concepts of metabolic engineering and methods to assess your cell factory. **Chapter 3** focuses on the results of **Paper I-II**, where we used the linear phosphoketolase pathway as a strategy for improved supply of the important precursor metabolite acetyl coenzyme A (acetyl-CoA) without carbon loss as CO_2. **Paper I** evaluates the effect of phosphoketolase expression on the physiology of *S. cerevisiae*. **Paper II** uses a combinatorial strategy of the phosphoketolase pathway for acetyl-CoA supply and overexpression of the gene coding for the transcription factor Stb5 to achieve activation of NADPH-generating pathways for fatty acid production. In **Chapter 4**, the linear phosphoketolase pathway is expanded to a circular pathway for the complete recycling of carbon to acetyl-CoA, potentially allowing for improved product yields. The functionality of a novel circular carbon-conserving pathway is demonstrated in **Paper III** and the implication of its usage on the physiology of *S. cerevisiae* is further investigated in **Paper IV**. **Chapter 5** summarizes the key conclusions and future perspectives of the work conducted in this thesis.

2 Background

Saccharomyces cerevisiae, commonly known as Baker's yeast, has been utilized by humans for thousands of years for its capability to ferment sugars to alcohol and to raise bread. The formation of alcohol was believed to be a spontaneous reaction until the middle of the 19th century when Louis Pasteur proved that the process required living cells [4]. Yeast for beer fermentation was first isolated by Emil Christian Hansen at the Carlsberg Laboratory in 1883 [5]. Because of its long use and popular products, *S. cerevisiae* genetics and physiology have been extensively studied. It was the first eukaryotic cell to have its whole genome sequenced in 1996 [6] and *S. cerevisiae* has been used as a model organism to study human cells and diseases, as many important cellular processes are conserved through evolution between yeast and humans [7].

Apart from being good at making alcohol, *S. cerevisiae* is susceptible to genetic engineering mainly through its efficient homologous recombination system for repairing its DNA [8]. The DNA contains instructions for the cellular machinery and exploiting the reparation system allows for gene deletions and integrations with high efficiency in *S. cerevisiae*. The central dogma in molecular biology describes the flow of genetic information from DNA to proteins which are needed to catalyze reactions, provide structure, and transport molecules in the cell. DNA is first transcribed by RNA polymerase to messenger RNA (mRNA), which is then translated to protein by the ribosomes. By changing the DNA of *S. cerevisiae* through genetic engineering, we can allow *S. cerevisiae* to produce new proteins and compounds from sugars. For example, the addition of the human gene for insulin to *S. cerevisiae* allowed the production of human insulin for the treatment of diabetes [9].

2.1 Metabolic engineering and metabolism

In metabolic engineering, we genetically engineer cells to efficiently convert sugars into our product of interest. Metabolism is the collection of thousands of reactions that allow cells to convert nutrients to energy and biomass. Metabolism can be divided into catabolism and anabolism. Catabolism generates energy, redox power and 12 precursor metabolites from nutrients, while anabolism uses the 12 precursor metabolites for the biosynthesis of building blocks and assembles them into the macromolecules needed for biomass formation. Energy generated from catabolism is captured through the formation of adenosine triphosphate (ATP), while the generated redox power is captured in nicotinamide adenine dinucleotide (NADH) or nicotinamide adenine dinucleotide phosphate (NADPH). NADH is mostly used for catabolism and energy generation, while NADPH is used for anabolism and synthesis of biomass components. By deleting genes, altering the expression level of existing genes and introducing heterologous genes, we can change the flux of carbon inside the metabolic network of the cell towards our product of interest. To create a commercially viable process, the goal is to optimize the fluxes to improve the titer, rate and yield (TRY) metrics of your cell factory [10]. *S. cerevisiae* is often used as a cell factory for industrial production due to a vast available knowledgebase, robustness of the organism and ease of genetic manipulations [11].

When designing your cell factory, it is important to evaluate different metabolic routes to your product of interest in terms of stoichiometry, energy requirements and redox balance. An

overview of the central carbon metabolism in *S. cerevisiae* can be seen in **Figure 1**. Glycolysis, or the Embden–Meyerhof–Parnas (EMP) pathway, is the pathway that converts glucose to two molecules of pyruvate, while generating two ATP and two NADH per glucose [12]. Glycolysis takes place in the cytosol and starts by investing one ATP through the phosphorylation of glucose to glucose-6-phosphate (G6P) by hexokinase (Hxk1 and Hxk2) or glucokinase (Glk1). G6P is then isomerized by phosphoglucose isomerase (Pgi1) to fructose-6-phosphate (F6P). A second ATP is invested by phosphorylation of F6P to fructose-1,6-bisphosphate (FBP) by phosphofructokinase (Pfk1 and Pfk2). The enzyme FBP aldolase (Fba1) splits FBP into glyceraldehyde-3-phosphate (GAP) and dihydroxyacetone-phosphate (DHAP). DHAP can be converted to a second GAP by triose phosphate isomerase (Tpi1). The energy generation phase of the glycolysis starts downstream of GAP. GAP is converted to 1,3 bis-phosphoglycerate (1,3BPG) by GAP dehydrogenase (Tdh1, Tdh2 and Tdh3), while generating one NADH. The first ATP is generated by dephosphorylation of 1,3BPG to 3-phosphoglycerate (3PG) by 3PG kinase (Pgk1). 3PG is converted by phosphoglycerate mutase (Gpm1 and Gpm2) to 2-phosphoglycerat (2PG), which is further converted to phosphoenolpyruvate (PEP) by phosphopyruvate hydratase (Eno1 and Eno2). Finally, the second ATP-generating reaction in the glycolysis involves the conversion of PEP to pyruvate by pyruvate kinase (Pyk1 and Pyk2).

The formed pyruvate can be transported to the mitochondria and consumed by the tricarboxylic acid (TCA) cycle if oxygen is available [13]. The TCA cycle completely oxidizes pyruvate to 3 molecules of CO_2, together with the generation of 4 NADH, 1 ATP and the reduction of 1 redox carrier flavin adenine dinucleotide (FAD) to $FADH_2$. Pyruvate is converted to acetyl coenzyme A (acetyl-CoA) by the pyruvate dehydrogenase (PDH) complex (subunits Pda1, Pdb1, Lat1, Lpd1 and Pdx1), while generating NADH and CO_2. Acetyl-CoA is combined with oxaloacetate (OA) to citrate (CIT) by citrate synthase (Cit1 and Cit3). CIT is converted to isocitrate (ICIT) by aconitase (Aco1 and Aco2). A second NADH and CO_2 is generated by the conversion of ICIT to alpha-ketoglutarate (AKG) by the ICIT dehydrogenase complex (Idh1 and Idh2). The $NADP^+$-specific ICIT dehydrogenase (Idp1) can also catalyze this reaction while releasing NADPH instead of NADH. The third NADH and CO_2 is generated by the conversion of AKG to succinyl-CoA (SUCCoA) by the AKG dehydrogenase complex (Kgd1, Kgd2 and Lpd1). The single ATP is generated by conversion of SUCCoA to succinate (SUC) by succinyl-CoA ligase (Lsc1 and Lsc2). The reduction of the redox carrier FAD to $FADH_2$ is performed by the SUC dehydrogenase complex (Sdh1, Sdh2, Sdh3 and Sdh4) during the conversion of SUC to fumarate (FUM). FUM is converted by fumarase (Fum1) to malate (MAL). MAL dehydrogenase (Mdh1) is closing the cycle by converting MAL to OA, while generating the final fourth NADH. The electrons stored in the NADH and $FADH_2$ generated from the TCA cycle are transferred to oxygen through the electron transport chain, where they are used to generate ATP through oxidative phosphorylation. In total, aerobic respiration of glucose in *S. cerevisiae* yields approximately 16 ATP [14].

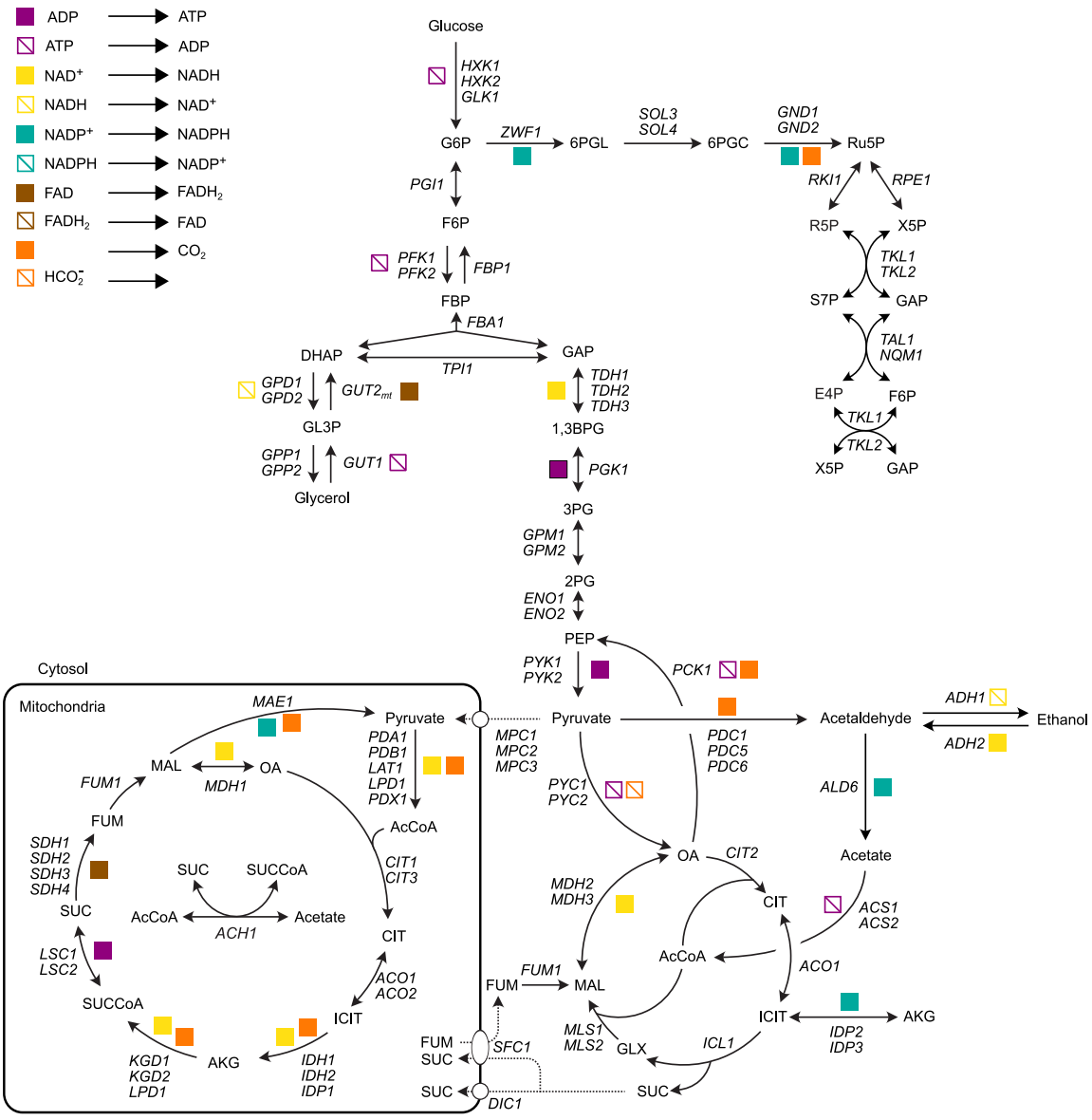

Figure 1. Overview of central carbon metabolism in *S. cerevisiae*. Abbreviations: AcCoA, acetyl-CoA; GL3P, glycerol-3-phosphate; GLX, glyoxylate; refer to text for other abbreviations.

The NADH and $FADH_2$ from the TCA cycle need oxygen to be reoxidized, which means that the TCA cycle cannot run at anaerobic conditions due to a finite pool of NAD^+ and FAD. The NADH generated through the glycolysis needs to be reoxidized by other means, otherwise, the depletion of NAD^+ will stop glycolysis. Glycolysis can instead become redox balanced during anaerobic conditions by converting cytosolic pyruvate to acetaldehyde and CO_2 by pyruvate decarboxylase (Pdc1, Pdc5 and Pdc6) and subsequent conversion of acetaldehyde to ethanol by alcohol dehydrogenase (mainly Adh1), while reoxidizing NADH to NAD^+. Ethanol formation can also occur in aerobic conditions when glucose is in excess. This is referred to as overflow metabolism, or the Crabtree effect, where *S. cerevisiae* is a Crabtree-positive yeast [15]. The Crabtree effect results in a lower ATP yield, but a higher ATP production rate, along with a lower requirement of protein mass for energy generation [16]. Overflow metabolism is suspected to be caused by limitations in NADH reoxidation from saturated respiration [17]. Accounting for protein cost and allocation suggests that overflow metabolism is caused by

protein limitations, as respiration requires more allocation of proteome mass than fermentation [18]. The produced ethanol can be later consumed by *S. cerevisiae* if oxygen is available, using the glyoxylate cycle (**Figure 1)**. Ethanol is converted to acetaldehyde by Adh2 and further converted to acetate by aldehyde dehydrogenase (Ald6), while generating NADPH. The formed acetate can be activated to acetyl-CoA by acetyl-CoA synthetase (Acs1 and Acs2) at the cost of 2 ATP. The acetyl-CoA enters the glyoxylate cycle, operating partly in the peroxisome and the cytosol. The succinate produced from the glyoxylate cycle can either be transported into the mitochondria to replenish the TCA cycle or be exchanged for fumarate, which in the end forms PEP that enters the gluconeogenesis pathway (reverse glycolysis) for the formation of precursor metabolites [19].

The major pathway for cytosolic NADPH generation in *S. cerevisiae* during growth on glucose is the pentose phosphate pathway (PPP), which is also used to provide precursors for nucleotide and amino acids biosynthesis. The first three steps of the PPP are responsible for the generation of 2 NADPH per G6P and are referred to as the oxidative PPP. The PPP starts by NADPH generation through the conversion of G6P to 6-phosphogluconolactone (6PGL) by G6P dehydrogenase (Zwf1). The second step involves the conversion of 6PGL to 6-phosphogluconate (6PG) by 6-phosphogluconolactonase (Sol3 and Sol4). The third and final step of the oxidative PPP is the conversion of 6PG to ribulose-5-phosphate (Ru5P) together with NADPH and CO_2 formation, catalyzed by 6PG dehydrogenase (Gnd1 and Gnd2). The remaining steps are referred to as the non-oxidative PPP. Ru5P is converted to ribose-5-phosphate (R5P) and xylulose-5-phosphate (X5P) by ribose-5-phosphate isomerase (Rki1) and ribulose-5-phosphate 3-epimerase (Rpe1), respectively. Through carbon rearrangement reactions, R5P and X5P are converted to sedoheptulose-7-phosphate (S7P) and GAP by the transketolases (Tkl1 and Tkl2), which are together converted to erythrose-4-phosphate (E4P) and F6P by the transaldolases (Tal1 and Nqm1). Finally, the PPP is linked back to the glycolysis through the conversion of X5P and E4P to F6P and GAP by the transketolases.

Acetyl-CoA is an important precursor metabolite for many different reactions in the cytosol, mitochondria, peroxisomes and the nucleus. The acetyl-CoA pools are compartmentalized as acetyl-CoA cannot traverse freely across membranes [20]. Therefore, the acetyl-CoA produced by the PDH complex in the mitochondria cannot easily be used in *S. cerevisiae* for acetyl-CoA consuming reactions in the cytosol, such as fatty acid biosynthesis. Instead, *S. cerevisiae* utilizes the PDH bypass to produce cytosolic acetyl-CoA from pyruvate. Like during ethanol formation, cytosolic pyruvate is converted to acetaldehyde, but with subsequent formation of acetyl-CoA like during ethanol consumption. Apart from being an important precursor in cellular metabolism, acetyl-CoA is also an important precursor metabolite in cell factories for the production of industrially relevant products, such as biopolymers, pharmaceuticals, dietary supplements and biofuels [21]. Therefore, several successful metabolic engineering strategies have been implemented in *S. cerevisiae* to optimize the central carbon metabolism for improved supply of cytosolic acetyl-CoA [22, 23], which will be discussed further in **Chapter 3** of this thesis.

The metabolic engineering process usually consists of repeated laps of the Design-Build-Test-Learn (DBTL) cycle [10]. In the design phase, you evaluate different pathways to your product

in terms of stoichiometry, enzyme kinetics, thermodynamics, cofactor usage and energy requirements. This is often aided by mathematical models and can help you find which pathway achieves the highest theoretical yield. It is important to assess the cultivation parameters and the toxicity of the product to achieve high TRY metrics. The build phase consists of constructing the necessary DNA parts and implementing them into your cell factory. In the test phase, the cell factory is cultivated and evaluated for strain performance. A large number of strains can be evaluated simultaneously in microtiter plates with automatic measurement of biomass formation. A less high-throughput method is to cultivate in shake flasks, which allows for larger volumes when needed during sampling and determining the TRY metrics. Bioreactors are usually used when strict control over the culture parameters (pH, temperature, aeration, mixing, etc.) are needed. The use of bioreactors also allows O_2 consumption and CO_2 production to be monitored. Tight control of the cultivation is ideal when analyzing different omics to gain more insights regarding the effect of your strategy on strain physiology. In the final phase, you learn from your results and adapt your strategy for the next round of the cycle to improve your cell factory further. For example, if the TRY metrics were not satisfactory, we can evaluate different homologous genes, delete competing pathways, or alter the expression of existing genes. My research has involved the entire DBTL cycle, and I will now introduce two different methods for high-throughput omics analysis that I used during the testing phase.

2.2 Transcriptomics analysis with RNAseq

A common method to access the cellular response of your cell factory to environmental perturbations, exposure to stress and changes in the genotype is to look at the transcriptome. The transcriptome is the collection of all transcribed genes in a cell and this information can tell us which genes are up- or downregulated as a response to a given change compared to a control. High-throughput determination of changes in gene expression between different cell factories is mainly performed with microarrays or RNA sequencing (RNAseq) [24, 25]. In microarrays, a chip is constructed with fluorescently labeled probes that can each bind to a specific mRNA molecule. By comparing the fluorescent intensities for the same probe between two samples, the relative abundance of each transcript between samples can be determined. RNAseq uses the next-generation sequencing (NGS) platforms to quantify each transcript as the number of times it was sequenced.

Microarray technologies were predominately used in the past, but the advent of NGS technologies allowed the invention of RNAseq in the mid-2000s, which started to replace microarrays due to its numerous advantages. The dynamic range of microarrays (10^3-10^4) is limited by fluorescence saturation, while the dynamic range in RNAseq (>10^5) is limited by the selected sequencing depth [26]. RNAseq is also not limited to predefined sets of transcripts or genomes, which allows it to detect novel genes and novel splicing events [25]. As a drawback, RNAseq is more expensive [26] and requires higher labor intensity for both sample preparation and data analysis compared to microarrays [27, 28].

In RNAseq, each transcript is quantified from sequencing reads, with higher abundant transcripts receiving more reads. Before sequencing, the mRNA is isolated by poly-A enrichment, fragmented, converted to complementary DNA (cDNA) by reverse transcription

and ligated to adapters to allow binding of sequencing primers. The transcripts are sequenced by synthesis with a DNA polymerase and each incorporated nucleotide is identified with its unique fluorescent label. There are options to sequence the transcript in one direction (single-end) or both directions (paired-end). Single-end sequencing is cheaper, but paired-end sequencing facilitates the alignment and is important for the detection of novel transcript splicing events [28]. The sensitivity of the RNAseq is dependent on the number of mapped reads, where 4 million and 30 million mapped reads can capture 80% and >90% of the transcripts, respectively, in *S. cerevisiae* [24]. Organisms with more complex splicing patterns need much larger coverage, where >200 million mapped reads might be required to detect novel splicing events in humans [29]. The reads are aligned to a genome, assigned to a transcript and counted. In the end, the raw reads from the sequencer are transformed to gene counts, which list how many times each transcript was counted.

The generated gene counts are used to determine which genes are differentially expressed (up- or downregulated) compared to a control. An important consideration is the normalization of the gene counts before calculating the $\log_2$ fold change (LFC) of each gene. Normalization is important to avoid effects from differences in the total amount of reads between samples. If one sample has more reads overall, the genes in that sample will also get more gene counts and skew the downstream analysis. Furthermore, differences in RNA composition will generate false positives. For example, a gene highly expressed in only one condition will take up a big portion of the reads for that condition and leave the other genes to appear downregulated compared to another condition. The normalization can be performed with the R-package DESeq2 [30], which normalizes for differences in sample preparation (library counts size) and sample type (RNA composition) by dividing the gene counts of each gene in each sample with the median of its scaled gene counts across all samples. DESeq2 calculates the LFC by pair-wise comparisons between the conditions and calculates the significance with the Wald test after fitting each gene with a negative binomial generalized linear model. Finally, the p-values are adjusted for multiple testing with the Benjamini-Hochberg method [31].

Trying to extract biological information from individual differentially expressed genes can be challenging, which is why genes are usually grouped into gene sets and evaluated in a gene set analysis (GSA) to find how the whole gene set is changing. These sets can be defined by Gene Ontology (GO) terms [32], which groups together genes with similar functions or those that are part of the same process. There exist several different GSA methods and a common method is to run multiple GSAs and combine the results in a consensus scoring approach, using the Platform for Integrated Analysis of Omics data (Piano) R-package [33]. Piano will tell you from each GSA method which gene sets are 1) enriched but without directional information, 2) enriched and changed in either or both directions and 3) enriched and changed in one direction. The results from different GSA methods are combined and each gene set receives a consensus score, calculated in a rank aggregation approach. RNAseq has been successfully used as a part of the DBTL cycle in *S. cerevisiae* to improve the octanoic acid titers [34], the productivity of S-adenosyl-L-methionine [35], the furfural tolerance [36], and the assimilation of xylose [37]. I used RNAseq during the test phase of **Paper I**, **II** and **IV** to gain more insight about our cell factories.

2.3 Proteomics analysis

Analysis of the transcriptome can tell us a lot about the response of a cell factory. However, it is the translated proteins that define the phenotype of the cell, as the proteins are needed to catalyze reactions, provide structure, and transport molecules. Analysis of the proteome has previously been limited to detecting a few proteins at a time through, for example, antibody-based techniques [38]. Recent advances in Liquid Chromatography–Mass Spectrometry (LC-MS) methods have allowed the quantification of more than half of the proteins in *S. cerevisiae* [39].

In LC-MS, the sampled proteins are first cut into peptides by trypsin digestion, separated by LC, converted to ions by applying high voltage to the liquid (electrospray ionization) and injected into the mass spectrometer. Inside the mass spectrometer, precursor ions of the peptides with specific masses can be selected, further fragmented and their intensities determined. The resulting spectra of different masses are matched against a database to determine the amino acid sequence of the peptides. Quantification between protein samples can be done with label-free methods by comparing ion intensities or spectral counting. Label-free variants of quantitative proteomics have minimal sampling handling and more cost-effective sample preparations, but can only run one sample at a time in the MS. Furthermore, they require very reproducible LC separations and multiple technical replicates.

Tandem mass tag (TMT) labeling is a chemical labeling method to allow multiplexing of global quantification of the proteome [40]. The TMT label consists of different combinations of ^{13}C and ^{15}N stable isotopes in a mass reporter, which can generate up to 16 unique masses when cleaved off. The weight of the mass tag is balanced by a mass normalizer so that all TMT tags have the same mass before cleavage. This allows up to 16 different protein samples to be analyzed simultaneously and limits the time needed to run the MS, which is an important factor for the cost of the analysis. TMT labeling also has better accuracy, precision and coverage compared to label-free variants of quantitative proteomics. The drawbacks of TMT are the cost of the reagents, extensive fractionation needed before the injection into the MS, and more hands-on time during labeling and sample preparation. We used the TMT labeling method in **Paper IV** to determine which genes are differentially expressed on the protein level.

The relative protein abundances of the quantified proteins should be $\log_2$ transformed before further analysis. We used the R-package DEqMS [41] to calculate the LFC and significance. DEqMS uses the number of peptide-spectrum matches (PSM) to estimate the prior variance. This means that proteins with low PSM get a larger variance than proteins with high PSM. Proteins with low PSM are usually excluded from the analysis, but DEqMS proposes this method to keep proteins with low PSM. After correcting the prior variance, DEqMS uses Limma to perform the statistical analysis. The Benjamini-Hochberg method [31] was used to correct the resulting p-values for multiple testing. Proteomics analyses have been used in metabolic engineering of *S. cerevisiae* to improve dicarboxylic acid production [42], improve the flavor of wine [43] and engineer oxygen-independent biotin biosynthesis [44]. I used global relative quantitative proteomics with TMT labeling in **Paper IV** along with RNAseq to assess my cell factory during the testing phase of the DBTL cycle.

3 Part I: The linear phosphoketolase pathway

With acetyl-CoA as an important precursor metabolite for many industrially relevant products, it can be beneficial to establish a platform strain [45] with a high flux towards acetyl-CoA formation, which can enhance the bioconversion into the product [21]. That platform strain can be used as a starting point for producing any industrially relevant product from acetyl-CoA. Most biosynthetic pathways for industrially relevant products are located in the cytosol, which means that the cytosolic pool of acetyl-CoA should be increased. Strategies for increasing the cytosolic acetyl-CoA supply in *S. cerevisiae* have included increasing the CoA biosynthesis [46] and upregulation of genes in the native PDH bypass [47]. A problem with the native PDH bypass is the cost of 2 ATP to activate acetate to acetyl-CoA, resulting in a final cost of 1 ATP per acetyl-CoA formed. This requirement of ATP to produce acetyl-CoA might limit the yields of products derived from cytosolic acetyl-CoA.

The PDH complex can convert pyruvate to acetyl-CoA directly without a cost of ATP, but the formed acetyl-CoA cannot be effectively transported to the cytosol. One solution is to move the entire production pathway to the mitochondria [48], but that might not be applicable for all production pathways. Instead, the usage of heterologous pathways for cytosolic acetyl-CoA supply has been explored to avoid the cost of ATP [22]. An alternative pathway is to use the acetylating acetaldehyde dehydrogenase (A-ALD), which can convert acetaldehyde to acetyl-CoA without ATP consumption [49]. This results in a net gain of 1 mol ATP per mol acetyl-CoA formed. However, an obstacle to efficient usage of the A-ALD pathway is a reduced biomass yield from acetaldehyde toxicity [49]. Moving the mitochondrial PDH complex to the cytosol would also allow a pathway that generates 1 mol ATP per mol acetyl-CoA formed. Expression of a cytosolic PDH complex was employed successfully in *S. cerevisiae* by using the PDH homolog from *Enterococcus faecalis*, with the drawback of the requirement of lipoic acid supplementation [50, 51]. Other implemented strategies in *S. cerevisiae* that generate 1 ATP/acetyl-CoA is through the oxygen-requiring pyruvate oxidase [52], the oxygen-sensitive pyruvate-formate lyase [53], or the supplementation-dependent export of acetyl-CoA from the mitochondria to the cytosol via the carnitine shuttle [54]. Oleaginous yeasts obtain a high flux towards acetyl-CoA for lipid formation by utilizing the citrate-oxaloacetate shuttle: citrate produced in the mitochondria is exported to the cytosol, where it is converted acetyl-CoA by ATP-citrate lyase [55]. Implementation of the citrate-oxaloacetate shuttle and ATP-citrate lyase provides an ATP neutral pathway from glucose to acetyl-CoA and has been successfully implemented in *S. cerevisiae* for improved cytosolic acetyl-CoA supply [56, 57].

Most strategies for increasing the acetyl-CoA supply result in carbon loss as CO_2, consequently limiting the maximal theoretical product yields. High product yields are important for process profitability, as the cost of the substrate could be up to 75% of the total costs of the production process [58]. Improvement of product yields is an important part to be able to compete with the petroleum-based industry and promote sustainable production to mitigate climate change. To increase product yields, strategies involving incorporation of CO_2 through synthetic carbon-fixation [59] have been deployed in *S. cerevisiae* through the expression of enzymes from the Calvin cycle [60, 61] and engineering of pyruvate carboxylase [62]. However, the fixation of CO_2 requires an energetic cost [63]. Another option is the utilization of pathways that avoid the

loss of carbon as CO_2. An enzyme related to the transketolase enzyme from the PPP is the phosphoketolase, which both are thiamin diphosphate dependent [64]. Like transketolase, phosphoketolase can convert X5P to GAP. However, while transketolase combines reversibly X5P with R5P or E4P to form GAP and S7P or F6P, phosphoketolase requires just a single sugar phosphate as substrate and converts X5P irreversibly to GAP and acetyl-phosphate (AcP). Apart from X5P-specific phosphoketolases (Xpk), there also exist phosphoketolases that can accept F6P as well (Xfpk). The two different phosphoketolase reactions are shown below:

$X5P+P_i \rightarrow GAP + AcP + H_2O$ (Xpk)

$F6P+P_i \rightarrow E4P + AcP + H_2O$ (Fpk)

The Xpk and Fpk reaction have an estimated change of Gibbs free energy at standard physiological conditions ($\Delta_rG'^m$) of -59.1 and -48.8 kJ/mol, respectively [65]. Phosphoketolases from different species differ in their relative activity towards X5P and F6P. For example, phosphoketolases from the Firmicute phylum (genus *Clostridium*, *Leuconostoc* and *Lactobacillus*) are usually more X5P-specific, with a X5P:F6P activity ratio of 5:1 for the phosphoketolase from *Leuconostoc mesenteroides* [66]. In comparison, the phosphoketolases from bifidobacterial are usually dual Xfpk versions, with a X5P:F6P activity ratio of 3:2 for *Bifidobacterium breve* [66]. In bifidobacteria, the dual Xfpk and the PPP form the bifid shunt, which can generate 1.5 mol acetate, 1 mol lactate and 2.5 mol ATP from 1 mol glucose [67]. This pathway can generate more ATP compared to lactic acid fermentation with the EMP pathway (2 mol ATP/mol glucose). Combining the phosphoketolase with the enzyme phosphotransacetylase (Pta), which converts AcP reversibly to acetyl-CoA, forms a linear pathway from glucose to acetyl-CoA without carbon loss as CO_2. There exist strategies to allow a circular pathway to fully recycle all carbon from F6P to 3 acetyl-CoA, which will be discussed in **Part II**. In **Part I**, we assume the use of the linear phosphoketolase pathway, as no genetic engineering efforts were made to promote the circular pathway. The phosphoketolase pathway has been used successfully in *S. cerevisiae* for the production of farnesene [68], fatty acid ethyl esters [69], β-amyrin [70], octanoic acid [71], polyhydroxybutyrate [72], 3-hydroxypropionic acid [73] and p-coumaric acid [74]. The phosphoketolase pathway has also improved lipid yields in the oleaginous yeast *Yarrowia lipolytica* [75, 76] and in cyanobacteria [77]. Utilization of the phosphoketolase pathway is not limited to growth on sugars as overexpression of the native phosphoketolase in *Methylomicrobium buryatense* resulted in an increased lipid yield from methane [78].

In **Part I** of this thesis, we investigated the effect of introducing the phosphoketolase pathway in *S. cerevisiae* (**Paper I**). In addition, we investigated the effect of a combinatorial strategy, where the phosphoketolase pathway provides additional acetyl-CoA and overexpression of the transcription factor Sbt5 provides extra NADPH, both needed for fatty acid biosynthesis (**Paper II)**.

3.1 Effect of phosphoketolase expression (Paper I)

The phosphoketolase gene can be found in some yeasts, for example, in the oleaginous yeast *Rhodosporidium toruloides* [79], but not in *S. cerevisiae*. Furthermore, the product AcP of the phosphoketolase is not produced from any other reactions in *S. cerevisiae*. We wanted to investigate the effect of AcP accumulation, caused by bottlenecks downstream of AcP, in a platform *S. cerevisiae* strain where the heterologous phosphoketolase pathway was implemented for additional acetyl-CoA supply. This bottleneck could arise from limitations in the conversion of AcP to acetyl-CoA, catalyzed by the Pta enzyme. Bottlenecks in acetyl-CoA consumption to the product of interest could lead to a build-up of acetyl-CoA, shifting the equilibrium of the reversible Pta reaction towards AcP formation.

In **Paper I**, we simulated the scenario of AcP accumulation by expressing only the phosphoketolase gene in the wild-type *S. cerevisiae* CEN.PK 113-5D strain, without the *pta* gene or additional acetyl-CoA sinks. The phosphoketolase we examined was from *Bifidobacterium breve*, which is a bifunctional phosphoketolase displaying the highest F6P activity among nine tested phosphoketolases, but with slightly higher activity towards X5P than F6P (3:2 ratio) [66]. The strains, with or without phosphoketolase expression, were cultivated in controlled bioreactor cultivations in both batch and chemostat mode at pH 5. We calculated the physiological parameters during exponential growth on glucose from continuous measurements of OD_{600}, cell dry weight (CDW), and extracellular metabolites by HPLC (**Table 1**). After the culture consumed all the glucose and reached the ethanol phase, the batch culture was turned into a carbon-limited chemostat at the dilution rate of 0.1 h^{-1}, with 0.75% glucose in the feed. The dilution rate is calculated by dividing the speed of the feeding pumping by the bioreactor culture volume.

Table 1. Physiological parameters calculated for control and phosphoketolase expressing strain xfpk(BB) during batch growth on glucose and carbon-limited chemostat.

	Batch – exponential phase		Chemostat	
Flux	Control	xfpk(BB)	Control	xfpk(BB)
μ(max) (h^{-1})	0.353 ± 0.008	0.266 ± 0.006	0.104 ± 0.002	0.103 ± 0.003
Y(x/s) (gCDW/gGlucose)	0.135 ± 0.00	0.123 ± 0.00	0.479 ± 0.01	0.409 ± 0.01
q(Glucose) (mmol $gCDW^{-1}$ h^{-1})	−14.42 ± 0.36	−12.19 ± 0.39	−1.18 ± 0.06	−1.36 ± 0.03
q(EtOH) (mmol $gCDW^{-1}$ h^{-1})	21.46 ± 0.75	17.26 ± 0.52	–	–
q(Acetate) (mmol $gCDW^{-1}$ h^{-1})	0.61 ± 0.04	1.38 ± 0.03	–	–
q(Glycerol) (mmol $gCDW^{-1}$ h^{-1})	1.13 ± 0.03	0.62 ± 0.04	–	–
q(Pyruvate) (mmol $gCDW^{-1}$ h^{-1})	0.13 ± 0.01	0.15 ± 0.00	–	–
q(Succinate) (mmol $gCDW^{-1}$ h^{-1})	0.02 ± 0.0	0.01 ± 0.0	–	–
q(CO_2) (mmol $gCDW^{-1}$ h^{-1})	30.01 ± 0.32	28.16 ± 0.97	2.91 ± 0.19	3.34 ± 0.09
q(Biomass) (mmol $gCDW^{-1}$ h^{-1})	14.37 ± 0.31	10.81 ± 0.25	4.13 ± 0.31	4.07 ± 0.25
q(O_2) (mmol $gCDW^{-1}$ h^{-1})	−5.49 ± 0.53	−7.63 ± 0.76	−2.61 ± 0.20	−3.35 ± 0.12
Carbon balance (%)	107 ± 2	107 ± 2	99 ± 3	92 ± 1

Strains were cultured with biological quadruplicates in minimal media with 2% glucose in batch and 0.75% glucose in the chemostat feed at pH 5. Values represent averages ± the standard deviation.

Expression of *xfpk* from *B. breve* in *S. cerevisiae* (xfpk(BB)) from the high copy plasmid pSP-GM1 [80] during the exponential phase at pH 5 reduced the maximum specific growth rate by 25%, biomass yield by 9% and the glucose uptake rate by 15%. Differences in the glucose uptake rate influence the other exchange fluxes from central carbon metabolism. Therefore, we converted the exchange fluxes to C-mol and normalized them to the glucose uptake rate for easier comparison (**Figure 2**). In the control, we can observe that 50% of the carbon is converted to ethanol, which is reduced by 5% after phosphoketolase expression, possibly caused by redirection of the carbon flux from the glycolysis by the phosphoketolase. Furthermore, the glycerol production rate decreased from phosphoketolase expression. Glycerol formation reoxidizes the NADH produced from biomass formation when the respiratory capacity is limited [81]. The lower glycerol formation could indicate that the phosphoketolase pathway is rerouting the carbon flux to bypass the NADH formation by glyceraldehyde-3-phosphate dehydrogenase (GAP → 1,3BPG) in the glycolysis, leading to less demand for NADH reoxidation.

We noticed an increased flux towards CO_2 (**Figure 2**) and an increase in oxygen consumption rate by 39% (**Table 1**), indicating increased respiration. Furthermore, estimating the respiration as the difference between the CO_2 flux and half the ethanol flux (both in relative C-mol) showed increased respiration in xfpk(BB). At the same time, the flux into biomass was decreased by 11%, indicating an increased energy demand that is met through increased respiration. Phosphoketolase expression more than doubles the acetate flux. Without the Pta enzyme, the AcP formed from the phosphoketolase cannot be directly converted to acetyl-CoA, but instead undergoes promiscuous hydrolysis to acetate by the glycerol-3-phosphate phosphatases (Gpp1 and Gpp2) [66, 68]. Acetate has a pK_a of 4.76 and will be deprotonated inside the cell due to the neutral pH of the cytoplasm. This leads to acidification of the cytoplasm [82] and excess protons and acetate anions need to be pumped out by ATP-dependent processes [83]. An extracellular pH below the pK_a will cause protonation of the majority of the acetate ions. This lipophilic protonated form of acetate can then be transported passively inside the cell again, creating a futile cycle that spends ATP [84]. This additional cost of energy could be met with increased respiration.

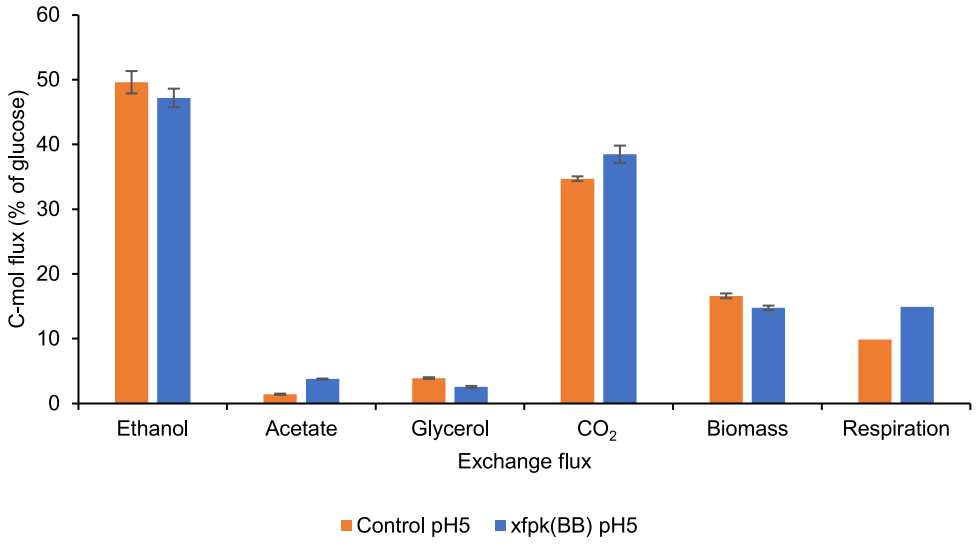

Figure 2. Carbon fluxes in C-mol normalized to the glucose uptake rate during batch growth on glucose in bioreactors at pH 5. The flux towards respiration is estimated as the difference between the CO_2 flux and half the ethanol flux.

To evaluate the effect of proton decoupling by acetate on cell growth, we conducted additional bioreactor experiments at pH 4 and pH 6, where the distribution of the lipophilic protonated form of acetate should be 85% and 5%, respectively. Increasing the pH from 4 to 6 in the control strain resulted in a slightly longer lag phase, but the maximum specific growth rate and biomass yield during the exponential phase was not affected (**Figure 3A**). Respiratory growth at pH 6 on the produced ethanol after glucose exhaustion showed a 27% reduction in growth rate and a 20% reduction in final biomass concentration for the control. Increasing the pH for xfpk(BB) did not affect the growth rate during the exponential phase. However, increasing the pH almost doubled the growth rate of xfpk(BB) during the ethanol phase, which was not significantly different from the control at pH 6. While the control showed reduced final biomass concentration at pH 6 compared to pH 4, the strain xfpk(BB) showed increased final biomass at higher pH.

Acetate production has previously been shown to increase with higher pH [85], and we observed a 205% increase of the acetate concentration for the control when increasing the pH from 4 to 6 (**Figure 3A**). At the same time, phosphoketolase expression increased the acetate concentration by 166% at pH 4 compared to the control, which in xfpk(B) was further increased by 130% at pH 6. The flux towards acetate increased from 0.4 to 1.4% of the carbon in the control (pH 4 vs pH 6), with xfpk(BB) showing an increase from 1.8 to 4.1% of the carbon converted to acetate (**Figure 3B).** The increased CO_2 and respiration flux during the glucose phase at pH 6 for the xfpk(BB) strain is believed to be caused by respiratory co-consumption of acetate [86]. In summary, the improved final biomass yield and growth rate during the ethanol phase of xfpk(BB) at pH 6 results in similar performance as the control strain. This suggests that the futile cycle caused by acetate transportation has a high effect on strain physiology at pH 4, which is relieved by increasing the pH to 6.

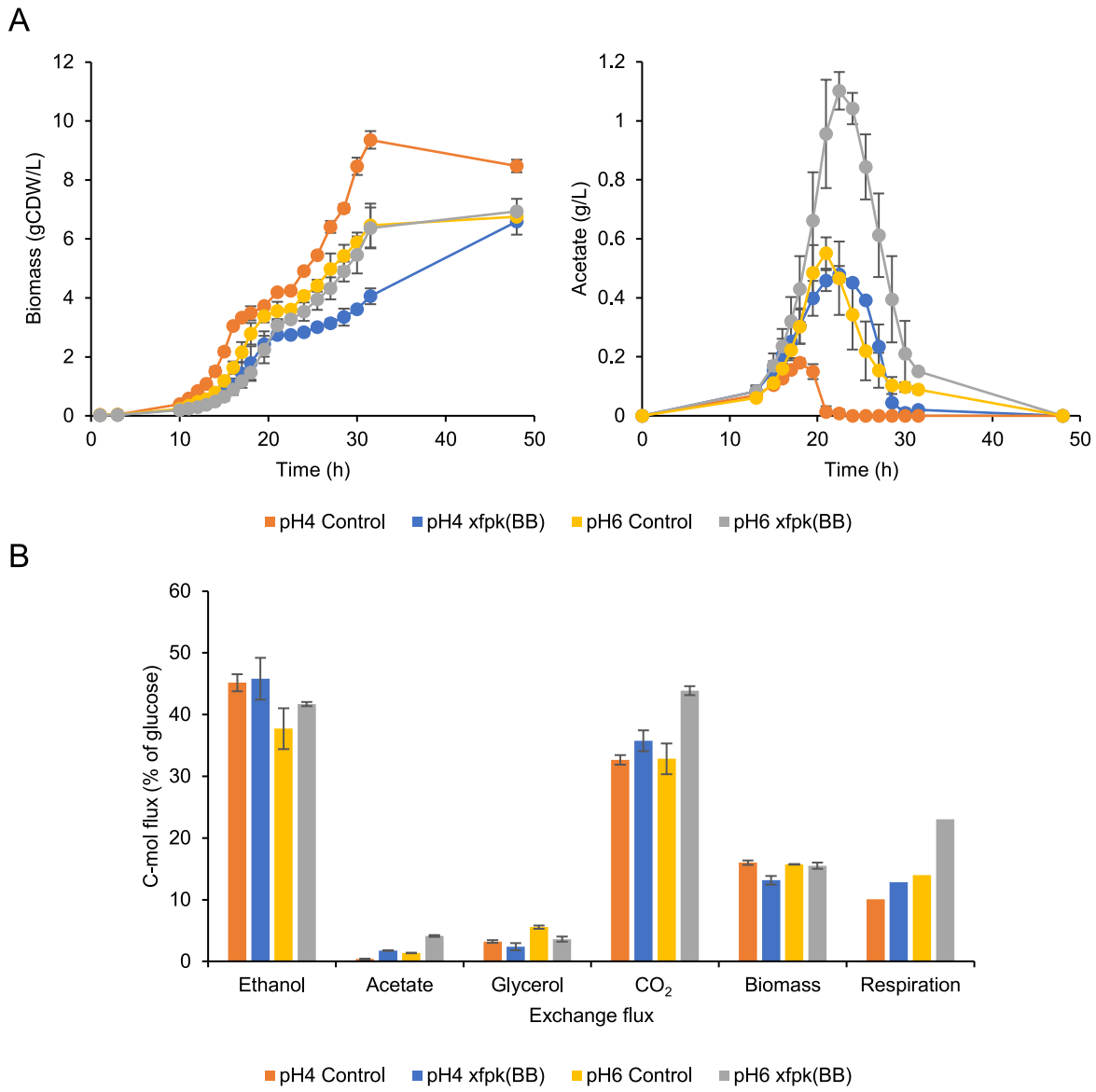

Figure 3. Bioreactor cultures of control and phosphoketolase expressing strain at pH 4 and pH 6. **A)** Profile of cell dry weight (CDW) and acetate production and **B)** comparison of the carbon fluxes in C-mol normalized to the glucose uptake rate.

After the batch bioreactor culture at pH 5 consumed all the glucose and reached the ethanol phase, the culture mode was turned into a chemostat at a dilution rate of 0.1 h^{-1}. During the chemostat, the growth rate is set by the dilution rate. The increased acetate concentration during batch in xfpk(BB) did not prevent it from reaching a purely respiratory steady-state, with no fermentation product accumulation (**Table 1**). Phosphoketolase expression in xfpk(BB) resulted in a 15% higher glucose uptake rate to be able to keep growing at the specific growth rate of 0.1 h^{-1}. Furthermore, the increased CO_2 production, increased oxygen consumption and 14% reduced relative C-mol flux to biomass indicate increased respiration and energy demand. Flux through the phosphoketolase bypasses the ATP generation from Pgk1 and Pyk1,2 in the glycolysis, and hydrolysis of the AcP from the phosphoketolase to acetate does not generate

any energy. To consume this acetate, 2 ATP need to be spent to convert acetate to acetyl-CoA with acetyl-CoA synthetase (Acs1 and Acs2), which can be consumed in the glyoxylate and TCA cycle. This extra demand of acetate consumption and ATP could explain the observed increase in respiration.

To further understand the effect of phosphoketolase expression in *S. cerevisiae* on a global level, we performed a RNAseq analysis from chemostat samples to determine the changes in genes expression. Identifying differentially expressed genes could give us clues about which pathways in metabolism are up- or downregulated, resulting in rearrangements of the carbon flux in response to phosphoketolase expression. It can also provide more evidence to strengthen our hypothesizes generated from the physiological data. Phosphoketolase expression in *S. cerevisiae* resulted in 120 differentially expressed genes (41 up- and 79 downregulated) with an absolute $\log_2$-fold change (LFC) above 1 and an adjusted p-value below 0.01. Reducing the filtering to absolute LFC above 0.5 reveals 447 differentially expressed genes (172 up- and 275 downregulated).

The effect of phosphoketolase expression in *S. cerevisiae* on transcript levels of genes involved in the central carbon metabolism is shown in **Figure 4**. The lower glycolysis was slightly downregulated, but only *ENO1* showed a LFC below -0.5. This downregulation could possibly be a result of the rerouting of carbon from the glycolysis by the phosphoketolase. Furthermore, the genes *PDC1*, *PDC6* and *ADH1* were downregulated, which are involved in ethanol formation from pyruvate. With the Pta enzyme missing, the AcP produced by the phosphoketolase can only be degraded to acetate by the promiscuous AcP hydrolysis by Gpp1 and Gpp2 [66, 68]. The downregulation of genes connected to acetaldehyde formation and consumption might be an attempt to reduce acetate formation. The cytosolic aldehyde dehydrogenase (Ald6), responsible for most of the acetate production from acetaldehyde in the cytosol [87], was not differentially expressed. However, the mitochondrial Ald4 and Ald5 were slightly downregulated.

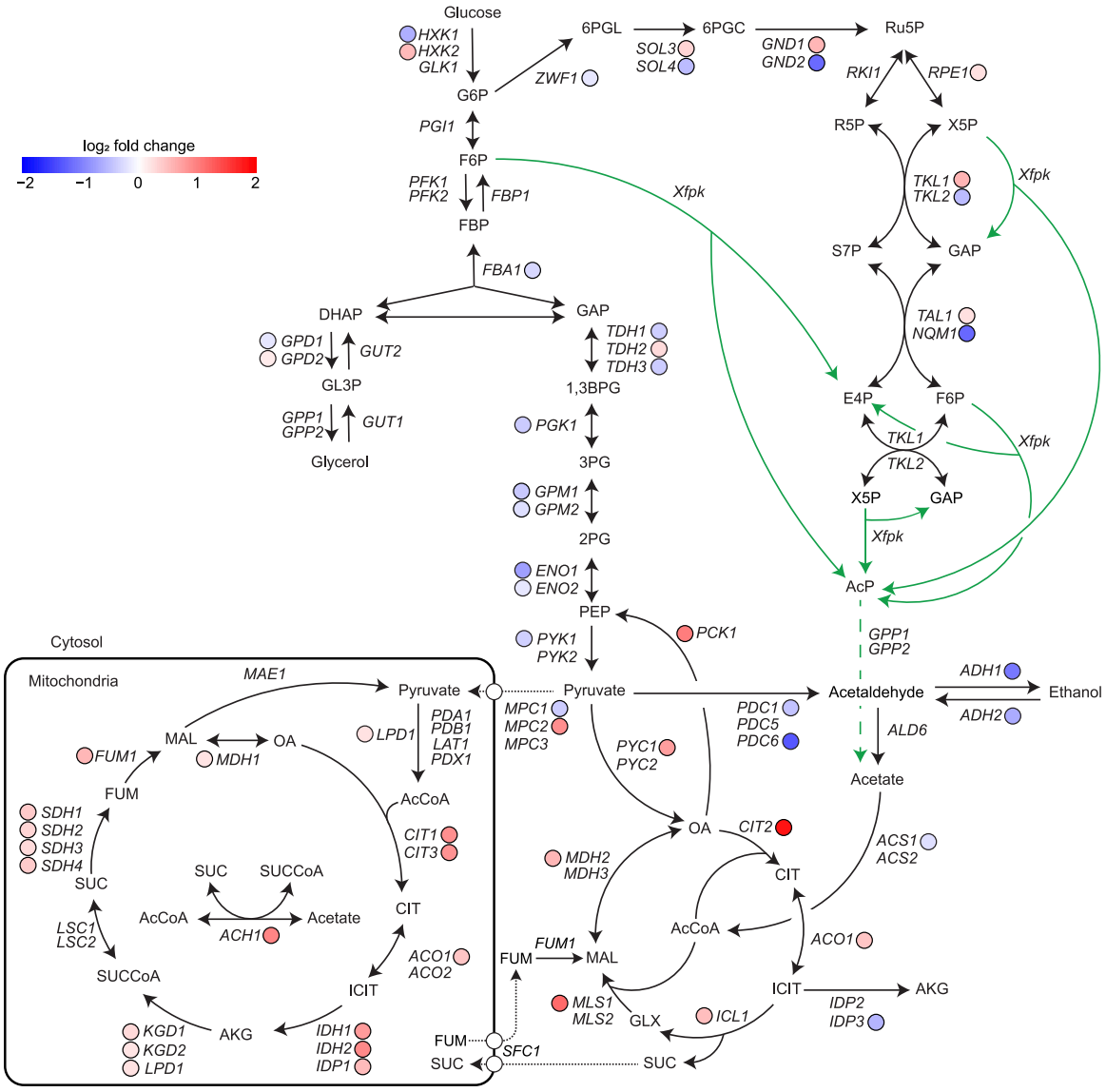

Figure 4. Differentially expressed genes in the central carbon metabolism from phosphoketolase expression during carbon-limited chemostat. The $\log_2$-fold change (LFC) values are filtered for adjusted p-value below 0.01 and visualized as intensities of red (up) and blue (down). Full green arrows indicate the introduced phosphoketolase reactions. The dashed green arrow highlights the promiscuous degradation of AcP to acetate by Gpp1 and Gpp2. Figure adapted from **Paper I** [88].

The increased acetate formation observed in the batch culture was consumed by xfpk(BB) in the chemostat, with no acetate detected in the outflow (**Table 1**), even though Acs1, the major isozyme during carbon-limited chemostat [89] was slightly downregulated. This could be connected to the upregulation of the glyoxylate cycle, the TCA cycle and gluconeogenesis, required for growth on acetate and other non-fermentable carbon sources. We also observe an upregulation of *ACH1*, which detoxifies mitochondrial acetate during growth on acetate [90]. GO-term analysis with the R-package Piano further highlights enrichment for upregulated genes in the TCA cycle (**Figure 5**). Furthermore, we can observe enrichment for upregulated genes in the GO-terms ‘mitochondrial translation’, ‘mitochondrial electron transport’, ‘cristae formation’, ‘ATP synthesis coupled proton transport’ and ‘aerobic respiration’, which supports the observation of the increased respiration deduced from the increased oxygen consumption

rate. Respiration is crucial for growth on acetate [91] and high respiratory capacity is needed to avoid overflow metabolism and accumulation of fermentation products in chemostat cultures [92]. The increased respiration in xfpk(BB) is possibly needed to consume the excess acetate generated from hydrolysis of the phosphoketolase product AcP. Additionally, the redirection of carbon from glycolysis by the phosphoketolase bypassed the ATP generation from the lower glycolysis, which might require upregulation of respiration to compensate for this loss of ATP.

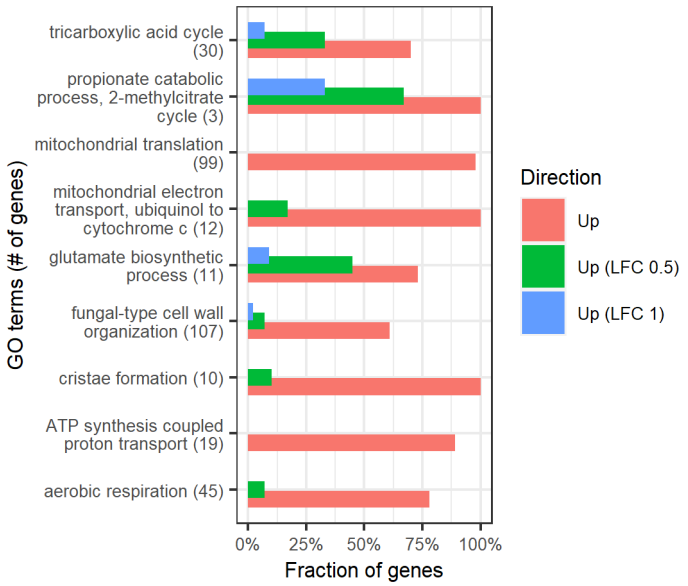

Figure 5. Enriched GO terms involved in biological processes from phosphoketolase expression during carbon-limited chemostat at pH 5. Data summarized from the consensus heatmap generated with the Piano R-package by filtering the median adjusted p-value below 0.1 for non-directional enrichment and below 0.05 for the distinct upregulated enrichment. The fraction of upregulated genes is shown without filtering (red) and LFC > 0.5 (green) or LFC > 1 (blue) together with an adjusted p-value below 0.01.

The isozymes from the PPP were differentially expressed in different directions, with the major isozymes upregulated and the minor ones downregulated. Combining the gene counts of these isozymes and rerunning the differential expression analysis results in a slight upregulation of the combined isozymes *GND1+2* and *TKL1+2*, with the combined isozymes of *SOL3+4* and *TAL1+NQM1* not being differentially expressed. Zwf1, catalyzing the first and the rate-limiting step of the oxidative PPP was slightly downregulated. Genes from the PPP were previously shown to be downregulated during growth on acetate [93], but we suspect that our observations here were due to a simultaneous growth on glucose and consumption of the excess produced acetate. Co-consumption of glucose and acetate might influence the expression of genes in the PPP differently compared to growth on acetate alone.

We observed that gene *URA3* was strongly downregulated in xfpk(BB). *URA3* is involved in uracil biosynthesis and is used as an auxotrophic marker to enable growth in minimal media for strains with a *ura3-52* genotype, ensuring that the cells keep the transformed plasmid. The downregulation of *URA3* indicates that it is beneficial to reduce the copy number of the high copy plasmid pSP-GM1 containing the phosphoketolase under the control of the *TEF1* promoter. The reduction in plasmid copy number could help to reduce the acetate formation and other negative effects caused by phosphoketolase expression without the Pta enzyme and

additional acetyl-CoA sinks. The copy number of the similar p426GPD plasmid is 17 per cell [94], but the transcript per million (TPM) of *xfpk* expressed from the *TEF1* promoter on the high copy plasmid was still lower than the native *TEF1* gene expressed from the genome. This could be the result of the reduction in pSP-GM1 copy number in xfpk(BB), however, the gene expression level is not exclusively defined by the promoter sequence, but also defined by other regulatory sequences, such as the coding sequence, 5' and 3' untranslated regions, and the terminator [95].

Measurement of changes in gene expression only gives an indirect overview of how the metabolism is rewired as a consequence of phosphoketolase expression in *S. cerevisiae*. Therefore, we performed targeted metabolomics to get a clearer picture of how the concentrations of a selected list of intracellular metabolites are changed. From **Figure 6**, we can see how the concentrations of 12 sugar phosphates are affected by phosphoketolase expression. The substrates F6P and X5P of the phosphoketolase were reduced by 25 and 75%, respectively, in the strain xfpk(BB), demonstrating that the phosphoketolase can efficiently redirect the carbon flux in *S. cerevisiae*. Even though the pool of F6P was approximately three times larger than X5P in the control strain, both substrates were reduced by 0.45 µmol/gCDW in xfpk(BB), possibly from the higher *in vitro* activity towards X5P [66]. At the same time, the products GAP and E4P from the phosphoketolase increased by 2- and 5.4-fold, respectively. E4P is a precursor of the aromatic amino acid (AAA) biosynthesis pathway, with AAAs being the substrates for the biosynthesis of aromatic compounds that can be used to make cosmetics, pharmaceuticals, and pigments [96]. The availability of E4P has been shown to be limiting in the AAA biosynthesis pathway in *S. cerevisiae* [97], and successful attempts have been made to utilize the phosphoketolase pathway to divert the carbon flux to E4P and increase the titers of the flavonoid precursor p-coumaric acid [74].

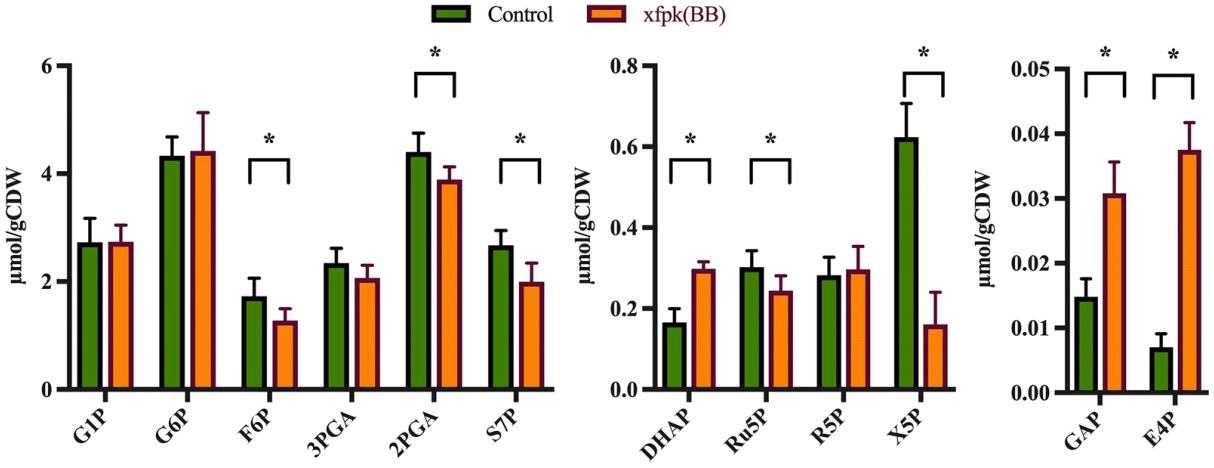

Figure 6. Quantification of sugar phosphates during carbon-limited chemostat for control and phosphoketolase expressing xfpk(BB) at a dilution rate of 0.1 h^{-1}. Biological quadruplicates were used: error bars show the standard deviation. Asterisks indicate significant changes calculated with a two-sided Student's t-test with unequal variance (* $p < 0.05$). Figure adapted from **Paper I** [88].

The reduction of 2PGA in the glycolysis could be a result of the redirection of F6P from glycolysis by the phosphoketolase. Lowering the X5P concentration by 75% might shift the equilibriums of the reactions in the PPP. This could explain the lower concentration of S7P,

caused by a phosphoketolase mediated reduction of X5P and increase of GAP that shift the transketolase reaction towards R5P and X5P formation. Reduction of X5P might also shift the equilibrium of the Rpe1 reaction towards X5P formation, leading to Ru5P consumption. The changes in the metabolites involved in the PPP might be responsible for the small upregulation of the combined isozymes *GND1+2* and *TKL1+2*.

In summary, we empathized the effect of bottlenecks in the phosphoketolase pathway at the Pta reaction (AcP ⇄ acetyl-CoA) and production formation pathways from acetyl-CoA by omitting the *pta* gene and additional acetyl-CoA sinks in the *S. cerevisiae* CEN.PK 113-5D strain expressing the phosphoketolase gene. This led to increased production of acetate, increased respiratory demand, and altered sugar phosphate pools. RNAseq analysis showed a downregulation of genes in the glycolysis and upregulation of genes involved in acetate consumption and respiration. Optimizing the AcP conversion to acetyl-CoA and product formation from acetyl-CoA is important for utilizing the phosphoketolase pathway efficiently for increased acetyl-CoA-derived product yields.

3.2 Coupling phosphoketolase expression to NADPH supply (Paper II)

Biofuels can be produced microbially with fatty acids (FA) as a building block from a great variety of feedstocks, allowing for a more sustainable alternative to plant- or animal-based fats [98]. Synthesis of FA is costly in terms of acetyl-CoA, but also requires reducing power in the form of NADPH. For example, the synthesis of one molecule of the saturated C_{16} fatty acid palmitic acid costs 8 acetyl-CoA and 14 NADPH. A common strategy for increased NADPH supply in *S. cerevisiae* is the upregulation of the PPP [57]. To meet the demand of acetyl-CoA and NADPH for FA synthesis, we designed a combinatorial strategy with the phosphoketolase pathway to provide the acetyl-CoA and overexpression of *STB5*, coding for a transcription factor (TF) that activates pathways that produce NADPH. Upon oxidative stress induced by diamide treatment, Stb5 has been shown to activate the expression of genes in the PPP (*ZWF1*, *SOL3*, *GDN1/2*, *RKI1*, *TKL1* and *TAL1*) to increase the NADPH generation [99]. The same study also showed that Stb5 mediated repression of *PGI1* to further direct the flux from the glycolysis to the PPP during oxidative stress. Other genes involved in NADPH generation shown to be activated by Stb5 in Larochelle et al. (2006) are: *YEF1*, an ATP-NADH kinase that catalyzes the phosphorylation of NAD(H) to NADP(H) [100]; *ALD4* and *ALD6*, mitochondrial and cytosolic aldehyde dehydrogenase, respectively, for the conversion of acetaldehyde to acetate; *GOR1*, glyoxylate reductase that reversibly converts glyoxylate to glycolate [101]; *ADH6*, medium-chain alcohol dehydrogenase; *IDP2*, cytosolic isocitrate dehydrogenase that converts isocitrate to alpha-ketoglutarate; *ILV5*, acetohydroxyacid reductoisomerase involved in the branched-chain amino acid synthesis. An overview of the targets of Stb5 in the central carbon metabolism can be seen in **Figure 7**. Taken together, we utilized *STB5* overexpression to simultaneously activate multiple genes involved in NADPH generation instead of overexpressing the targets of Stb5 themselves.

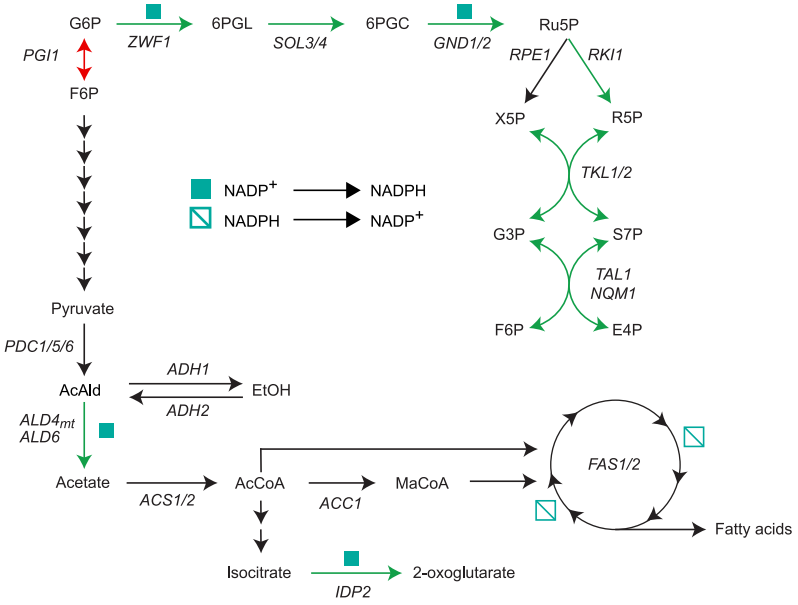

Figure 7. Overview of targets of Stb5 in central carbon metabolism. Green and red arrows indicate genes that are activated or repressed, respectively, by Stb5. Abbreviations: AcAld, acetaldehyde; MaCoA, malonyl-CoA; refer to text for other abbreviations. Figure adapted from **Paper II** [102].

To implement the strategy of *STB5* overexpression, we replaced the native promoter of *STB5* with four different endogenous promoters: the weak *CYC1* promoter (P_{CYC1}) and the stronger promoters of *ADH1*, *TPI1* and *PCK1* (P_{ADH1}, P_{TPI1} and P_{PCK1}) [103, 104]. The promoter replacements were done in the wild-type *S. cerevisiae* CEN.PK 113-5D without phosphoketolase expression during the early characterization. The promoter replacement of *STB5* yielded a reduction of the growth rate compared to control. *STB5* overexpression has previously been able to increase the NADPH concentration by 2.5-fold in *S. cerevisiae* BY4727 [105], but we failed to detect any differences in NADPH concentration compared to the control in our strains. Instead, we evaluated if *STB5* overexpression could supply additional NADPH for oxidative stress tolerance, for example to the glutathione system [106]. We induced oxidative stress in our strain and estimated survival from spot tests on agar plates. We included a strain with deletion of *ZWF1* as a negative control, resulting in a strain where the flux through the oxidative PPP is blocked. In **Figure 8**, we can observe that the control strain shows a small reduction in viability from the H_2O_2 treatment. Blocking the oxidative PPP through *zwf1*Δ results in a low survival at higher concentrations of H_2O_2. Overexpression of *STB5* with a weak promoter (P_{CYC1}-*STB5*) shows a reduction in viability when increasing the H_2O_2 concentration. Utilizing a stronger promoter (P_{TPI1}-*STB5*) reduces the viability even further, with a similar pattern of reduction in viability as *zwf1*Δ when increasing the H_2O_2 concentration. This indicates that *STB5* overexpression fails to redirect the flux to the PPP, which is important for oxidative stress tolerance [107].

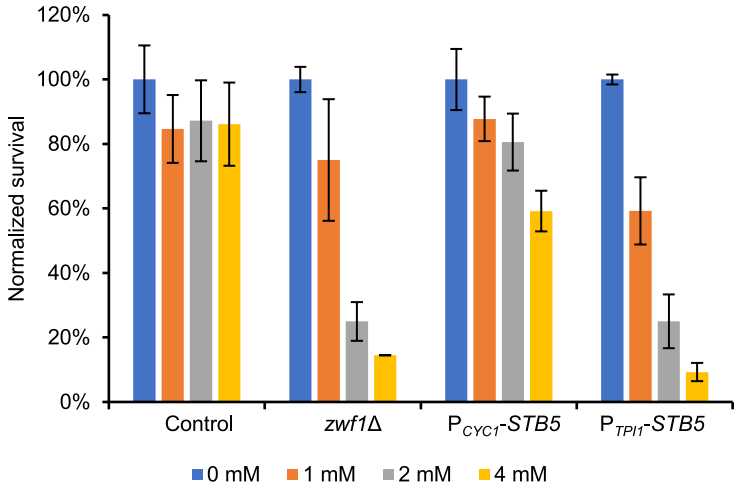

Figure 8. Survival of control *S. cerevisiae* CEN.PK 113-5D, *zwf1*Δ negative control and strains with the native *STB5* promoter exchanged with the *CYC1* or *TPI1* promoter during different degrees of oxidative stress from H_2O_2. The fraction of surviving cells is normalized against the 0 mM H_2O_2 treatment for each strain. The experiment was conducted with two biological and two technical replicates. Average values are shown with the standard deviation as errors bars. Figure adapted from **Paper II** [102].

Even if *STB5* overexpression failed to activate the PPP, we still evaluated if *STB5* overexpression could work as a strategy to increase the titers of FA. To evaluate this, we created an NADPH sink by deleting *FAA1* and *FAA2*, leading to free fatty acid (FFA) accumulation [108]. Introducing different levels of *STB5* overexpression in a *faa1*Δ *faa4*Δ strain resulted in increased levels of FFA, normalized to the biomass concentration, at glucose exhaustion during fermentative growth (**Figure 9A**). However, after 72 h, when all the produced ethanol was

consumed, the normalized titers of FFA were unchanged by the weak promoter replacement (P_{CYC1}-*STB5*) and reduced by strong promoter replacement (P_{ADH1}-*STB5*, P_{TPI1}-*STB5* and P_{PCK1}-*STB5*). We conducted an additional experiment to validate if *STB5* overexpression could activate the PPP in this genetic background by including strains with *ZWF1* deletions. We observed that *ZWF1* deletion did not affect the normalized FFA titers at the end of the glucose phase but reduced the titers at the end of the ethanol phase (**Figure 9B**). Furthermore, introducing P_{TPI1}-*STB5* in a *zwf1*Δ strain showed that *STB5* overexpression could increase the normalized FFA titers independently of the PPP flux at the end of the glucose phase. Respiratory growth on the produced ethanol was not possible for the strain with *zwf1*Δ P_{TPI1}-*STB5*, which is why the normalized FFA titers remain unchanged after 72 h. Taken together, this suggests that *STB5* overexpression positively affects the FFA production during the glucose phase by other means than through activation of the PPP.

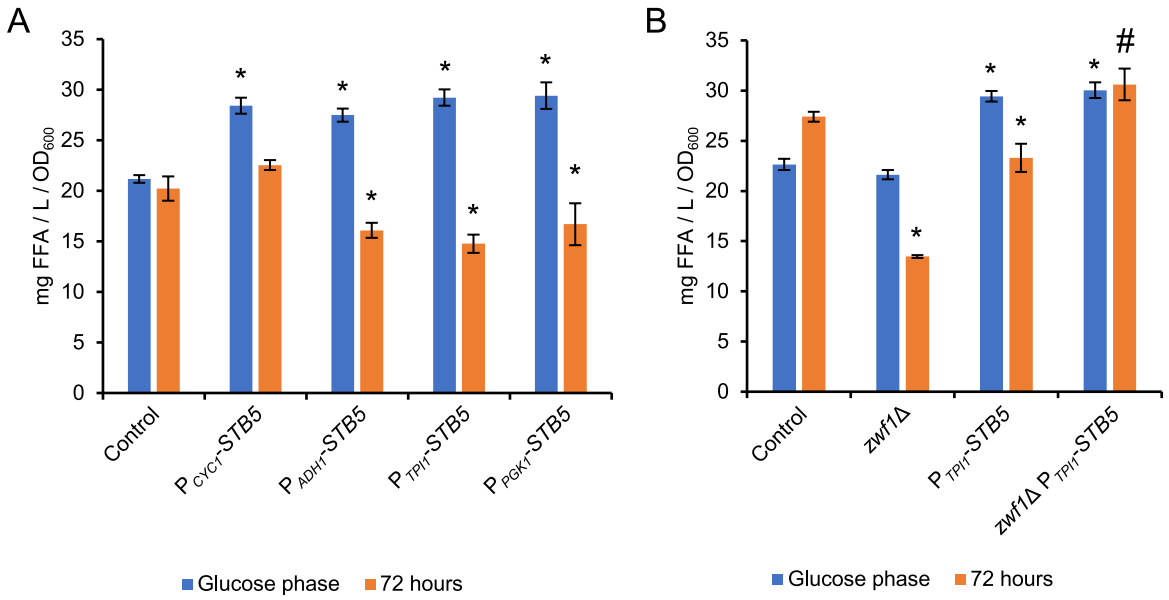

Figure 9. Production of free fatty acids (FFA) normalized to biomass in the *faa1*Δ *faa4*Δ background strain after glucose depletion and at the end of the ethanol phase (72 h). **A)** Effect on FFA production by overexpression of *STB5* with different promoters and **B)** effect on FFA production by *ZWF1* deletion in control and in a strain with *STB5* overexpressed with the *TPI1* promoter (# indicates no growth during the ethanol phase). Strains were cultured with three biological replicates in shake flasks with minimal media supplemented with 2% glucose and 60 mg/L uracil. Average values are shown with the standard deviation as errors bars. Asterisks indicate significant changes calculated with a two-sided Student's t-test with unequal variance (* $p < 0.05$). Figure adapted from **Paper II** [102].

Even though the oxidative PPP was not necessary for FFA production during the glucose phase, we could still see an improvement in normalized FFA titers from *STB5* overexpression. Next, we evaluated the combinatorial strategy of utilizing *STB5* overexpression for increased NADPH supply and the phosphoketolase pathway for increased acetyl-CoA supply to improve the FFA titers. Introduction of the phosphoketolase from *B. breve* and the *pta* from *Clostridium kluyveri* on a high copy plasmid (pAB10) to the *faa1*Δ *faa4*Δ control strain did not improve the normalized FFA titers at the end of the glucose phase (**Figure 10**). To enhance the phosphoketolase pathway and reduce the promiscuous breakdown of AcP to acetate by the glycerol-3-phosphate phosphatases [66, 68], we deleted the *GPP1* gene. Deletion of *GPP1* in the control strain increased the normalized FFA titers by 12%, which was further increased by

25% after the introduction of the phosphoketolase pathway. Implementation of *STB5* overexpression in the *gpp1*Δ control strain increased the normalized FFA titers by 22%. The addition of the phosphoketolase pathway to the *gpp1*Δ P_{TPI1}-*STB5* strain improved FFA production by 37%. In summary, the combinatorial strategy of *STB5* overexpression and the phosphoketolase pathway increased the FFA production by 67% in the *gpp1*Δ control at the end of the glucose phase. This shows a synergistic effect in FFA production when combining both strategies.

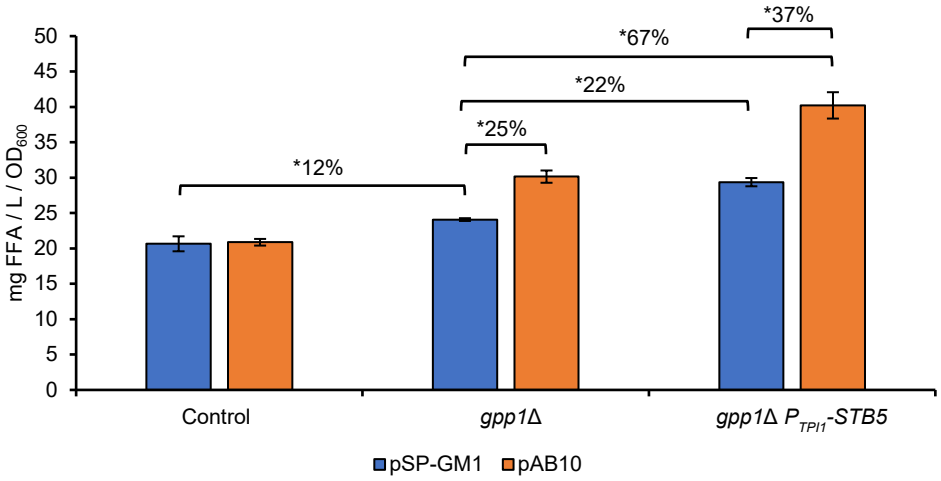

Figure 10. Effect on normalized FFA titers by the implementation of the phosphoketolase pathway for increased acetyl-CoA supply in different host strains. pSP-GM1 is the empty plasmid control, while the plasmid pAB10 contains the *xfpk* from *B. breve* and the *pta* from *C. kluyveri* under the *TEF1* and *PGI1* promoter, respectively. Strains were cultured with three biological replicates in shake flasks with minimal media supplemented with 2% glucose. Average values are shown with the standard deviation as errors bars. Asterisks indicate significant changes calculated with a two-sided Student's t-test with unequal variance (* $p < 0.05$). Figure adapted from **Paper II** [102].

We wanted to investigate the global effect of *STB5* overexpression to gain more understanding as to why we observe downregulation of the PPP pathway, even though Stb5 has previously been reported to activate the PPP. Therefore, we conducted controlled bioreactor cultures in quadruplicates to be able to calculate the physiological parameters and to sample for RNAseq analysis, to gain a deeper understanding of the cellular response to *STB5* overexpression. To simplify the comparison, we used an unmodified strain as control (CEN.PK 113–5D) and overexpressed *STB5* with the *TPI1* promoter. The phosphoketolase pathway was not included in these strains.

We sampled for extracellular metabolites and cell dry weight during the exponential phase on glucose to be able to calculate the physiological parameters. When the culture entered the ethanol phase, the culture condition was turned to a carbon-limited chemostat at a dilution rate of 0.1 h^{-1}. Samples for transcriptomics were taken in the mid-glucose phase, early ethanol phase and during chemostat. *STB5* overexpression in CEN.PK 113–5D during the glucose phase reduced the maximum specific growth rate by 36% and reduced the normalized C-mol flux of ethanol, glycerol, CO_2, and biomass. *STB5* overexpression did not prevent respiratory growth at a dilution rate of 0.1 h^{-1} in the chemostat culture, as no accumulation of fermentation products

was detected. The biomass yield was reduced by 9% in P_{TPI1}-*STB5*, but with no significant change in glucose uptake rate (**Paper II: Table S7**).

Differential expression analysis revealed 665, 347 and 121 differentially expressed genes during the glucose phase, ethanol phase and chemostat, respectively (absolute LFC > 1 and adjusted p-value < 0.01). Overexpression of *STB5* with the glycolytic *TPI1* promoter resulted in a LFC of 4.83, 1.75 and 3.29 during growth on glucose, ethanol and during chemostat, respectively. The strong upregulation of *STB5* in the glucose phase is reflected by the high number of differentially expressed genes, showing that roughly half of the genes in *S. cerevisiae* are changed from *STB5* overexpression during the glucose phase, if filtering only for adjusted p-value below 0.01. The differentially expressed genes involved in the central carbon metabolism are shown in **Figure 11**. During the glucose phase, we can observe that many of the targets activated by Stb5 (green arrows) are downregulated instead of upregulated: *ZWF1* (responsible for the first and rate-limiting step of the oxidative PPP), *SOL3* (the second step in the oxidative PPP), *GND1* (the last step of the oxidative PPP), *RKI1*, *TKL1*, and *TAL1* (involved in the non-oxidative PPP), and *ALD6* (cytosolic acetate production from acetaldehyde). The minor isozymes *SOL4*, *GND2*, *TKL2* and *NQM1* are upregulated, but combining the gene counts of these isozymes show that only *GND* is slightly upregulated. Taken together, the major pathways for cytosolic NADPH supply were downregulated (*ZWF1* and *ALD6*), except for the upregulation of *IDP2* and the combined *GND1+2*. The glyoxylate reductase *GOR1* was one of the few upregulated targets of Stb5, with an LFC of 1.72. *GOR1* uses NADPH when reducing glyoxylate to glycolate, and could potentially be used as a sink for NADPH overconsumption [109]. In addition, there was a small upregulation of *ACC1* and *FAS1*, which could be one of the reasons for the increased FFA titers during the glucose phase (**Figure 9**). The constitutively expressed acetyl-CoA synthetase *ACS2* was downregulated and the glucose repressed isozyme *ACS1* was upregulated. Combining the gene counts of these isozymes gives a LFC of -0.22. The upregulated Acs1 has a lower K_M than Acs2 (0.3 and 9 mM, respectively) [89], but the low TPM of 11 for *ACS1* compared to 288 for *ACS2* suggests that the flux through acetyl-CoA synthetase is still reduced from *STB5* overexpression. Further investigations are needed, however, to evaluate if the cytosolic acetyl-CoA levels are affected by *STB5* overexpression.

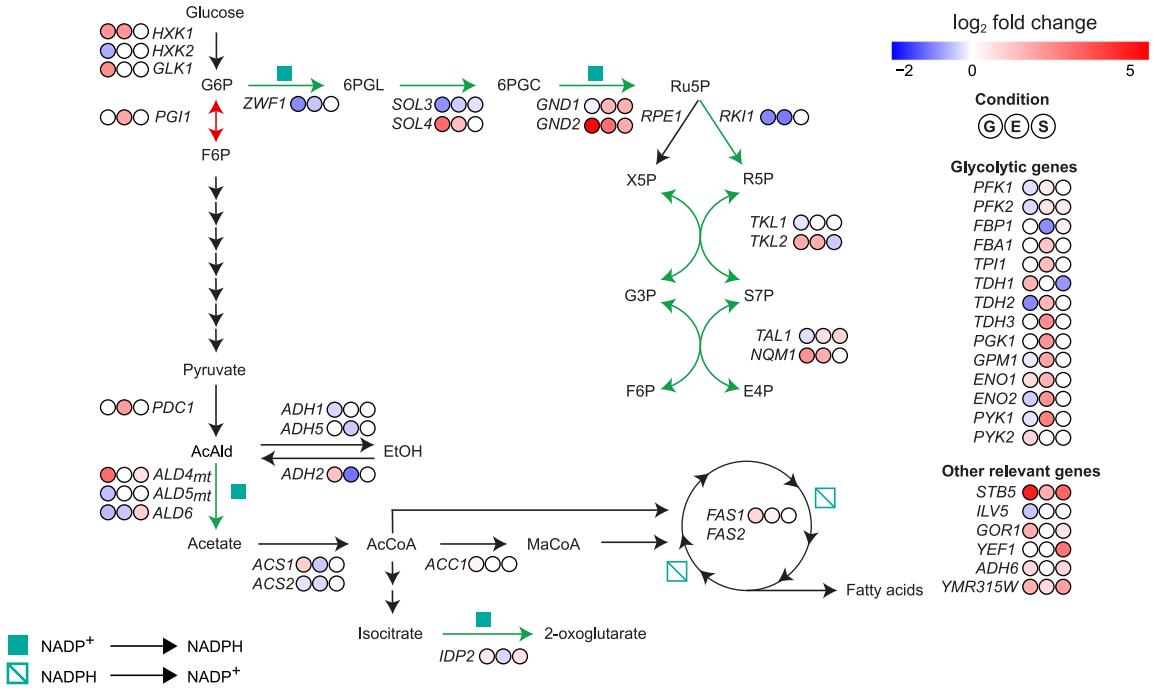

Figure 11. Differentially expressed genes in the central carbon metabolism from *STB5* overexpression during the glucose phase (G), the ethanol phase (E) and steady-state carbon-limited chemostat (S). The $\log_2$-fold change (LFC) values are filtered for adjusted p-value below 0.01 and visualized as intensities of red (up) and blue (down). Figure adapted from **Paper II** [102].

The effect of *STB5* overexpression during the ethanol phase also included downregulation of *ZWF1*, the rate-limiting step of the oxidative PPP (**Figure 11**). Furthermore, *PGI1*, which is documented to be negatively regulated by Stb5, is upregulated. Upregulation of *PGI1* and downregulation of *ZWF1* is the opposite result of what was intended with *STB5* overexpression, possibly limiting the flux through the PPP. Flux through the PPP is important for FFA production during the ethanol phase, as seen with the observation that *ZWF1* deletion reduced the normalized FFA titers during the ethanol phase but not during the glucose phase (**Figure 9B**). A reduced flux through the PPP caused by P_{TPI1}-*STB5* could explain the lower FFA titers during the ethanol phase (**Figure 9A**). The remaining steps of the oxidative PPP are upregulated. The transketolases and transaldolases in the non-oxidative PPP are upregulated, but *RKI1*, generating one of the substrates for the transketolase, is downregulated. There is an upregulation of glycolytic genes and a downregulation of genes involved in the gluconeogenesis, possibly redirecting the flux away from G6P and further reducing the flux through the oxidative PPP.

Overexpression of *STB5* did have a smaller effect during the chemostat culture compared to the glucose phase, with 121 and 665 differentially expressed genes in the chemostat and the glucose phase, respectively. Unlike in the glucose and ethanol phase, *ZWF1* and *RKI1* were not downregulated in the chemostat culture. Apart from the small downregulation of *SOL3* and *TKL2*, the remaining genes involved in the PPP were either upregulated (*GND1/2* and *TAL1*) or unchanged (*ZWF1*, *SOL4*, *RPE1*, *RKI1*, *TKL1* and *NQM1*) (**Figure 11**). *STB5* overexpression in chemostat does not seem to be counteracted as in the glucose or ethanol phase, as we can see upregulation of the activating targets of Stb5 proposed by Larochelle et

al. (2006) (*GND1/2*, *TAL1*, *ALD4*, *ALD6*, *IDP2*, *GOR1*, *YEF1*, *ADH6*), and from Hector et al. (2009) (*YMR315W)*.

We performed GO-term analysis with the R-package Piano to identify enriched GO-terms from *STB5* overexpression. During the glucose phase, we observed enrichment for upregulated genes in the GO terms involving mitochondrial translation, respiration, and TCA cycle (**Figure 12A**). Upregulated genes in these processes could stem from increased energy demand, also reflected in the lower growth rate, reduced biomass yield, and increased O_2 consumption, because of *STB5* overexpression during the glucose phase. Upregulation of genes in the TCA cycle has been observed during reduced growth rates from unfavorable environmental conditions [85]. GO-terms enriched for downregulated genes during the glucose phase involved translation, rRNA processing, ribosomes, and amino acid synthesis (**Figure 12B**). These are processes that are downregulated at lower growth rates [110].

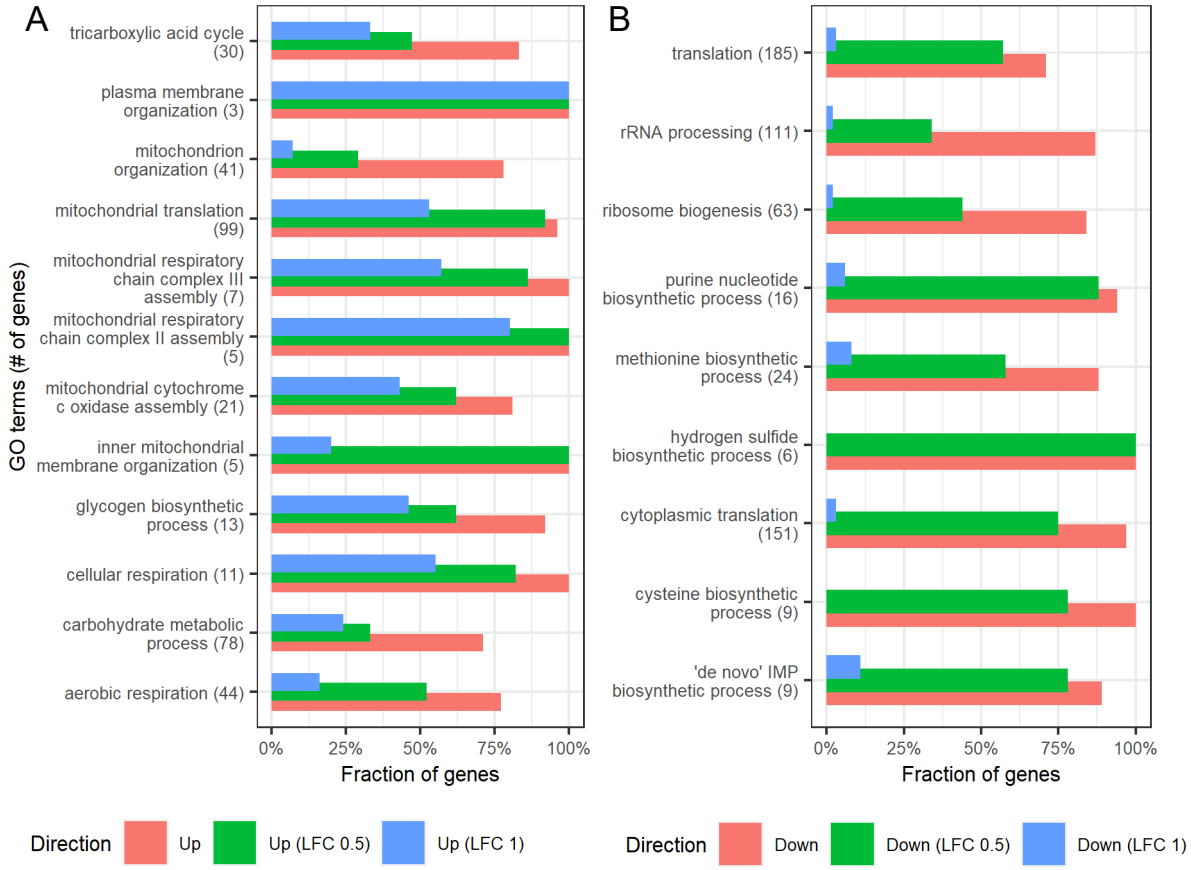

Figure 12. GO-terms involved in biological processes that are enriched for **A)** upregulated or **B)** downregulated genes from *STB5* overexpression during batch growth on glucose at pH 5. Data summarized from the consensus heatmap generated with the Piano R-package by filtering the median adjusted p-value below 0.1 for non-directional enrichment and below 0.05 for the distinct up- or downregulated enrichment. The fraction of up- or downregulated genes is shown without filtering (red) and absolute LFC > 0.5 (green) or absolute LFC > 1 (blue) together with an adjusted p-value below 0.01.

GO term enrichment analysis during the ethanol phase showed enrichment for upregulated genes in the GO terms 'response to heat' and 'protein refolding', both connected to stress responses. GO terms enriched for downregulated genes were 'ATP synthesis coupled proton

transport', mitochondrial translation', and 'cristae formation', indicating reduced respiratory capacity from *STB5* overexpression during the ethanol phase. During the chemostat culture, we could observe enrichment for downregulated genes in GO-terms connected to translation, and enrichment for upregulated genes for the GO-terms 'ATP synthesis coupled proton transport' and 'TCA cycle', indicated increased respiration. These changes in the transcriptome align well with the 9% reduced biomass yield and the non-significant increase of CO_2 production and O_2 consumption for the P_{TPI1}-*STB5* strain during the chemostat.

We conducted a TF reporter analysis to find which TFs are enriched for differentially expressed targets, using the database Yeastract [111] to connect TFs to genes based on both binding and expression evidence. During the glucose and ethanol phase, we could observe enrichment for upregulated genes for the TFs Msn2 and Msn4, involved in activation of stress-response genes [112] (**Figure 13A**). The glucose phase also showed enrichment of upregulated genes for the TF Adr1, required for activation of glucose-repressed genes during growth on non-fermentable carbon sources [113]. *ADR1* is a proposed target of Stb5, but was shown to be negatively regulated by Stb5 [114], but is strongly upregulated by *STB5* overexpression (**Figure 13B**). Interestingly, Stb5 was only enriched for upregulated genes during the chemostat culture, further highlighting that the effects of *STB5* overexpression were counteracted during the glucose and ethanol phase. The extent of the LFC of the targets of the TFs Adr1, Msn2, Msn4 and Stb5 is shown in **Figure 13C**.

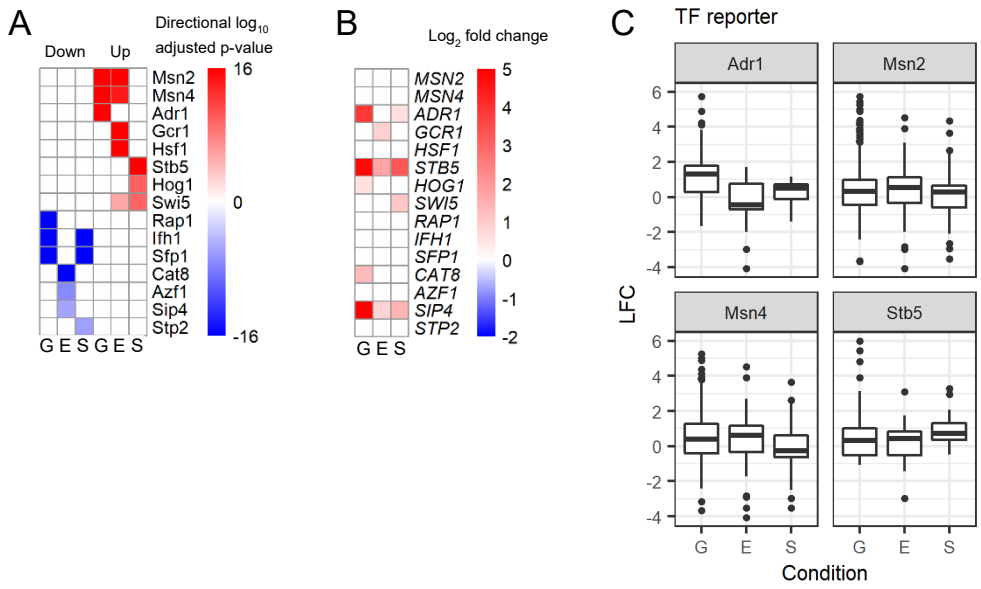

Figure 13. Transcription factor (TF) reporter analysis of *STB5* overexpression compared to control. The enrichments are shown from the glucose phase (G), ethanol phase (E) and steady-state carbon-limited chemostat (S). **A)** The top three enriched TFs, whose targets are either down- or upregulated in each sampling condition (adjusted p-value below 10^{-5}). **B)** Differential expression analysis of the top three TFs (absolute $\log_2$-fold change >0.5 and adjusted p-value <0.01). **C)** Boxplot showing the $\log_2$-fold changes (LFC) of the target genes of the TFs Adr1, Msn2, Msn4 and Stb5 from *STB5* overexpression in each sampling point.

Taken together, *STB5* overexpression can increase the specific FFA titers during the glucose phase, but independently of the PPP. Transcriptome analysis revealed that many of the genes reported to be activated by Stb5 are instead downregulated during the glucose and ethanol phase. This effect was not seen during the carbon-limited chemostat. *STB5* overexpression might lead to NADPH overproduction during the glucose and ethanol phase, which is counteracted by the cell. NADPH overproduction might be less harmful during chemostat growth, as more biomass is produced compared to the glucose phase (56.9 and 16.2% relative C-mol, respectively), creating an effective NADPH sink. This suggests that the strategy of *STB5* overexpression for improved NADPH supply should be applied in a strain already equipped with a strong flux towards product formation requiring a lot of NADPH. A recent example of *STB5* overexpression as a strategy for increased NADPH supply was in combination with the NAD^+ kinase EcyjfB from *Escherichia coli* to improve the production of isoflavonoids in *S. cerevisiae* [115].

4 Part II: Carbon-conservation with the cyclic phosphoketolase pathway

The phosphoketolase pathway (Xfpk + Pta) can generate one acetyl-CoA from one F6P or X5P without carbon loss as CO_2, but is it possible to recycle the other phosphoketolase products (E4P or GAP) to acetyl-CoA as well? In bifidobacterial, there exists a bifid shunt that uses the Xfpk together with the PPP to generate 1.5 mol acetate (converted from AcP with acetate kinase) and 1 mol lactate from 1 mol F6P, while generating 2.5 mol ATP/glucose [67]. Theoretically, it should be possible to further increase the yield of 1.5 mol AcP/glucose to 3 mol AcP/glucose by combining the Xfpk with carbon rearrangement reactions and recycle all the carbon from F6P into AcP [116, 117]. Schramm and Racker postulated the "F6P shunt" (**Figure 14)** in 1957 [116]. Xfpk converts F6P to E4P, which can be combined with another F6P into GAP and S7P by the transaldolase. GAP and S7P can further be converted to X5P and R5P by the transketolase. R5P can be converted into GAP again by Rpi, Rpe and Xfpk. The X5P formed by the transketolase can be converted into DHAP by Xfpk and Tpi1. This leaves us GAP and DHAP, which can be converted into FBP by Fba. Finally, the cycle is closed by conversion of FBP to F6P again by fructose-1,6-bisphosphatase (Fbp) from the gluconeogenesis. In summary, three AcP are released from the cycle from one F6P without carbon spent as CO_2.

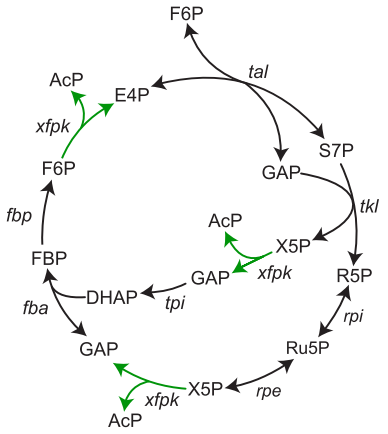

Figure 14. The F6P shunt, nowadays referred to as the non-oxidative glycolysis (NOG) pathway. Phosphoketolase reactions are marked with green arrows. Abbreviations: rpe, ribulose-5-phosphate 3-epimerase; rpi, ribose-5-phosphate isomerase; refer to text for other abbreviations. Figure adapted from **Paper III** [118].

The formed AcP from the F6P shunt can either be converted to acetyl-CoA by Pta without generating energy or to acetate by acetate kinase while generating 1 ATP/acetate. The cost of 2 ATP to activate acetate to acetyl-CoA makes coupling the F6P shunt with the Pta enzyme for acetyl-CoA production more beneficial in terms of energy cost. Coupling the F6P shunt with the Pta enzyme allows the synthesis of 3 mol acetyl-CoA from 1 mol of glucose, with the net cost of 1 ATP (**Table 2**). Usage of the F6P shunt + Pta instead of the native PDH bypass avoids the ATP cost in activating acetate to acetyl-CoA and lowers the total ATP cost per acetyl-CoA formed from 1 to 1/3 ATP.

Table 2. Stoichiometric comparison in acetyl-CoA formation from glucose with the native PDH bypass and the F6P shunt, nowadays referred to as the non-oxidative glycolysis (NOG) pathway, together with Pta.

Pathway	Stoichiometry
Native PDH bypass	glucose + 4 $NAD(P)^+$ + 2 ATP + 2 CoA + 2 H_2O → 2 acetyl-CoA + 4 $(NAD(P)H + H^+)$ + 2 CO_2 + 2 $(ADP + P_i)$
F6P shunt (NOG) + Pta	glucose + ATP + 3 CoA → 3 acetyl-CoA + ADP + P_i + 2 H_2O

4.1 Non-oxidative glycolysis (NOG)

In 2013, Bogorad et al. demonstrated the functionality of the F6P shunt *in vitro* with purified enzymes, where the Xfpk from *Bifidobacterium adolescentis* converted 10 mM F6P to 30 mM AcP [119]. Bogorad et al. (2013) renamed the F6P shunt to the non-oxidative glycolysis (NOG) pathway and could also demonstrate a yield of 2.2 mol acetate per mol xylose *in vivo* (approaching the theoretical yield of 2.5 mol/mol). They used an *E. coli* strain that expressed *xfpk* from *B. adolescentis*, overexpressed the native Fbp and contained disrupted pathways to succinate, lactate, formate and ethanol, while also culturing it anaerobically to reduce the amount of carbon converted to biomass. Acetate formation from xylose through the glycolysis alone would yield 1.67 mol/mol.

A limitation of the NOG pathway is that it does not generate any reducing power or energy needed to support growth by itself. This limits the use of the NOG pathway to achieve full carbon-conservation. Lin et al. (2018) from the same group wanted to create a system where the NOG can be used for growth on glucose aerobically, but with inhibition of growth and full carbon-conservation during anaerobic cultivation [120]. They needed to disrupt the native glycolysis to remove competing pathways while still being able to provide essential C_3 precursor metabolites (PEP, pyruvate and 3PG) from the NOG. After extensive genetic engineering and adaptive laboratory evolution, they managed to create a strain (NOG21) that could grow aerobically on glucose by using the NOG. Anaerobically, the strain could convert 83% of the glucose to acetate without any growth (glycolysis alone can theoretically convert 67% of the glucose to acetate).

The NOG pathway has been utilized for acetyl-CoA supply in *E. coli* to increase the product yield of acetone [121]. Acetone is produced commercially with help of *Clostridium acetobutylicum* [122] and can be formed from acetyl-CoA: two acetyl-CoA can be combined by thiolase to one acetoacetyl-CoA, which can be converted to acetoacetate by coenzyme A transferase, before converted to acetone by acetoacetate decarboxylase (Adc). Adding this pathway to *E. coli* allows a maximum theoretical yield of acetone of 1 mol acetone/mol glucose if utilizing glycolysis and pyruvate dehydrogenase to produce acetyl-CoA. The loss of two carbons as CO_2 during acetyl-CoA formation and one by Adc gives a carbon molar yield of 0.5 C-mol acetone/C-mol glucose. As acetone formation does not require any cofactors, utilizing the NOG for acetyl-CoA supply can increase the maximum theoretical yield from 1 to 1.5 mol/mol [121]. Accounting for the ATP cost of the NOG (**Table 2**) gives a maximum theoretical yield of 1.487 mol acetone/mol glucose [123]. Yang et al. (2016) implemented the NOG in an acetone-producing *E. coli* strain by expressing the *xfpk* from *B. adolescentis* and

overexpressing the endogenous *fbp*, and could demonstrate an increased yield from 0.38 to 0.47 mol acetone/mol glucose [121]. They could possibly have gained an even bigger improvement by utilizing the FBPase GlpX that is not inhibited by AMP instead of using Fbp [120, 124]. Overexpressing FBPase without reducing *pfk* expression might result in a futile cycle that consumes ATP. Furthermore, additional genomic modifications might be required to reach the maximum theoretical yield of 1.487 mol acetone/mol glucose. These modifications could include knocking out genes from the glycolysis and overexpressing transketolase and transaldolase to force flux through the NOG.

4.2 Combining the NOG with other pathways

Acetone and acetate production with the NOG pathway alone is beneficial, as they do not require NAD(P)H or ATP. For other products that require energy or reducing power, the NOG needs to be combined with other pathways. By combining the NOG pathway with the oxidative PPP (**Figure 15**), Wang et al. (2019) created the pathway EP-bifido, which sacrifices some of the high yield of the NOG for NADPH formation (from 3 acetyl-CoA/glucose to 2.5 acetyl-CoA and 2 NADPH/glucose) [125]. To enable EP-bifido in *E. coli*, they expressed the *xfpk* from *B. adolescentis* and overexpressed the native *fbp*. Furthermore, to ensure flux through EP-bifido, they downregulated the flux to glycolysis by deleting *pfkA* and deleted 6-phosphogluconate dehydratase (*edd*) to remove the breakdown of 6PGC to GAP and pyruvate. Finally, they deleted the acetate kinase (*ackA*), which would otherwise convert the excess AcP from EP-bifido to acetate. Flux through the EP-bifido was demonstrated with a ^{13}C labeling experiment. In addition, Wang et al. (2019) used mevalonate as a proof-of-concept product, which requires 3 acetyl-CoA and 2 NADPH per mol mevalonate formed and demonstrated that EP-bifido could increase the product yield from 0.434 to 0.643 mol mevalonate/mol glucose [125]. Finetuning the flux between EMP and the PPP (1:6) in the EP-bifido can theoretically achieve a product yield of 0.86 mol mevalonate/mol glucose [125]. In a later paper, the same group improved the mevalonate yield from 0.643 to 0.687 mol/mol by optimizing the flux ratio between NOG and the PPP through promoter replacement of *zwf* and downregulation of *pfkA* through CRISPR-interference [126].

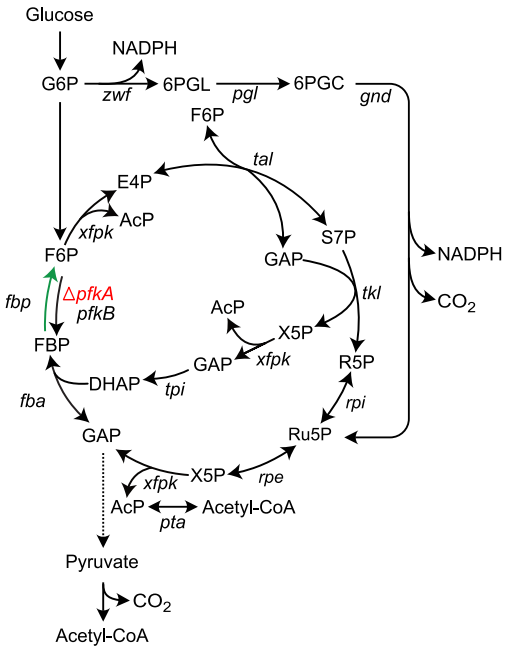

Figure 15. The EP-bifido [125] pathway for carbon-conservation and NADPH generation. Reactions with overexpressed genes are shown with green arrows. Gene deletions are marked in red.

In a recent paper, Wang et al. (2021) modeled different distributions of fluxes between the PPP, the glycolysis and the NOG to finetune the acetyl-CoA yield and the ratio of NAD(P)H gained per acetyl-CoA (N/A ratio) [127]. Only using the PPP, glycolysis or NOG alone would yield a N/A ratio of 3.19, 2 and 0, respectively, and an acetyl-CoA yield of 55.7, 66.7 and 100%, respectively [127]. The authors aimed to match the N/A ratio of product formation with the N/A ratio of the precursor supply pathways to increase the maximum theoretical yield. For example, biosynthesis of 3-hydroxybutyrate (3HB) needs three enzymatic steps from acetyl-CoA and requires two acetyl-CoA and one NADH in total to produce 1 mol of 3HB, resulting in a N/A ratio of 0.5. Distributing the fluxes equally between NOG and glycolysis would yield a N/A ratio of 0.8. They could show computationally that distributing 33% of the flux from glucose through glycolysis and 67% through NOG would increase the maximum theoretical yield of 3HB from 1 to 1.33 mol/mol. Through deletion of *edd* and *pfkB* in *E. coli* and finetuning of the expression of the NOG genes *tklA*, *glpX* and *xfpk* from *Lactococcus lactis*, they increased the 3HB yield from 0.61 mol/mol with the native metabolism to 1.02 mol/mol by coordinating the native metabolism with the NOG in shake flask cultures. Using fed-batch fermentation, they could increase the yield of 3HB to 1.13 mol/mol, which is 13% higher than the maximum theoretical yield of the native metabolism.

A hybrid EMP-NOG was also established in *Corynebacterium glutamicum* by overexpressing the native *tal* and *glk,* deleting *pfkA* and expressing *xfpk* from *B. adolescentis* [128]. After balancing the phosphate supply, the authors could demonstrate a 19% increase in acetyl-CoA levels and a 10% reduction in CO_2 production. However, they did not overexpress the native *glpX*, which might be needed to fully utilize the NOG during growth on glucose. A summary of how the utilization of the NOG in combination with other pathways can increase the theoretical maximum yields for several different products is shown in **Table 3**.

Table 3. Estimated theoretical maximum yield (TMY) for different products, using different strategies for acetyl-CoA supply. The flux distribution for the strategies that combine the NOG with other pathways is shown within parenthesis.

Product	Strategy	TMY (mol/mol)	Reference
Mevalonate	EMP	0.66	[125]
	EP-bifido: EMP+PPP (1:6)	0.86	
Poly-3-hydroxybutyrate	EMP	1.0	[129]
	Threonine bypass	1.26	
	NOG+PDH (2:1)	1.285	[123]
3-Hydroxybutyrate	EMP	1.0	[127]
	NOG+EMP (2:1)	1.33	
Acetone	EMP	1.0	[121]
	NOG+PDH (38:1)	1.487	[123]
Farnesene	EMP	0.205	[22]
	NOG+PDH (0.44:0.56)	0.261	
	NOG+PDH (1.8:2.24)	0.271	[123]
Palmitic acid	EMP	0.203	[22]
	NOG+PDH (13:7)	0.232	
Citric acid	EMP	1.0	[22]
	NOG	1.2	
L-Glutamate	EMP	1.0	[123]
	NOG+EMP (4:6)	1.2	

4.3 A second NOG configuration

The NOG contains three reactions that require two substrates: the transketolase (S7P+GAP), the transaldolase (E4P+F6P) and the fructose 1,6-bisphosphate aldolase (DHAP+GAP). An imbalance in the availability of one of these substrates might result in a reduction of the reaction rate of the NOG. Andersen et al. (2019, initially published in 2017) explored different configurations of the NOG computationally to optimize it and reduce the number of reactions [130]. In their model, a novel phosphoketolase reaction (Spk) was added:

$S7P+P_i \rightarrow R5P + AcP + H_2O$ (Spk)

The Spk reaction has an estimated $\Delta_rG'^m = -55.2$ kJ/mol [65] and there are indications that this reaction also can occur *in vitro* [131]. By utilizing a trifunctional phosphoketolase that could react on X5P, F6P and S7P (Xfspk) in the model, they could eliminate the transketolase reaction and generate a second configuration of the NOG (**Figure 16**).

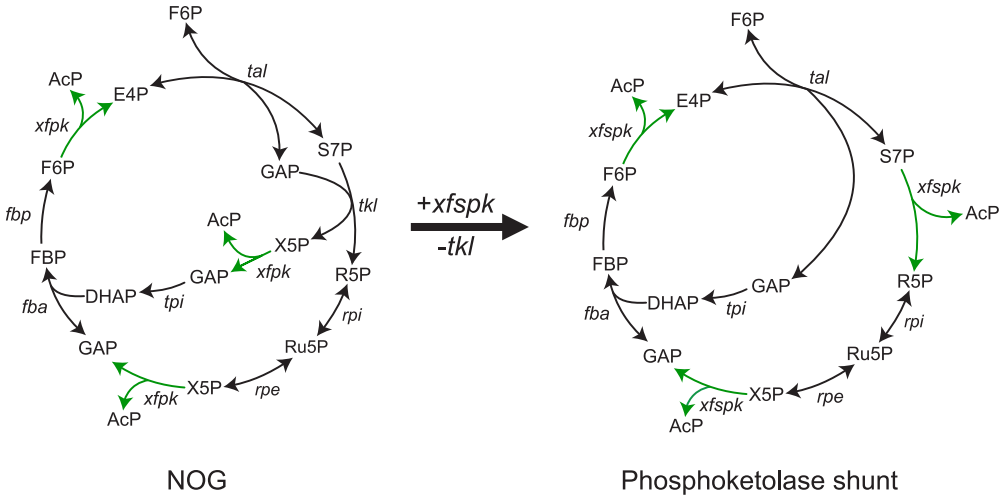

Figure 16. Enabling a second configuration of the NOG, the phosphoketolase shunt. Phosphoketolase reactions are shown with green arrows. Figure adapted from **Paper III** [118].

Krüsemann et al. (2018) overexpressed the phosphoketolase from *B. adolescentis* that was suspected to have Xpk, Fpk and Spk activity. They could through different gene deletions isolate the Xpk, Fpk, and Spk activities and show that the second NOG configuration, now referred to as the phosphoketolase shunt, could support growth [132]. Firstly, they showed that the deletion of ribose-5-phosphate isomerase (Δ*rpiAB*) needed the Xpk reaction to supply GAP during growth on xylose. Secondly, in a transketolase deletion strain (Δ*tktAB*), growth on glucose was rescued by the Fpk activity to provide E4P needed for aromatic amino acid synthesis [133]. Combining Δ*tktAB* Δ*rpiAB* created a strain background where only the Spk activity could provide R5P, needed for nucleotide and histidine synthesis, which was also rescued by phosphoketolase expression. Finally, they demonstrated flux through the phosphoketolase shunt in a strain where the glucose-6-phosphate dehydrogenase (*zwf*) and transketolases were deleted (no native pathways to E4P or R5P), both in a growth experiment and in a ^{13}C-labelling experiment by measuring the labeling patterns of histidine.

4.4 Implementing a third NOG configuration (Paper III)

Andersen et al. (2019) proposed a third configuration of the NOG by removing the transaldolase reaction and replacing the Fba and Fbp reaction with the sedoheptulose-1,7-bisphosphate aldolase (Sba) and the sedoheptulose-1,7-bisphosphatase (Sbp) (**Figure 17A**). Sba can combine the E4P created by the phosphoketolase with DHAP to form sedoheptulose-1,7-bisphosphate (SBP). SBP can then be dephosphorylated by Sbp to generate S7P, which is the substrate for the phosphoketolase, allowing a third NOG configuration: **G**lycolysis **A**l**T**ernative **H**igh **C**arbon **Y**ield **C**ycle (GATHCYC). The Sba and Sbp reactions are part of the Calvin-cycle that fixates carbon from CO_2 into C_3 metabolites in photosynthetic organisms [134]. The Sba and Sbp reactions also occur in non-photosynthetic microorganisms such as *E. coli* [135, 136], *Bacillus methanolicus* [137] and *C. glutamicum* [138], with the Sba reaction catalyzed by Fba and the Sbp reaction by GlpX. In *S. cerevisiae*, the Sba and Sbp reaction can be catalyzed by Fba1 and Shb17, respectively, which are important steps in the riboneogenesis pathway that can produce R5P without NADPH generation when NADPH requirements are low [139]. In **Paper III**, we simulated all three NOG configurations in the COPASI software

[140], where we identified a possible bottleneck in the first NOG configuration that lead to accumulation of S7P (**Figure 17B)** [118]. After conducting a sensitivity analysis of the parameters of the first NOG configuration (**Paper III: Table S1**), we obtained a strong correlation of the S7P concentration with the equilibrium constants of Tpi and Fba, which could indicate that the concentration of GAP is limited. The transketolase reaction needs both S7P and GAP simultaneously to generate X5P and R5P and limitations of GAP in the NOG could create a bottleneck, resulting in S7P accumulation. Simulation of the phosphoketolase shunt and the GATHCYC (both without the transketolase reaction) did not result in accumulation of S7P (**Figure 17B).**

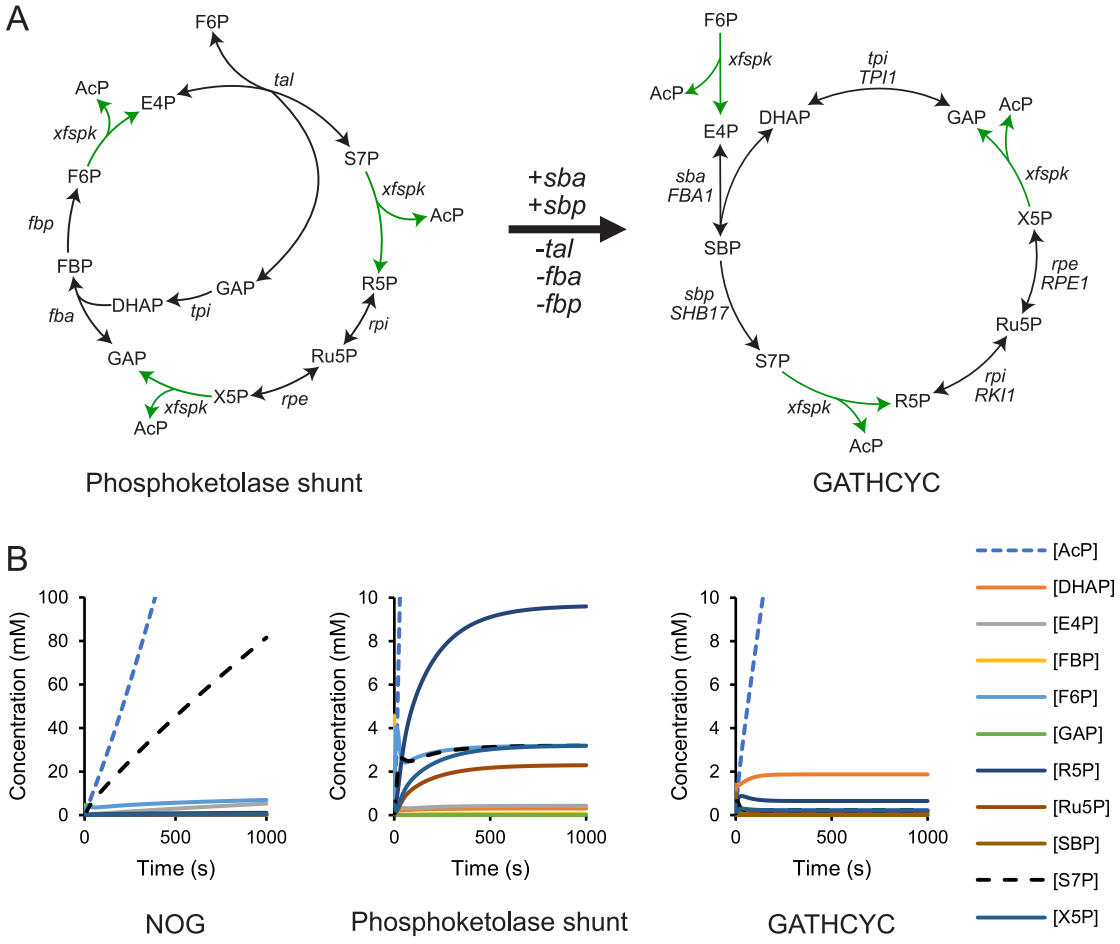

Figure 17. Introduction of the third NOG configuration. **A)** Adding the Sba and Sbp reaction to the model removes the need for the Tal, Fba and Fbp reaction and enables the **G**lycolysis **A**l**T**ernative **H**igh **C**arbon **Y**ield **C**ycle (GATHCYC). Native genes from *S. cerevisiae* are shown in the GATHCYC. **B**) Kinetic time course simulations in COPASI of the NOG, phosphoketolase shunt and the GATHCYC. Figure adapted from **Paper III** [118].

To establish the GATHCYC in *S. cerevisiae*, we first eliminated competing reactions by deleting the transketolases (*tkl1*Δ *tkl2*Δ) and the transaldolases (*tal1*Δ *nqm1*Δ). Furthermore, we promoted flux through the GATHCYC by overexpressing of the native SBPase *SHB17* [139] by exchanging the native promoter to the strong *TDH3* promoter. To preserve S7P for the Spk reaction, we deleted the *PHO13* phosphatase because it can produce the dead-end metabolite sedoheptulose from S7P [141]. Finally, we expressed the Xfspk from *Bifidobacterium longum*, an Xfpk phosphoketolase [142] that had reported S7P activity in

patent literature [131], from the high-copy plasmid pBS01A [143]. We demonstrated *in vitro* activity of the GATHCYC through a whole-pathway assay, using crude cell-free extracts prepared from *S. cerevisiae* strains with the genotype for the GATHCYC and measuring AcP formation from F6P in a colorimetric phosphoketolase assay with the ferric acetyl hydroxamate method [66, 144]. We included a "pathway negative" strain by disrupting the GATHCYC through *SHB17* deletion (**Figure 18A**). If the pathway is functional *in vitro*, the disruption of *SHB17* should result in three times less AcP compared to the "pathway positive" strain with *SHB17* overexpressed. These two strains were evaluated in the phosphoketolase assay, which also contained the inhibitor iodoacetate to block the activity of glyceraldehyde-3-phosphate dehydrogenase in the lower glycolysis [145]. The pathway negative strain produced 2.7 times less AcP than the pathway positive strain (**Figure 18B**), which aligns very well with the expected difference between the strains, suggesting that the pathway is functional *in vitro*.

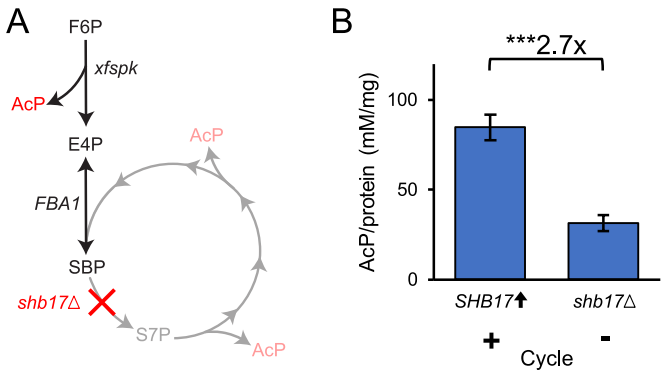

Figure 18. *In vitro* evaluation of AcP production on crude cell-free extracts from *S. cerevisiae* containing the genotype for the GATHCYC. **A)** Deleting *SHB17* stops utilization of the full cycle (faded) and should result in three times less AcP from F6P compared to *SHB17* overexpression. **B)** *In vitro* AcP formation from GATHCYC strains with *SHB17* overexpression or *SHB17* deletion. Statistical significance was evaluated with a two-sided Student's t-test with unequal variance (***$p < 0.001$). Figure adapted from **Paper III** [118].

Activity *in vitro* does not necessarily mean activity *in vivo*. Inspired by the growth experiments by Krüsemann et al. (2018) to prove that the phosphoketolase shunt could restore growth in Δ*tktAB* Δ*zwf* [132], we added the *ZWF1* deletion to the GATHCYC strain. As in *E. coli*, deletion of the transketolases and G6P dehydrogenase in *S. cerevisiae* is lethal because of the lack of additional pathways to E4P and R5P, precursors for AAA and nucleotides, respectively [146]. E4P deficiency is rescued by the Fpk activity from the phosphoketolase but the R5P needs to be generated from a functional GATHCYC (**Figure 19A**). Before we deleted *ZWF1*, we further engineered the GATHCYC strain by integrating the phosphoketolase into the genome instead of expressing it from a plasmid. One copy of *xfspk* under the *TEF1* promoter in the genome was not sufficient to allow efficient growth in minimal media, as that strain (JH18) displayed a lag time of 20 h and a maximum specific growth rate of 0.13 h^{-1} (**Paper III: Figure S5**). To improve growth, we added a second copy of the *xfspk* under the control of the enhanced *TDH3* promoter (e*TDH3*) [147] and introduced the *pta* under the e*TEF1* promoter to allow acetyl-CoA formation from AcP. Finally, we created the strain JH25 by deleting *GPP1* to reduce the promiscuous hydrolysis of AcP to acetate by the glycerol-3-phosphate phosphatases [66, 68]. Compared to the parental strain JH18, the new strain JH25 showed an increased μ_{max} from 0.13 to 0.20 h^{-1} and a reduced lag time from 20 to 4.8 h. The improvement

in strain performance is likely connected to the increased supply of E4P from the second copy of the phosphoketolase, needed to rescue the deficiency of AAA from the *tkl1*Δ *tkl2*Δ genotype [146]. In JH25, we could delete *ZWF1* and generated a strain (JH40), which could utilize the GATHCYC alone to supply R5P, albeit at a reduced growth rate from 0.20 to 0.10 h^{-1} and an increased lag time from 4.8 to 6.7 h, without affecting the final biomass yield (strain JH25 and JH40, **Figure 19B)**. Since we could not delete *ZWF1* in *shb17*Δ (or *SHB17* in *zwf1*Δ), we downregulated *ZWF1* by placing it under the *GAL1* promoter, which is highly active at galactose conditions but strongly repressed on glucose conditions [148]. With a disrupted GATHCYC through *shb17*Δ (strain JH46), the only pathway to R5P is through Zwf1 and the oxidative PPP. A strain with downregulated *ZWF1* in the *shb17*Δ background (JH45) is expected to grow on galactose but not on glucose, serving as a negative control in this experiment. While deletion of *ZWF1* in the cycle strain reduced the strain performance (JH40), downregulation of *ZWF1* in the cycle strain (JH44) had a minimal effect on growth, indicating leaking expression from the *GAL1* promoter during growth on glucose. Promoter replacement of *ZWF1* in JH46 (*shb17*Δ, disrupted cycle) reduced the growth rate on glucose, indicating a lower supply of R5P in this strain background. The reasons for growth on glucose in JH45 could be from a leaky expression of *ZWF1* under the *GAL1* promoter, which can supply R5P through the oxidative PPP. Taken together, the functionality of the GATHCYC was demonstrated *in vitro* and the GATHCYC can support growth in a *zwf1*Δ *tkl1*Δ *tkl2*Δ strain, which otherwise would not grow [146].

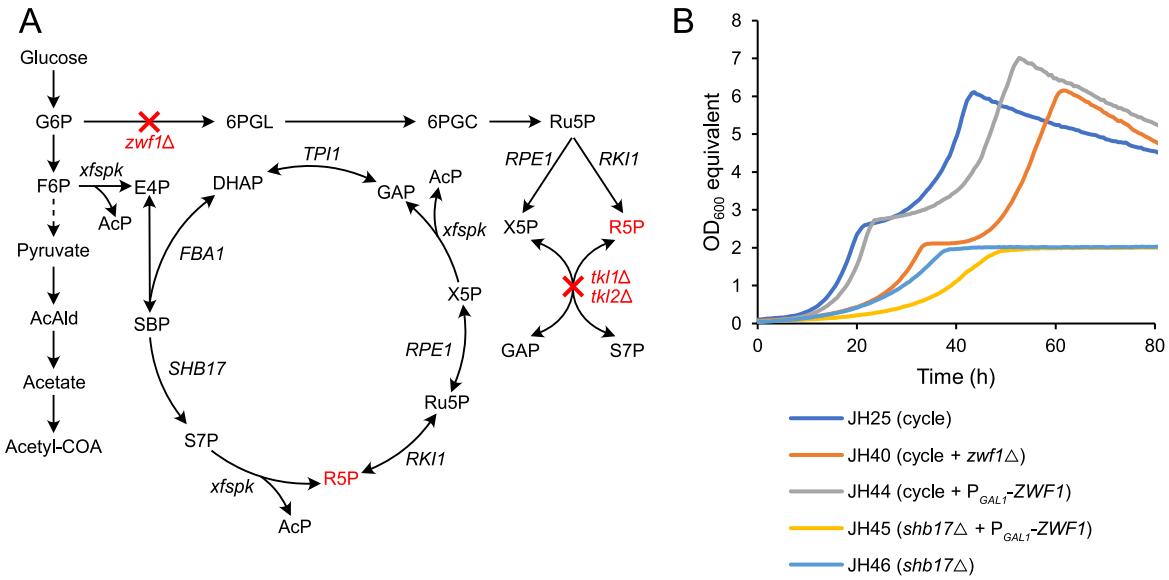

Figure 19. Demonstration of *in vivo* activity of the GATHCYC. **A)** Deletion of *ZWF1* and the *TKL1/2* requires a functional GATHCYC to provide R5P (marked in red) to allow growth on glucose. **B)** Growth in microtiter plates for the GATHCYC strain (JH25), GATHCYC strain with deleted *ZWF1* (JH40), GATHCYC strain with downregulated *ZWF1* on glucose (JH44), a strain with disrupted GATHCYC through *SHB17* deletion, and a strain with disrupted GATHCYC and downregulation of *ZWF1* on glucose. Strains were grown in microtiters plates with minimal media supplemented with 2% glucose and 100 mg/L uracil, with three biological and technical replicates. The strain JH45 was precultured in rich media with galactose before washed and resuspended in the growth media. Figure adapted from **Paper III** [118].

We have now demonstrated flux through the GATHCYC both *in vitro* (**Figure 18)** and *in vivo* (**Figure 19**), but does it also improve product yields of acetyl-CoA-derived products? The introduction of the linear phosphoketolase pathway (without additional modifications to promote any of the NOG configurations) has been shown to increase the production of acetyl-CoA-derived products, for example, farnesene [68] and fatty acid ethyl esters [69] in *S. cerevisiae*. We wanted to evaluate the benefit of expanding the linear phosphoketolase pathway (**Figure 20A)** to a circular one (**Figure 20B)**. Therefore, the GATHCYC strains were compared to a phosphoketolase control lacking the modifications to enable the GATHCYC (*tkl1*Δ *tkl2*Δ *tal1*Δ *nqm1*Δ *pho13*Δ and overexpression of *SHB17*). Similar to the NOG, the GATHCYC can recycle all carbon from 1 mol F6P to 3 mol AcP, but does not produce any NAD(P)H. This makes it suitable for acetate production, as acetate formation requires no cofactors and generates 2 ATP/glucose when the NOG is coupled to acetate kinase. Products that require NAD(P)H or ATP cannot be produced by the NOG alone. Therefore, we did not force all flux from glucose through the GATHCYC by deleting *ZWF1*, *PFK1*/*2*, *TDH1*/*2*/*3* and *PGK1*, but instead allowed a combinatorial configuration of the GATHCYC, glycolysis and the PPP. Depending on the product, different distributions of fluxes between a carbon-conserving pathway and additional pathways to acetyl-CoA might be needed to balance carbon-conservation with cofactor demand for optimal product yield [22, 123, 127].

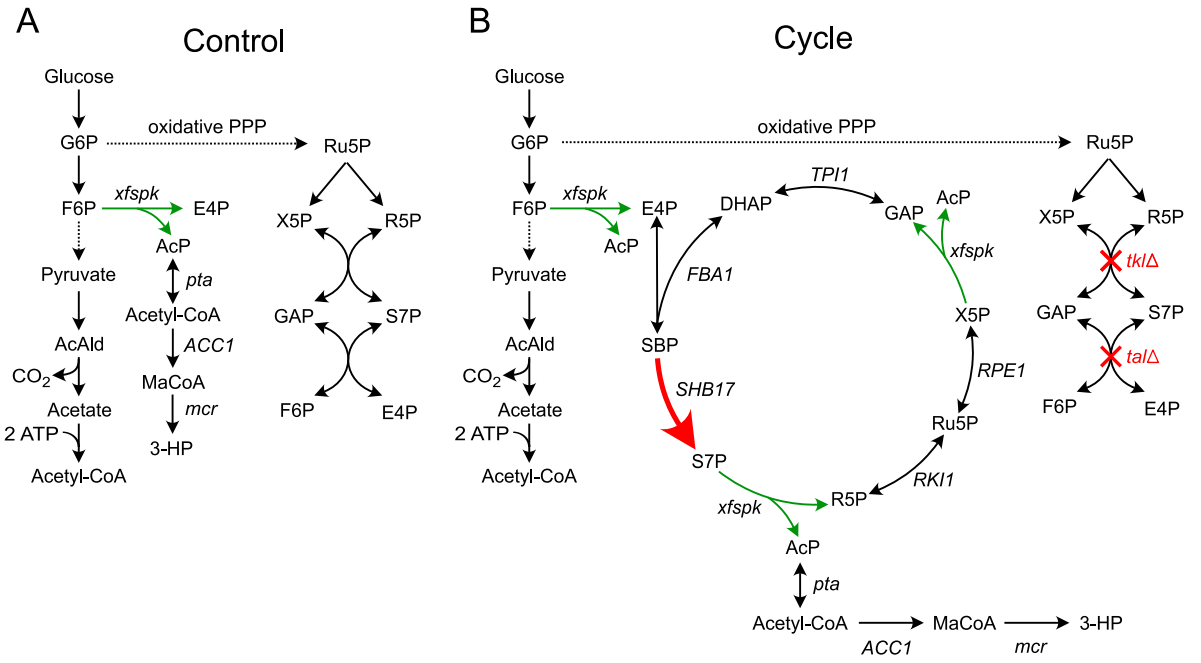

Figure 20. Overview of central carbon metabolism in *S. cerevisiae* strains using **A)** the linear phosphoketolase pathway (control) or **B)** the GATHCYC for additional cytosolic acetyl-CoA supply. Phosphoketolase reactions on metabolites from the PPP are not shown. Green arrows depict phosphoketolase reactions and red arrows show overexpressed genes. Gene deletions are shown with a red cross. Both control and cycle strain have 2 copies of $xfspk_{BL}$, 1 copy of pta_{CK}, *gpp1*Δ and overexpression of $ACC1^{S659A,S1157A}$ (*ACC1***).

We chose 3-hydroxypropionic acid (3-HP) as a proof-of-concept product to evaluate the benefit of the GATHCYC for additional precursor supply. 3-HP is a precursor for acrylic acid and biodegradable plastics [149] and microbial production of 3-HP can be achieved in pathways from β-alanine, glycerol and malonyl-CoA [150]. 3-HP can be formed from acetyl-CoA in two

steps, using the malonyl-CoA pathway. Acetyl-CoA is converted to malonyl-CoA by acetyl-CoA carboxylase (Acc1 in *S. cerevisiae*), which can be further converted to 3-HP in a two-step NADPH-dependent reaction by the malonyl-CoA reductase from *Chloroflexus aurantiacus* (mcr_{CA}) [151]. Increased supply of acetyl-CoA has previously been shown to increase the titers of 3-HP [152], which is why we chose to evaluate the performance of the GATHCYC by measuring the production of 3-HP. Both the phosphoketolase control and the GATHCYC strains were further engineered by integrating $ACC1^{S659A,S1157A}$ (*ACC1***) to avoid bottlenecks in acetyl-CoA to malonyl-CoA conversion from Snf1-dependent inhibition of Acc1 [153]. 3-HP production was achieved by separating the two subdomains of the mcr_{CA} [154] and integrating them into the genome, with the DNA constructs kindly provided by Xiaowei Li (unpublished data).

We evaluated if the acetyl-CoA supply can be increased by expanding the phosphoketolase pathway to the GATHCYC by measuring the concentration of 3-HP in the supernatant from shake flask cultures with yeast strains using either the phosphoketolase pathway or the GATHCYC for additional acetyl-CoA supply. Expanding the phosphoketolase pathway to the GATHCYC increased the 3-HP titers at the end of the glucose phase by 109% (**Figure 21A**), indicating an increased supply of acetyl-CoA. Introduction of the GATHCYC to a phosphoketolase expressing strain also increased the acetate concentration from 1.4 to 2.0 g/L at glucose exhaustion. These are high levels of acetate, as wild-type CEN.PK 113-5D produced 0.55 g/L acetate at glucose exhaustion, which was increased to 1.10 g/L after introducing the *xfpk* from *B. breve* on a high copy plasmid (**Figure 3A**). To efficiently utilize the GATHCYC for precursor supply of acetyl-CoA, the formation of acetate needs to be reduced as it requires an extra cost of 2 ATP/acetate to be activated to acetyl-CoA. This cost can be avoided if AcP from the GATHCYC is converted to acetyl-CoA by Pta instead of promiscuous hydrolysis of AcP to acetate without ATP formation. Furthermore, as investigated in **Paper I**, higher acetate production increases the respiratory demand from futile transportation of acetate.

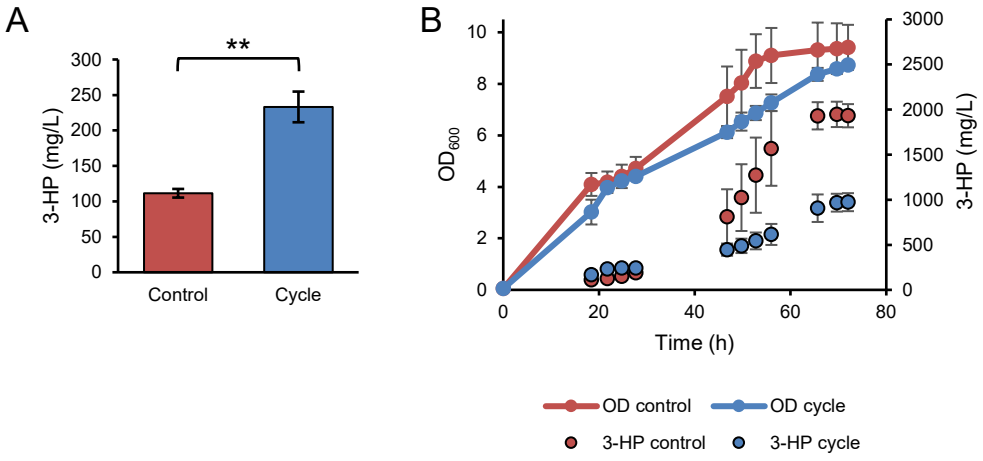

Figure 21. Comparison in 3-HP formation between the linear phosphoketolase pathway (control, strain JH36) and the GATHCYC (cycle, strain JH29) for additional supply of acetyl-CoA. **A)** 3-HP titers at glucose exhaustion and **B)** optical density (OD_{600}) and 3-HP concentration profile. Strains were cultured with biological triplicates in shake flasks with minimal media supplemented with 2% glucose and 100 mg/L uracil. Values are shown as averages, with error bars as the standard deviation. Statistical significance was evaluated with a two-sided Student's t-test with unequal variance (**$p < 0.01$). Figure adapted from **Paper III** [118].

During aerobic batch growth on glucose, *S. cerevisiae* displays respiro-fermentative growth, with ethanol as the main product. After the respiratory growth on the produced ethanol, expansion of the phosphoketolase pathway to the GATHCYC reduced the 3-HP titers by 50% (**Figure 21B**). Phosphoketolase expression has previously been shown to increase the titers of FFA at glucose depletion, while reducing the titers at the end of the ethanol phase [155]. During growth on ethanol, cytosolic acetyl-CoA can already be formed by alcohol dehydrogenase (Adh2), aldehyde dehydrogenase (Ald6) and acetyl-CoA synthetase (Acs1/2) without carbon loss as CO_2. This means that using the phosphoketolase pathway during growth on ethanol will reduce the yield, as assimilation of 4 mol acetyl-CoA to 1 mol F6P through the gluconeogenesis costs 2 mol CO_2. Converting this assimilated F6P to 3 mol of acetyl-CoA through the GATHCYC will result in a net loss of 2 mol CO_2 per acetyl-CoA, effectively just converting acetyl-CoA to CO_2. Flux through the NOG in the phosphoketolase control during growth on glucose is not likely, as Fbp1 is glucose-repressed. However, this is not the case during growth on ethanol, possibly allowing some flux through the NOG in the phosphoketolase control, even if the genes in the NOG are not overexpressed. This makes it challenging to determine if the GATHCYC would increase the theoretical yield on ethanol compared to the phosphoketolase control, as the NOG and the GATHCYC both produce 3 mol acetyl-CoA from 1 mol F6P.

Deleting the transketolases and transaldolases, which is required for the GATHCYC, might not be beneficial during respiratory growth on ethanol as they connect the gluconeogenesis pathway with the non-oxidative PPP for the supply of the precursor metabolites E4P and R5P. This function is replaced by the GATHCYC in the cycle strain, where bottlenecks in the GATHCYC could lead to growth defects and reduced 3-HP titers. In flask culture, the cycle strain showed high concentrations of acetate during the ethanol phase (**Paper III: Figure S9**). This prolonged exposure to high concentrations of acetate could lead to increased energy demand from acetate detoxification, contributing to the 50% reduction in 3-HP titers in the cycle strain at the end of the fermentation (**Figure 21B**). Consumption of the nonfermentable carbon source acetate needs oxygen, where oxygen limitation in shake flask cultures [156] can reduce the capacity of consuming the excess acetate formed by the cycle. We also observed an accumulation of glycerol at the end of the fermentation. Glycerol formation is needed to oxidize excess NADH from biomass formation [81] and accumulation of glycerol could indicate a redox imbalance caused by the GATHCYC. The *S. cerevisiae* CEN.PK strains cannot grow with glycerol as their sole carbon source, but they can grow on glycerol when co-consumed with ethanol [157]. However, the prolonged acetate exposure and possible oxygen limitation could reduce the consumption of glycerol, which is also a nonfermentable carbon source.

The GATHCYC should preferably be utilized in growth conditions where ethanol formation is limited. Exposure to high concentrations of glucose during batch fermentation triggers overflow metabolism (the Crabtree effect) [15], where the majority of the carbon is converted to ethanol instead of your product of interest. This can be avoided by slowly adding glucose to the culture in a fed-batch fermentation mode, which is also beneficial for 3-HP production [158]. The phosphoketolase pathway has been successfully used during a fed-batch fermentation to produce 0.173 g/g farnesene from glucose, which is 53% of the chemical limit [68]. Further modifications to the cycle strain might be needed to efficiently use the

GATHCYC: **i**) assess and balance the X5P, F6P and S7P activities of the Xfspk, **ii**) reduce the acetate formation and **iii**) efficiently convert AcP to acetyl-CoA and the product of interest.

In conclusion, we analyzed three different configurations of the NOG pathway through mathematical modeling and could show that implementing a Xfspk phosphoketolase could solve a potential bottleneck at the transketolase step in the original NOG pathway. Experimentally, we demonstrated *in vitro* activity of the third configuration, the GATHCYC, which also showed *in vivo* activity by rescuing growth in a *tkl1*Δ *tkl2*Δ *zwf1*Δ strain. Finally, we showed that the introduction of the GATHCYC to a phosphoketolase expressing strain yielded increased acetyl-CoA supply, with a 109% increase in the titers of the acetyl-CoA-derived product 3-HP at glucose exhaustion.

4.5 Effect of cyclic phosphoketolase expression (Paper IV)

We wanted to gain more insight regarding the effect on the metabolism of *S. cerevisiae* from the introduction of the GATHCYC, which replaces the non-oxidative PPP. This information could aid in understanding the cell factory and finding clues on how to identify and overcome bottlenecks. In **Paper IV**, we analyzed the GATHCYC strains from **Paper III** further by culturing them in bioreactors, as having control over pH, temperature, agitation, and dissolved oxygen make them superior to shake flask cultures. Bioreactors are also ideal for taking samples for omics analysis, as control over the culture parameters is important for reducing variability and for promoting reproducibility. By taking samples for proteomics and transcriptomics from bioreactor cultures, we hoped to be able to understand which pathways and processes are up- or downregulated because of the introduction of the GATHCYC to a phosphoketolase expressing strain.

First, we constructed a phosphoketolase control and a cycle strain with two copies of the native mcr_{CA} instead of using the split version. Like the split mcr_{CA} in **Paper III**, the use of two copies of the native mcr_{CA} resulted in a 118% increase of 3-HP titers when the GATHCYC was implemented in a phosphoketolase expressing strain in flask culture (**Figure 22**). During exponential growth on glucose, implementation of the GATHCYC reduced the maximal specific growth rate by 7.5% and increased the acetate concentration by 61% at glucose exhaustion (**Paper IV: Figure S2**). After respiratory growth on the produced ethanol, the GATHCYC reduced the final 3-HP titers by 49%, reduced the final OD_{600} by 23%, and accumulated glycerol. The lower 3-HP titer and biomass yield could be caused by the prolonged exposure of acetate during the ethanol phase, with 3.5 and 2.3 g/L acetate in the supernatant for the cycle strain at 44 and 68 h, respectively. At the same time points, the phosphoketolase control had 0.8 and 0 g/L acetate, respectively. All acetate was consumed however after 5 d in the cycle strain. The cycle strain with the split mcr_{CA} in **Paper III** consumed all acetate after 70 h (**Paper III: Figure S9**), possibly due to a higher flux towards 3-HP. A high flux from acetyl-CoA to product formation is important, as bottlenecks in acetyl-CoA consumption will lead to a buildup of acetyl-CoA, which can shift the equilibrium of the reversible reaction catalyzed by Pta (AcP ⇄ acetyl-CoA) towards AcP formation. Excess AcP from the cycle can then be promiscuously degraded into acetate by Gpp1/2 [66, 68] or by additional unidentified hydrolases, with less AcP converted to 3-HP.

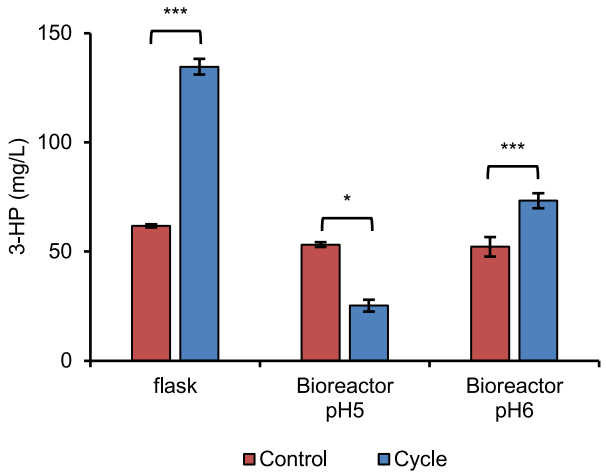

Figure 22. Comparison of 3-HP titers between strains with the phosphoketolase pathway (control) or the GATHCYC (cycle) for additional acetyl-CoA supply in shake flask culture or bioreactor controlled at pH 5 or 6. Strains were cultured with biological triplicates in shake flasks using minimal media supplemented with 2% glucose and 100 mg/L uracil. Bioreactor cultures contained the same media, but with lower nitrogen content (reduced from 7.5 to 5 g/L $(NH_4)_2SO_2$) and phosphate content (reduced from 106 to 22 mM KH_2PO_4). Biological duplicates and quadruplicates were used for the bioreactor culture at pH 5 and 6, respectively. Average values are shown with the standard deviation as errors bars. Asterisks indicate significant changes calculated with a two-sided Student's t-test with unequal variance (* $p < 0.05$, *** $p < 0.001$).

The strains with two copies of the native *mcr*$_{CA}$ were further characterized during batch growth in controlled bioreactors. Initially, we ran the fermentation in minimal media with the pH-controlled according to standard conditions (pH 5). Expansion of the phosphoketolase pathway to the GATHCYC did not affect the final biomass yield during bioreactor fermentation at pH 5 (**Paper IV: Figure S3**). Furthermore, there was no longer any accumulation of glycerol, possibly due to the higher aeration in bioreactors compared to shake flask cultures [156]. However, the final concentration of 3-HP was reduced by 53% in the cycle strain (**Figure 22**). We suspected that the increased acetate concentration in the cycle strain might cause energy to be wasted on futile transportation of acetate, as investigated in **Paper I**, and result in lower 3-HP titers for the cycle strain. Acetate has a pK_a of 4.76, which means that it will be deprotonated inside the cell because of the neutral pH. Disassociated protons and anions from acetate need to be exported by ATP-dependent processes to avoid acidification of the cytoplasm [82, 83]. Outside the cell, the distribution between the protonated and deprotonated form of acetate is defined by the extracellular pH, with the lipophilic protonated form present at 85% and 5% at pH 4 and pH 6, respectively. The lipophilic protonated form of acetate can be transported passively inside the cell, where the subsequent deprotonation of acetate establishes a futile cycle that spends energy [84]. At pH 5, the fraction of the lipophilic form of acetate is 36% and we decided to investigate if increasing the pH to 6 would lower the amount of energy spent on futile transport of acetate, which otherwise could reduce the benefit of the GATHCYC. Increasing the pH to 6 would also mimic the shake flask conditions, which used buffered minimal media at a starting pH of 6.5. After batch growth on glucose in bioreactors with the pH controlled to 6, the feeding and outflow pumps were turned on during the early ethanol phase and the culture mode was turned into a carbon-limited chemostat.

Increasing the pH from 5 to 6 in the bioreactor did not affect the concentration of 3-HP of the phosphoketolase control at glucose exhaustion. However, implementation of the GATHCYC at pH 6 increased the 3-HP titer by 40% compared to the control (**Figure 22**), which indicates a reduced degree of futile transportation of acetate and an improved supply of acetyl-CoA by the GATHCYC. Surprisingly, the titer of 3-HP for the cycle strain was lower in the bioreactor compared to the shake flask at glucose exhaustion. The higher aeration and pH control in bioreactors generally result in faster growth compared to flask cultures, which made us expect higher 3-HP concentrations in the bioreactors. The minimal media used in both cultures were the same, except for a lower nitrogen concentration in the bioreactor compared to the flask (5 and 7.5 g/L $(NH_4)_2SO_2$, respectively). Furthermore, the content of the potassium phosphate buffer was reduced because of the pH control in the bioreactor (from 106 to 22 mM KH_2PO_4). Phosphate limitation was observed when combining the NOG and the lower glycolysis for increased acetyl-CoA supply in *C. glutamicum*, which showed less accumulation of trehalose as a response to phosphate starvation when the phosphate content was increased from 13 to 130 mM [128]. The phosphate content could possibly be limiting when using the GATHCYC, as each phosphoketolase reaction requires one inorganic phosphate, thus lowering the phosphate content might reduce the activity of the GATHCYC and result in lower titers of 3-HP. However, the phosphate-limited condition for *S. cerevisiae* is 0.15 mM KH_2PO_4 [159], making phosphate limitation unlikely in our study.

During the glucose phase in the bioreactor at pH 6, we sampled continuously for biomass and extracellular metabolites to be able to calculate the physiological parameters, summarized in **Table 4**. Implementing the GATHCYC in a phosphoketolase expressing strain reduced the maximum specific growth rate and the glucose uptake rate by 14% and 13%, respectively. Furthermore, the production rate of ethanol and CO_2 was reduced by 23 and 17%, respectively, while the acetate production rate was increased by 21%.

Table 4. Physiological parameters for strains using the phosphoketolase pathway (control) or the GATHCYC (cycle) for additional acetyl-CoA supply in bioreactors controlled at pH 6 during batch growth on glucose or in chemostat.

Parameter	Batch – exponential phase		Chemostat	
	Control	Cycle	Control	Cycle
μ_{max} (h^{-1})	0.32 ± 0.006	0.28 ± 0.002 (***)	0.105 ± 0.002	0.104 ± 0.004 (ns)
Biomass concentration (g/L)	2.88 ± 0.06	2.79 ± 0.10 (ns)	2.94 ± 0.059	2.08 ± 0.14 (***)
Yx/s (g/g)	0.14 ± 0.001	0.13 ± 0.005 (ns)	0.40 ± 0.008	0.29 ± 0.019 (***)
Residual glucose (g/L)	–	–	0.07 ± 0.003	0.09 ± 0.016 (ns)
q(Glucose) (mmol $gCDW^{-1}$ h^{-1})	–12.91 ± 0.32	–11.19 ± 0.41 (***)	–1.44 ± 0.054	–2.00 ± 0.19 (**)
q(EtOH) (mmol $gCDW^{-1}$ h^{-1})	13.19 ± 0.32	10.12 ± 0.77 (**)	–	0.07 ± 0.066 (ns)
q(Acetate) (mmol $gCDW^{-1}$ h^{-1})	2.35 ± 0.11	2.84 ± 0.10 (***)	–	1.33 ± 0.24 (**)
q(Glycerol) (mmol $gCDW^{-1}$ h^{-1})	1.05 ± 0.07	1.00 ± 0.04 (ns)	–	0.15 ± 0.02 (***)
q(CO_2) (mmol $gCDW^{-1}$ h^{-1})	16.03 ± 0.70	13.38 ± 0.26 (**)	3.30 ± 0.24	3.79 ± 0.23 (*)
q(Biomass) (mmol $gCDW^{-1}$ h^{-1})	12.98 ± 0.24	11.17 ± 0.08 (***)	4.28 ± 0.10	4.21 ± 0.15 (ns)
q(3-HP) (mmol $gCDW^{-1}$ h^{-1})	0.07 ± 0.009	0.10 ± 0.007 (**)	0.030 ± 0.002	0.013 ± 0.001 (***)
Carbon balance (%)	82 ± 1	80 ± 1	89 ± 1	94 ± 3

*Strains were cultured with biological quadruplicates in minimal media, supplemented with 100 mg/L uracil, with 2% glucose in batch and 0.75% glucose in the chemostat feed at pH 6. Values represent averages ± the standard deviation. Asterisks indicate significant changes compared to control (two-sided Student's t-test with unequal variance; ns: not significant, * p <0.05, ** p < 0.01, *** p < 0.001).*

Changes in glucose uptake rate and growth rate will influence the other production rates. Therefore, we converted the production rates during the glucose phase to C-mol fluxes and normalized them to the glucose uptake rate. This makes it easier to follow how carbon is redistributed in the two strains. From **Figure 23** we can observe that the amount of carbon converted to ethanol in the cycle strain is 13% lower than the control, while the reduction in CO_2 production is not significant when accounting for the lower glucose uptake rate in the cycle strain. The flux into 3-HP is increased by 63% but is a very small portion of all the carbon (0.27 and 0.44% relative C-mol flux in control and cycle, respectively). This small increase in 3-HP could mask the benefit of the GATHCYC in terms of capacity to reroute glucose to acetyl-CoA without wasting carbon as CO_2. Another effect of implementing the GATHCYC is that the amount of glucose converted to acetate increased from 6.1 to 8.5% relative C-mol. Efficient use of the GATHCYC should supply more AcP for 3-HP production, but it seems that the majority is converted to acetate instead. A flux of 6.1% relative C-mol into acetate for the phosphoketolase control is also high, compared to 1.4 and 4.1% in wild-type CEN.PK 113-5D and xfpk(BB), respectively (**Figure 3B**). Deletion of glycerol-3-phosphate phosphatases (Gpp1 and Gpp2) can reduce AcP hydrolysis, with Gpp1 responsible for the majority of the breakdown [66, 68], but double deletion is not preferable as it can cause a severe growth defect [155]. Furthermore, the double deletion of *GPP1*,*2* did not abolish all hydrolysis of AcP to acetate in a synthetic Crabtree negative strain featuring deletion of *PDC1*,*5*,*6* to stop all flux

from pyruvate to acetaldehyde [52]. With AcP provided from the heterologous expression of pyruvate oxidase, this strain had a relative C-mol flux of 14% into acetate during batch growth, even if acetate could not be produced from acetaldehyde. This indicates that there are alternative major pathways for AcP degradation to acetate in *S. cerevisiae*.

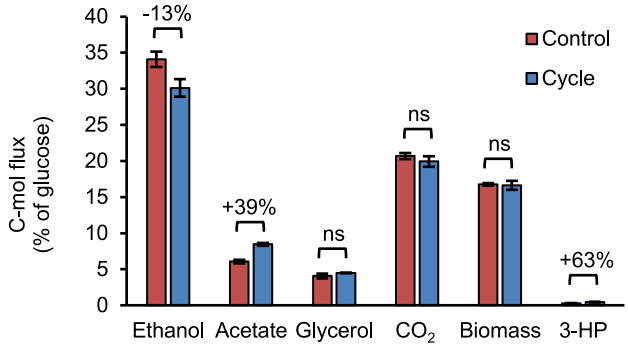

Figure 23. Comparison of the carbon fluxes during the glucose phase in C-mol normalized to the glucose uptake rate between strains with the phosphoketolase pathway (control) or the GATHCYC (cycle) for additional acetyl-CoA supply in bioreactors at pH 6. Average values are shown with the standard deviation as errors bars. Statistical significance was calculated with a two-sided Student's t-test with unequal variance; ns: no significant change ($p>0.05$).

The GATHCYC has so far been demonstrated to be beneficial during growth on glucose, but not during growth on the produced ethanol. We wanted to use a carbon-limited chemostat to avoid overflow metabolism and ethanol formation to fully utilize the potential of the GATHCYC to increase the yields of acetyl-CoA-derived products. A chemostat is also beneficial for the comparison of different yeast strains as the growth rate can be controlled by the dilution rate and thus avoid effects from differences in growth rates. The higher acetate flux in the phosphoketolase control compared to xfpk(BB) from **Paper I** did not prevent the phosphoketolase control to achieve a purely respiratory steady-state without accumulation of fermentation products (**Table 4** and **Figure 24**). However, the cycle strain reached a steady-state with respiro-fermentative metabolism and accumulation of 1.56 g/L acetate, which corresponds to a 22% relative C-mol flux from glucose to acetate (**Figure 24**). Wild-type *S. cerevisiae* can grow completely respiratory at dilution rates below 0.28 h^{-1} [160–162]. At higher dilution rates, overflow metabolism is initiated and fermentation products such as ethanol and acetate accumulate while respiration is reduced [15, 162]. Hypotheses for the onset of overflow metabolism involve limitations in the capacity of NADH reoxidation [17] and protein limitation [18]. The critical dilution rate for overflow metabolism is strain-dependent and can be reduced from heat stress [163], uracil limitations [164], ergosterol limitation [165], and low respiratory capacity [92].

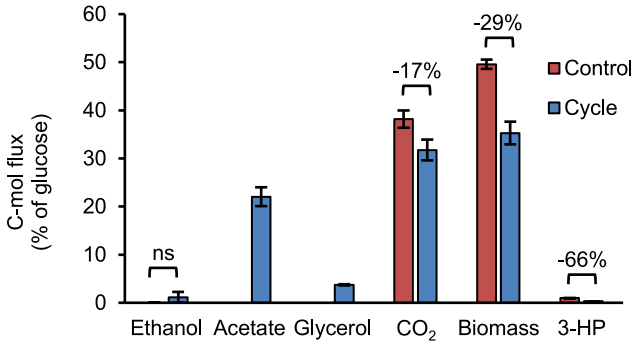

Figure 24. Comparison of the carbon fluxes during chemostat in C-mol normalized to the glucose uptake rate between strains with the phosphoketolase pathway (control) or the GATHCYC (cycle) for additional acetyl-CoA supply in bioreactors at pH 6. Average values are shown with the standard deviation as errors bars. Statistical significance was calculated with a two-sided Student's t-test with unequal variance; ns: no significant change ($p>0.05$).

Two NADH are formed from glucose during glycolysis, which can be regenerated to two NAD^+ through ethanol formation by alcohol dehydrogenase during fermentative growth. Without regeneration of NAD^+, glycolysis stops as NAD^+ is required by GAP dehydrogenase to convert GAP to 1,3BPG. Purely respiratory growth generates in total 10 NADH and 2 $FADH_2$ per glucose through the glycolysis and the TCA cycle, which is regenerated to NAD^+ and FAD through the respiratory chain while generating ATP from oxidative phosphorylation. During high growth rates, the respiratory capacity to regenerate NAD^+ might not be sufficient [17], which leads to repression of respiration and activation of alcohol fermentation to keep NAD^+ available for glucose consumption. A study in *E. coli* hypothesized that the respiratory capacity was insufficient at high growth rates due to membrane crowding, which is why respiration was repressed and overflow metabolism initiated [166]. In *S. cerevisiae*, the overflow metabolite is mostly ethanol, as its synthesis regenerates NAD^+. A chemostat study showed that a dilution rate of 0.28 h^{-1} (the critical dilution rate) resulted in a 1.1% relative C-mol flux to ethanol, which increased to 41.7% at a dilution rate of 0.4 h^{-1} [162]. In our study at a dilution rate of 0.1 h^{-1}, the cycle strain had no significant accumulation of ethanol, but instead 22% relative C-mol to acetate as the main overflow metabolite (**Figure 24**). A study exploring uracil limitations at a dilution rate of 0.1 h^{-1} also observed mostly ethanol accumulation (24.5% relative C-mol), with lower amounts of acetate (6.1% relative C-mol) [164]. Acetate as the major overflow metabolite during respiro-fermentative growth in chemostat is unusual in *S. cerevisiae* and could be connected to excess AcP hydrolysis to acetate in the cycle strain. I will address this further later in this chapter.

To better understand how the carbon fluxes are redirected upon the implementation of the GATHCYC, we analyzed the changes in gene expression on protein and mRNA level during the mid-glucose phase and on mRNA level during the early ethanol phase and chemostat. Up- or downregulated genes can indirectly give clues on how the carbon flux is distributed. During the glucose phase, implementation of the GATHCYC to a phosphoketolase expressing strain resulted in 103 differentially expressed genes on the protein level (95 up- and 8 downregulated) and 297 on mRNA level (254 up- and 43 downregulated) if filtering for an absolute LFC above 1 and adjusted p-value below 0.01. GO-term analysis with Piano revealed enrichment for upregulated genes in the TCA cycle, oxidative PPP and NADPH generation in

both datasets (**Figure 25**). Upregulation of genes in the TCA cycle was observed in **Paper I** when expressing the phosphoketolase gene in wild-type *S. cerevisiae* (**Figure 4**), where the excess acetate formation increased the respiratory demand (**Table 1**). The addition of the GATHCYC resulted in enrichment for upregulated genes in the GO-term 'mitochondrial electron transport chain' in the protein dataset (**Figure 25**), hinting at increased respiration. Furthermore, the GO-terms 'aerobic respiration 'and 'ATP synthesis coupled proton transport' are enriched on both protein and mRNA level, but only when analyzing just the upregulated genes (**Paper IV: Figure S5 and S6**). The potential increase in respiration in the cycle strain needs to be verified, as malfunctioned oxygen sensors prevented us from determining if the GATHCYC increases the oxygen consumption rate. The cycle strain displayed a lower growth rate during the glucose phase and GO-terms enriched for downregulated genes involved RNA metabolism, translation, ribosomes, and amino acid biosynthesis, which is usually observed in mutants with lower growth rates [110].

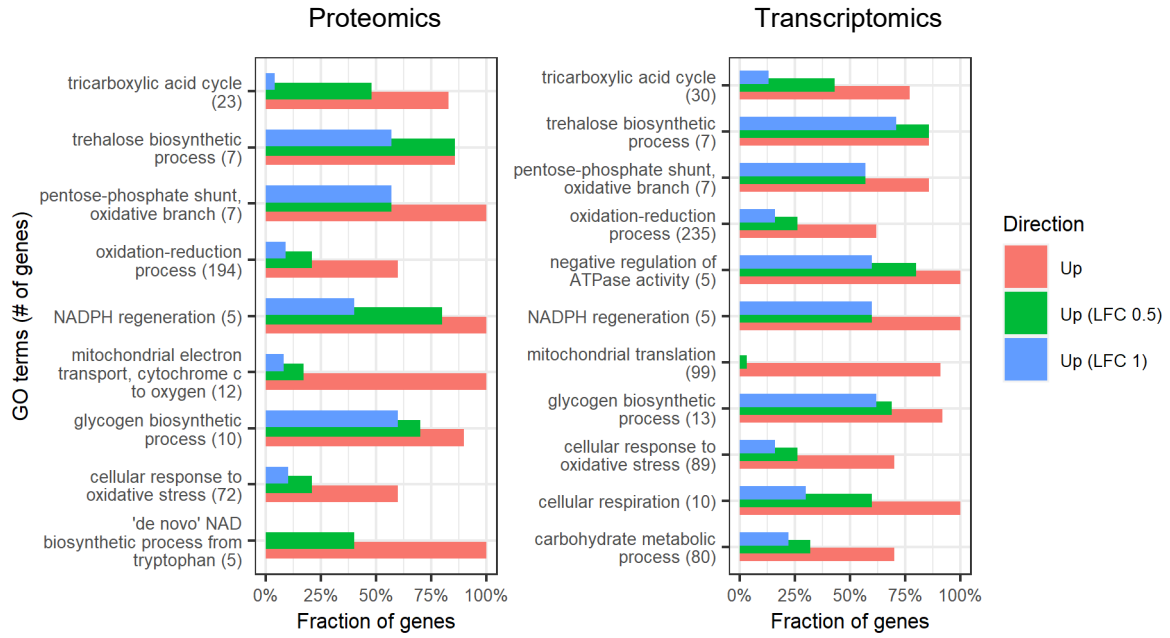

Figure 25. GO-terms involved in biological processes that are enriched for upregulated genes from implementing the GATHCYC to a phosphoketolase expressing strain during batch growth on glucose at pH 6. Proteomics or transcriptomics data were summarized from the consensus heatmap generated with the Piano R-package by filtering the median adjusted p-value below 0.1 for non-directional enrichment and below 0.05 for the distinct up- or downregulated enrichment. The fraction of upregulated genes is shown without filtering (red) and LFC > 0.5 (green) or LFC > 1 (blue) together with an adjusted p-value below 0.01.

We could observe enrichment for upregulated genes in the stress responses 'trehalose biosynthesis process', 'glycogen biosynthesis process' and 'cellular response to oxidative stress' in both datasets during the glucose phase (**Figure 25**). Genes involved in stress responses can be upregulated by reducing the growth rate alone, which can complicate the analysis of mutants with lower growth rates [110]. The consequence might be that the mutant is assumed to experience stress, even though the upregulated genes involved in that stress response could be an artifact from the reduced growth rate. The upregulation of stress response genes was predominantly occurring during the reduction of the growth rate from 0.25 to 0.02 h^{-1} [110], while implementation of the GATHCYC reduced the growth rate slightly from 0.32

to 0.28 h^{-1}. The enrichment for upregulated genes involved in oxidative stress in combination with upregulated genes involved in NADPH generation made us suspect that the cycle strain is experiencing oxidative stress, even though the strains differ in growth rate. NADPH is needed for neutralizing reactive oxygen species (ROS) with the glutathione and the thioredoxin system [106]. Upregulated proteins involved in NADPH generation were: Gnd1/2, catalyzing the final reaction of the oxidative PPP; Ald6 and Ald4, responsible for acetate production in the cytosol and mitochondria, respectively; and Idp2/3, catalyzing the formation of alpha-ketoglutarate (**Figure 26**). The GATHCYC increased the acetate flux by 21% (**Table 4**) and acetate can cause oxidative stress in *S. cerevisiae* [167, 168]. This oxidative stress is probably caused by acetate-mediated activation of the mitochondrial respiratory chain [168], which is the main endogenous source of ROS through leakage of electrons from the electron transport chain that form superoxide anions [169]. Exposure to 6 g/L acetic acid for 0-45 min was shown previously to generate ROS in the form of hydrogen peroxide, while longer treatment (60-90 min) resulted in the generation of primary superoxide anions [170]. In the cycle strain, we could see an upregulation of the glutathione-dependent disulfide oxidoreductases Grx1/2 and the glutathione transferase Gtt1 on protein level. Furthermore, upregulation on protein level was also observed for the mitochondrial peroxiredoxin Prx1 and the cytosolic peroxiredoxin Ahp1. However, the total ROS levels were lower in the cycle strain compared to the control when stained with dihydrorhodamine 123 (DHR123) (**Paper IV: Figure S8**). DHR123 has been reported to not measure superoxide anions directly [171] and a specific dye for superoxide anions might be needed to validate the suspected oxidative stress, as superoxide anions were the major ROS species during long term acetic acid stress [170]. Another possibility is that the increased oxidative stress response is enough to counteract the suspected oxidative stress caused by increased acetate production. Further experiments are needed to validate if the cycle strain is experiencing oxidative stress and, if it does, how to reduce it to improve strain performance.

If upregulation of genes involved in NADPH generation is not needed to combat ROS production, the upregulation of NADPH generating pathways might indicate a general limitation of NADPH supply in the GATHCYC strain. The major routes for cytosolic NADPH generation are the PPP and acetate formation by Ald6, which contribute by 80 and 20%, respectively, during normal conditions [172]. An increased NADPH demand can saturate the oxidative PPP and lead to more acetate formation [172]. 3-HP production from malonyl-CoA by Mcr_{CA} consumes two NADPH per 3-HP formed, but the low titer of 3-HP (52 and 73 mg/L for control and cycle, respectively) is unlikely to cause an NADPH limitation in the cycle strain. Deletion of the transketolases and the transaldolases in the GATHCYC might interfere with the NADPH generation of the oxidative PPP. The last step of the oxidative PPP produces Ru5P, which now must be fed into the GATHCYC as the transketolases and the transaldolases are deleted (**Figure 26**). Thus, bottlenecks in the GATHCYC could limit the flux through the oxidative PPP. Of the genes involved in the GATHCYC, only *SHB17* was upregulated during the glucose phase (LFC of 3.34 and 5.29 on protein and mRNA level, respectively). The upregulation of *SHB17* was expected, as *SHB17* was overexpressed during strain construction by replacing its native promoter with the strong *TDH3* promoter.

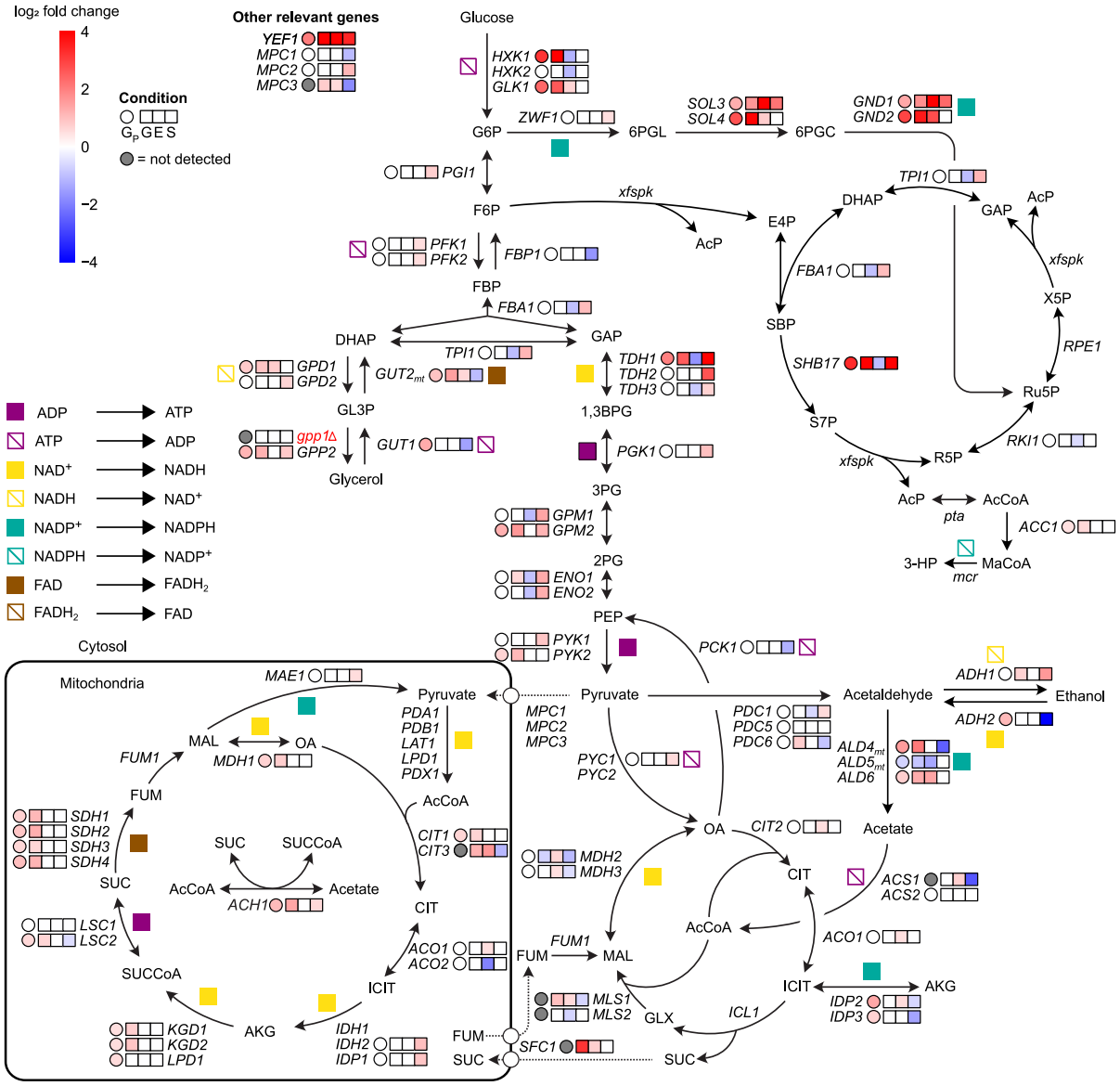

Figure 26. Differentially expressed genes in the central carbon metabolism from implementing the GATHCYC to a phosphoketolase expressing strain. The log_2-fold change (LFC) values are filtered for absolute LFC >0.5 and adjusted p-value below 0.01 and visualized as intensities of red (up) and blue (down). The changes on protein level during the glucose phase (Gp) are shown in the circles and changes on mRNA level in the glucose phase (G), ethanol phase (E) and steady-state carbon-limited chemostat (S) in the squares.

Implementation of the GATHCYC resulted in a small upregulation of *ACC1* (**Figure 26**). Acc1 is responsible for the conversion of acetyl-CoA to malonyl-CoA and is the rate-limiting step of fatty acid biosynthesis. A bottleneck in acetyl-CoA conversion to malonyl-CoA could shift the equilibrium of the Pta reaction (AcP ⇄ acetyl-CoA) towards AcP formation. The consequence of this could be that the AcP released from the cycle is not efficiently converted to acetyl-CoA, but instead hydrolyzed to acetate. The upregulation of *ACC1* in the cycle strain made us suspect that there is a bottleneck at this step. We had already integrated one copy of the *ACC1***, engineered to abolish Snf1-dependent inactivation at low glucose conditions [153], under the *HXT7* promoter. As the *HXT7* promoter is stronger during the ethanol phase [103], we decided to add an additional copy of *ACC1*** under the *TPI1* promoter to get a higher expression level of *ACC1*** during the glucose phase. Additional overexpression of *ACC1***

in the cycle strain increased the 3-HP titers from 137 to 327 mg/L at glucose exhaustion, while not affecting the growth rate (**Figure 27A-B**). The 3-HP titers at the end of the ethanol phase also increased from 297 to 550 mg/L by the additional overexpression of *ACC1*** in the cycle strain. However, we could no longer see a benefit of the GATHCYC as overexpression of *ACC1*** in the phosphoketolase control achieved 3-HP titers that were not significantly different from the cycle strain. Furthermore, the overexpression of *ACC1*** in the phosphoketolase control was more beneficial after the ethanol phase, with a final 3-HP titer of 730 mg/L. We expected that overexpression of *ACC1*** should relieve the bottleneck in acetyl-CoA consumption and reduce acetate formation in the cycle strain, however, the acetate titers were unchanged both at glucose exhaustion and mid ethanol phase (**Figure 27C**). After overexpressing *ACC1*** further, we lost the benefit of expanding the linear phosphoketolase pathway to the GATHCYC. It could be that there exist additional bottlenecks that prevent efficient use of the GATHCYC for improved supply of acetyl-CoA. We still observe excess formation of acetate that could reduce the formation of 3-HP. Efforts should be focused on enhancing the conversion of AcP to acetyl-CoA to avoid build-up of AcP that can be degraded to acetate. Ideally, *ACC1*** should be overexpressed in a strain where the Pta reaction and the Mcr reaction is improved to ensure efficient flux from the cycle to a product.

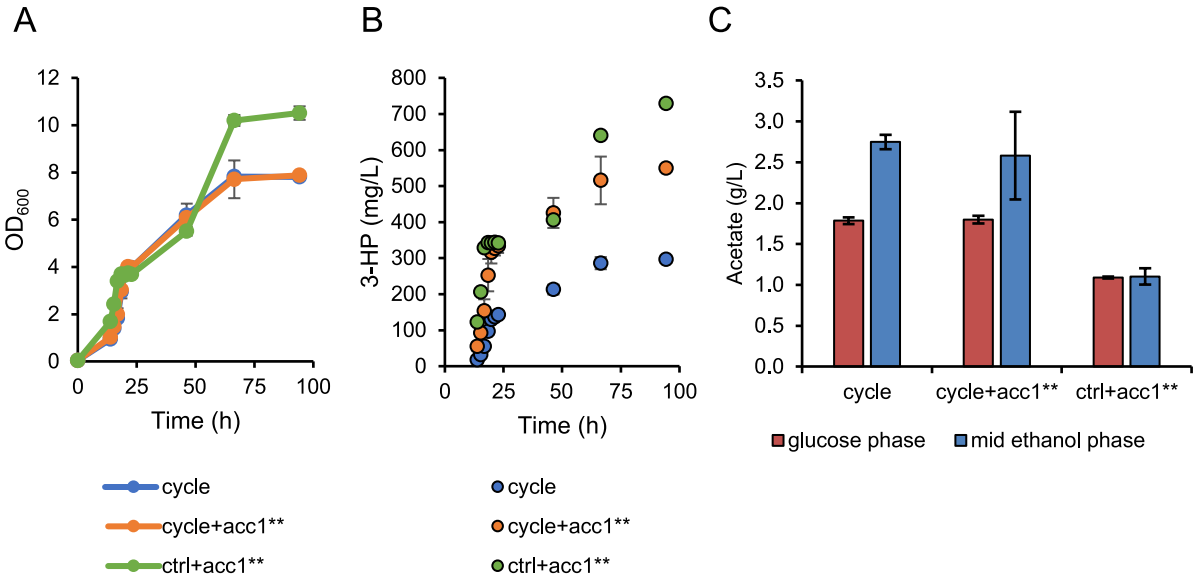

Figure 27. Effect of additional *ACC1*** overexpression in strains with the phosphoketolase pathway (ctrl) or the GATHCYC (cycle) for additional acetyl-CoA supply on **A)** OD_{600} profile, **B)** 3-HP profile and **C)** acetate concentrations. Strains were cultured with biological triplicates in shake flasks using minimal media supplemented with 2% glucose and 100 mg/L uracil. Average values are shown with the standard deviation as errors bars.

Next, we investigated the changes in gene expression during the ethanol phase and chemostat. Even if the GATHCYC might not be beneficial during the ethanol phase, we still wanted to investigate the response of utilizing the GATHCYC during respiratory growth on ethanol. Furthermore, the chemostat culture would be the ideal condition for analyzing the changes in gene expression from the GATHCYC, as controlling the growth rate of both strains eliminates changes in gene expression caused by differences in growth rates, as seen in the batch growth on glucose. However, analyzing the dataset from the chemostat turned out to be challenging as the cycle strain displayed respiro-fermentative growth instead of growing purely respiratory as

the control. This different mode of growth imposes changes on gene expression that can be challenging to separate from changes in gene expression caused by the implementation of the GATHCYC.

Using the GATHCYC in the ethanol phase resulted in 342 differentially expressed genes (91 up- and 251 downregulated), compared to 326 genes in the chemostat (161 up- and 165 downregulated) and 297 genes in the glucose phase (254 up- and 43 downregulated), with an absolute LFC > 1 and adjusted p-value <0.01. As observed in the glucose phase, most of the downregulated genes in the ethanol phase were involved in translation and ribosomal processes, which indicates a slower growth rate during the ethanol phase for the cycle strain. The strains were only sampled once during the early ethanol phase before the feed was initiated, so further experiments are needed to evaluate the growth rate of the cycle strain on ethanol in bioreactor cultures at pH 6. By comparing all three datasets, we found 17 genes that were upregulated in all conditions. *YRO2* was upregulated in all conditions, coding for a protein with a putative role in response to acetic acid stress. Furthermore, we observed an upregulation of genes involved with NADPH generation in all three conditions: *GND1* and *SOL3* from the oxidative PPP; *GCY1*, a glycerol dehydrogenase involved in an alternative glycerol consumption via dihydroxyacetone (DHA) instead of GL3P; *YEF1*, an ATP-NADH kinase that can phosphorylate NAD(H) to NADP(H) [100]; *GOR1*, glyoxylate reductase that converts glyoxylate to glycolate [101]; and *YMR315W*, an NADP(H) oxidoreductase that can increase NADPH levels during NADPH deletion [105]. In **Paper III**, we deleted *PHO13* to reduce the formation of the dead-end metabolite sedoheptulose from S7P [141] to increase the availability of S7P for the phosphoketolase reaction in the GATHCYC. However, deletion of *PHO13* alone resulted in upregulation of *GND1*, *SOL3*, *GCY1*, *YEF1* and *GOR1* in *S. cerevisiae* BY4742 [173]. Therefore, GATHCYC strains without *PHO13* deletion should be investigated to make sure that the upregulation of these genes in all conditions is caused by the GATHCYC and not *PHO13* deletion alone.

During growth on ethanol, genes within the GATHCYC were downregulated in the cycle strain (*FBA1*, *SHB17*, *RKI1* and *TPI1*) (**Figure 26**). Downregulation of *FBA1* and *SHB17* could limit the supply of S7P for the phosphoketolase, resulting in a lower flux through the cycle. The high availably of S7P was important for the phosphoketolase shunt to allow a sufficient reaction rate with the phosphoketolase from *B. adolescentis* due to its high K_M towards S7P (68.1 mM) [132]. In **Paper III**, *SHB17* was overexpressed by exchanging its native promoter with the strong *TDH3* promoter, the 2nd and 9th strongest native promoter in *S. cerevisiae* during growth on glucose and ethanol, respectively [174]. While this resulted in a strong upregulation during the glucose phase (LFC of 5.29), it was instead downregulated during the ethanol phase (LFC of -1.05). Titers of 3-HP after the ethanol phase could possibly be increased by adding an additional copy of the downregulated cycle genes (*FBA1*, *SHB17*, *RKI1* and *TPI1*) under the control of a promoter that is strong during the ethanol phase (*CIT2*, *JEN1* or *ICL1*). However, as discussed earlier, the phosphoketolase pathway or the GATHCYC is preferably used during glucose conditions as acetyl-CoA can already be produced by the native pathway from ethanol without loss of carbon as CO_2.

ALD6 (acetate formation from acetaldehyde) and *ACS1* (activation of acetate to acetyl-CoA) were upregulated in the cycle strain during growth on ethanol (**Figure 26**). Furthermore, genes in the glyoxylate cycle were upregulated, and the GO-term 'TCA cycle' was enriched for upregulated genes (**Paper IV: Figure S10**). The glyoxylate and TCA cycles are needed for growth on acetate and their upregulation could be a response to the high concentration of extracellular acetate for the cycle strain during the ethanol phase. Three hours after glucose exhaustion, the control strain started to consume the acetate, which was reduced from 1.35 to 1.30 g/L. In the cycle strain, however, the acetate concentration 4 h after glucose exhaustion was instead increased from 1.72 to 2.27 g/L. A similar acetate profile was observed in shake flasks (**Paper IV: Figure S2**): at 44 h the control had reduced the concentration of acetate after glucose exhaustion (1.1 to 0.8 g/L), while the level of acetate in the cycle was increased after glucose exhaustion (1.8 to 3.5 g/L). This prolonged high concentration of acetate is probably due to a reduced capacity for acetate consumption in combination with excess acetate production in the cycle strain. The respiration chain is the major source of ROS generation in *S. cerevisiae* through leakage of electrons that forms superoxide anions [169]. The prolonged acetate exposure during the ethanol phase might result in increased oxidative stress [167, 168]. We noticed enrichment for upregulated genes in the GO-term 'cellular response to oxidative stress', but only when analyzing just the upregulated genes (**Paper IV: Figure S10**). Evaluation of the ROS levels during the ethanol phase is needed to determine if oxidative stress is contributing to the lower 3-HP titers in the cycle strain during the ethanol phase.

Running the chemostat at a dilution rate of 0.1 h^{-1} resulted in a respiro-fermentative growth of the cycle strain with an accumulation of acetate and glycerol (**Figure 24**). As mentioned earlier, dilution rates below 0.28 h^{-1} usually result in respiratory growth without accumulation of fermentation products [160–162], unless the strains are exposed to stress [163], are under nutrient limitations [164, 165], or have reduced respiratory capacity [92]. The phosphoketolase control did not show overflow metabolism at a dilution rate of 0.1 h^{-1}. Overflow metabolism in *S. cerevisiae* usually involves the accumulation of ethanol, as it reoxidizes the NADH that is generated during glycolysis. The formation of glycerol allows reoxidation of NADH that is generated from biomass formation [81] and can accumulate during a redox imbalance. Another study deleted the major enzymes that shuttle cytosolic NADH to the mitochondria (*NDE1*, *NDE2* and *GUT2*), which resulted in a high glycerol accumulation (0.63 mol/mol) without ethanol formation during a carbon-limited chemostat at a dilution rate of 0.1 h^{-1} [175]. The low glycerol accumulation in the cycle strain (0.07 mol/mol) might indicate problems with redox shuttling of cytosolic NADH to the mitochondria, as no significant accumulation of ethanol was detected. In the cycle strain, *GUT2* and *NDE2* were downregulated (LFC of -1.04 and -0.83, respectively), while *NDE1* was slightly upregulated (LFC of 0.32).

In the chemostat, the cycle strain showed an upregulation of genes involved in glycolysis and production of ethanol and downregulation of *ADH2*, required for ethanol consumption (**Figure 26**). A recent study investigating the level of mRNA, protein, and phosphorylated proteins in chemostat cultures at different dilution rates (from 0.027 to 0.379 h^{-1}) found that the transcript levels of glycolytic genes are downregulated during overflow metabolism at high dilution rates [176]. They could show that the high glycolytic flux at high dilution rates is

instead achieved by a higher degree of dephosphorylation of the glycolytic enzymes. Similarly, glycolytic genes were downregulated during overflow metabolism from 38°C heat stress [163]. A ^{13}C-based metabolic flux analysis and a phosphoproteomics analysis should be performed to determine if the glycolytic flux in the cycle strain is affected by the upregulation on mRNA level during the overflow metabolism. This might help us understand why we do not see any significant ethanol accumulation in the cycle strain (**Figure 24**).

Accumulation of acetate instead of ethanol in the chemostat could indicate a shortage of NADPH, as the formation of acetate from acetaldehyde by Ald6 generates NADPH. As discussed earlier, a saturation of the PPP during NADPH limitations can increase acetate formation [172]. In the wild-type metabolism, 1 mol G6P can be completely oxidized to 12 mol NADPH and 6 mol CO_2 through the combined use of the oxidative PPP, transketolase, transaldolase and gluconeogenesis when demands for NADPH are high. Deletion of the transketolase and transaldolase is required for the GATHCYC and prevents usage of the PPP in this way. Combining the oxidative PPP and the GATHCYC limits the conversion of 1 mol G6P to 4 mol NADPH, 2 mol AcP and 2 mol CO_2. Complete oxidation of G6P might not be possible anyway during batch growth on glucose as *FBP1* is strongly repressed. However, it might have a physiological effect during a carbon-limited chemostat as *FBP1* is strongly upregulated in the chemostat compared to the glucose phase. In any case, it seems unlikely that the deletion of the transketolase and transaldolases is causing a profound NADPH deficiency that requires 22% of the carbon to be converted to acetate.

Changes in gene expression during the chemostat that are consistent with overflow metabolism are the downregulation of glucose-repressed genes in the cycle strain: *ALD4*, converting mitochondrial acetaldehyde to acetate; *ACS1*, converting acetate to acetyl-CoA; *FBP1* and *PCK1* from the gluconeogenesis; and *MLS1*, *MDH2/3* and *IDP2/3* from the glyoxylate cycle (**Figure 26**). These downregulations are also observed during overflow metabolism due to high dilution rates (increasing from 0.1 to 0.379 h^{-1}, dataset from [176]) or 38°C heat stress at a dilution rate of 0.1 h^{-1} [163]. Conducting a TF reporter analysis reveals that Adr1, responsible for activating glucose-repressed genes [177], is enriched for downregulated genes in the chemostat (**Paper IV: Figure S12**). The enrichment of Adr1 for downregulated genes further indicates that glucose repression is occurring in the cycle strain at a dilution rate of 0.1 h^{-1}. The downregulation of *ACS1* and the glyoxylate cycle from glucose repression might lead to reduced acetate consumption and contribute to acetate accumulation. Acetate consumption might be increased by overexpressing acetyl-CoA synthetase, but a glucose pulsing experiment showed that overexpression of either *ACS1* or *ACS2* did not reduce the acetate levels [178]. Overexpressing the acetylation insensitive variant of the acetyl-CoA synthetase from *Salmonella enterica* [179] might be an option, but the focus should be on determining the reason for the repression of *ACS1*. Furthermore, running another chemostat at a lower dilution rate (0.025–0.05 h^{-1}) might be beneficial for reducing the acetate accumulation.

From GO-term analysis of the chemostat, we found enrichment for upregulated genes in the GO-terms ‘translation’, ‘amino acid biosynthesis’, and ‘methionine biosynthetic processes’ (**Figure 28**). Enrichment of these processes usually happens during an increased growth rate [110]. Steady-state cultures in a chemostat should have their growth rate defined by the dilution

rate. The dilution rate for the control and cycle was the same, indicating that the upregulation of amino acid biosynthesis processes is caused by another mechanism. It has been reported that upregulation of amino acid biosynthesis can occur during NADPH limitations [172], which could support acetate formation from Ald6. Another study showed that elevated pools of methionine in *E. coli* mutants led to increased acetic acid resistance [180]. However, measurements of the amino acid pools in control and cycle strains, in combination with follow-up experiments, are needed before any conclusions can be drawn from the upregulation of amino acid biosynthesis processes. We also observed enrichment for upregulated genes in the GO-term 'purine nucleotide biosynthetic process' (**Figure 28**), which could indicate shortages of nucleotide precursors. However, this process was shown to be upregulated in response to increased glucose uptake rate in *E. coli* [181] and we observed a 39% increase in the glucose uptake rate in the cycle strain (**Table 4**). A metabolomics experiment is needed to determine if specific metabolites are limiting.

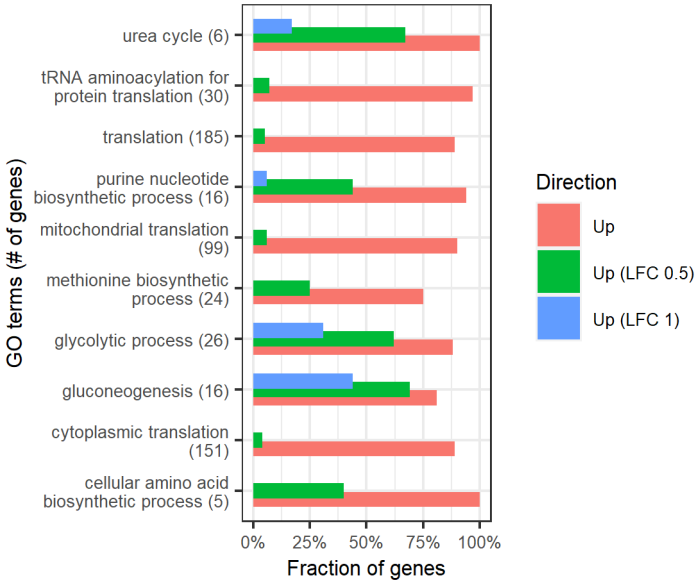

Figure 28. GO-terms involved in biological processes that are enriched for upregulated genes from implementing the GATHCYC to a phosphoketolase expressing strain during chemostat at pH 6. Transcriptomics data were summarized from the consensus heatmap generated with the Piano R-package by filtering the median adjusted p-value below 0.1 for non-directional enrichment and below 0.05 for the distinct up- or downregulated enrichment. The fraction of upregulated genes is shown without filtering (red) and LFC > 0.5 (green) or LFC > 1 (blue) together with an adjusted p-value below 0.01.

Another source of the excess acetate could be the degradation of AcP released from the GATHCYC. AcP can be degraded by Gpp1 and Gpp2 to acetate, with Gpp1 contributing to the majority of the degradation [66, 68]. The addition of the phosphoketolase to a wild-type strain increased the acetate concentration from 0.55 to 1.10 g/L during batch growth (**Figure 3**). With *GPP1* deleted, expanding the phosphoketolase pathway to the GATHCYC increased the acetate concentration from 1.35 to 1.72 g/L at glucose exhaustion (**Table 4**), corresponding to 6.1 and 8.5% relative C-mol flux (**Figure 23**), without affecting the biomass yield. Without acetate kinase, acetate formation from AcP hydrolysis does not generate ATP. Producing acetyl-CoA by hydrolyzing AcP from the GATHCYC and converting it to acetyl-CoA with acetyl-CoA synthetase, instead of converting AcP directly to acetyl-CoA by Pta, adds a cost of

2 ATP per formed acetyl-CoA. As the GATHCYC bypasses the ATP generation from the lower glycolysis, the total cost will be 2.3 ATP/acetyl-CoA from glucose instead of 0.3 ATP/acetyl-CoA if the GATHCYC was used in combination with Pta. The cost of utilizing the PDH bypass for producing cytosolic acetyl-CoA from glucose is 1 ATP/acetyl-CoA. The extra cost in ATP to consume acetate might make it more energetically favorable to export acetate rather than to consume it. In the native metabolism, flux through the PPP can undergo carbon rearrangements by the transketolase and transaldolase to form GAP or F6P that can reenter the glycolysis. Now, with the transketolase and transaldolases deleted, the flux through the oxidative PPP must produce AcP by the Xpk reaction before forming GAP that can reenter the glycolysis (**Figure 26**). As the flux through the oxidative PPP increases from 16% of the glucose uptake rate during batch growth to 45% during chemostat at a dilution rate of 0.1 h^{-1} [182], even more AcP might be produced during the chemostat in the cycle strain. This could result in an acetate production rate that is exceeding the consumption rate, leading to increased export of acetate to avoid acidification of the cytoplasm. To determine the source of the acetate, a ^{13}C-based metabolic flux analysis should be performed.

In conclusion, we further analyzed a *S. cerevisiae* strain that was utilizing the GATHCYC for an additional supply of acetyl-CoA. We showed that in the current state of the GATHCYC, pH 6 was needed during bioreactor fermentation to achieve higher 3-HP titers compared to the phosphoketolase control at the end of the glucose phase. We analyzed the effect of implementing the GATHCYC on a global level by analyzing the proteome and transcriptome during the glucose phase, where we observed an upregulation of genes involved in stress responses and genes involved in NADPH formation. Furthermore, we analyzed the transcriptome during the ethanol phase and chemostat. From the ethanol phase, we observed downregulation of genes within the cycle, which could contribute to the lower titers achieved after the growth on the produced ethanol. Finally, the chemostat culture yielded respiro-fermentative growth at a dilution rate of 0.1 h^{-1}, with acetate as the unusual overflow metabolite and lower 3-HP titers. The acetate overflow could originate from a metabolic imbalance and extensive hydrolysis of AcP to acetate. Resolving the acetate overflow in the GATHCYC is crucial before the cycle can be utilized commercially as part of a platform strain with increased acetyl-CoA supply.

5 Conclusions and perspectives

The work in this thesis focused on the use of the phosphoketolase pathway in the yeast *S. cerevisiae* to increase the supply of the precursor metabolite acetyl-CoA. Acetyl-CoA was chosen because it can be used as a starting point in the production of many industrially relevant products. The aim of this thesis was to investigate if the use of phosphoketolase pathways can enable carbon-conservation in *S. cerevisiae* to improve product yields. Increased product yields would contribute to the profitability of the process and make microbial production of industrially relevant products more attractive compared to petroleum-based sources. This can be a key step towards more sustainable production.

5.1 Part I: The linear phosphoketolase pathway

In **Part I**, we used the phosphoketolase pathway without conducting additional genetic modification to enable the NOG. The linear phosphoketolase pathway requires two enzymes: the phosphoketolase to convert X5P or F6P to AcP and GAP or E4P without carbon loss as CO_2, and Pta to reversibly convert AcP to acetyl-CoA. In **Paper I**, we investigated the effect of adding only the phosphoketolase gene to *S. cerevisiae*. This simulates a scenario in the DBTL cycle where there is a limitation in acetyl-CoA consumption to a production pathway, leading to accumulation of AcP. Without the Pta enzyme, AcP produced from the phosphoketolase cannot be directly converted to acetyl-CoA and is instead degraded to acetate by Gpp1 and Gpp2 [66, 68]. We showed that heterologous expression of the phosphoketolase gene in *S. cerevisiae* increased the flux towards acetate, increased the respiratory demand, and altered the sugar phosphate pool. The reduction in biomass yield in the phosphoketolase expressing strain can be mitigated by cultivating at a higher pH, which reduces the energy wasted on futile transportation of acetate.

To efficiently use the phosphoketolase pathway in the future, efforts should be made to reduce the acetate formation and increase the flux from AcP into acetyl-CoA-derived products. This can be achieved by optimizing Pta through enzymatic engineering to promote acetyl-CoA formation instead of acetyl-CoA consumption. Furthermore, even if AcP hydrolysis to acetate can be reduced by *GPP1* and *GPP2* deletion, extensive acetate formation from AcP hydrolysis still occurred in a synthetic Crabtree-negative *S. cerevisiae* lacking major pathways to acetate through disruption of the PDH bypass by *PDC1*,*5*,*6* deletion [52]. This suggests that there exist additional enzymes in *S. cerevisiae* that can promiscuously degrade AcP to acetate. AcP hydrolysis to acetate does not seem to occur in *Y. lipolytica* [76]. Comparing the degree of AcP breakdown in different yeast species might aid in uncovering the mechanism for AcP hydrolysis in *S. cerevisiae* without Gpp1 or Gpp2.

The phosphoketolase pathway can also be used to supply E4P, demonstrated in **Paper I** with the 5.4-fold increase in E4P concentration in the xfpk(BB) strain. The phosphoketolase pathway was used previously in *S. cerevisiae* to increase the titer of the E4P-derived flavonoid precursor p-coumaric acid in a fed-batch culture with feedbeads [74]. However, the phosphoketolase pathway reduced the titers of 2-phenylethanol [183] and tyrosol [184] during batch cultivation in flasks. The positive effect of the phosphoketolase pathway could only be achieved for tyrosol production when the *pta* gene was not included [184]. This could be

connected to the negative effect on FFA titers from the phosphoketolase pathway during the ethanol phase [155]. The acetyl-CoA produced from ethanol assimilation can be converted to AcP by Pta and further to acetate by Gpp2 or other AcP hydrolyzing activities, where the excess acetate formation could possibly contribute to the lower titers. This suggests that the phosphoketolase pathway should be deployed at conditions where ethanol formation is avoided, for example, in fed-batch cultures.

In **Paper II**, we investigated a combinatorial strategy to improve FFA titers, involving additional acetyl-CoA supply through the phosphoketolase pathway together with additional NADPH supply through overexpression of the TF Stb5. Stb5 has been reported to positively affect NADPH generation by rerouting the flux towards the PPP and activating the expression of several genes coding for enzymes that catalyze reactions with NADPH formation. *STB5* overexpression in our study failed to activate the oxidative PPP during the glucose phase, with H_2O_2 survivability similar to *ZWF1* deletion. However, *STB5* overexpression could increase the titers of FFA during the glucose phase but independently of the oxidative PPP. After the ethanol phase, *STB5* overexpression reduced the FFA titers. Combining the phosphoketolase pathway with *STB5* overexpression also increased the FFA titers only at the end of the glucose phase. RNAseq analysis showed that many targets of Stb5 were regulated in the opposite direction than previously reported during the glucose and ethanol phase, indicating a counteractive response to *STB5* overexpression, possibly due to NADPH overproduction. This counteractive response was not observed in chemostat cultures, with targets of Stb5 being upregulated, possibly due to a higher NADPH demand from increased biomass yield compared to batch culture. Taken together, the strategy of *STB5* overexpression to increase NADPH generation could be effective in strains with a high flux towards product formation requiring NADPH.

Overexpressing a TF to activate multiple targets at once could be an effective solution, however, we lose the control of adjusting the expression of individual genes with this approach. When enhancing the NADPH supply, the whole production pathway should be considered to assure redox balance. Flux in *Y. lipolytica* was pushed through the PPP by phosphofructokinase deletion, which needed implementation and fine-tuning of the phosphoketolase pathway to abolish the resulting growth defects, restore redox balance, and reach improved lipid yields in the end [76]. Instead of increasing the flux through the PPP, another very successful strategy in *Y. lipolytica* recycled NADH to NADPH through the expression of $NADP^+$-dependent GAP dehydrogenase and malic enzyme and could achieve a yield of 0.269 g/g fatty acid methyl esters on glucose, representing 74% of the maximum theoretical yield [185]. More progress needs to be made before *S. cerevisiae* can be utilized as a production host for lipid production, as current lipid content and yields are much lower compared to oleaginous yeasts [98]. Selecting an oleaginous yeast as a production host might be beneficial to have an effective NADPH sink and thus avoiding the counteractive effects from NADPH overproduction.

5.2 Part II: Carbon-conservation with the cyclic phosphoketolase pathway

In the second part of this thesis, we expanded the phosphoketolase pathway to a new configuration of the cyclic NOG that can recycle all the carbon from F6P into 3 mol of acetyl-CoA to enable a further increase of product yields. By using a generalist phosphoketolase that could also convert S7P to AcP, we obtained a configuration of the NOG that does not require the transketolase, transaldolase, or fructose-1,6-bisphosphatase reaction. This new cycle also includes two native reactions from the yeast riboneogenesis pathway. In **Paper III**, we showed through kinetic modeling that this new configuration, the GATHCYC, overcomes the potential limitations of the original NOG. We implemented the GATHCYC in an *S. cerevisiae* strain and could demonstrate *in vitro* activity of the GATHCYC using crude cell-free extracts. We also demonstrated *in vivo* activity of the GATHCYC, which could rescue growth on minimal media by providing R5P in the *tkl1*Δ *tkl2*Δ *zwf1*Δ background. Finally, we used 3-HP as an acetyl-CoA sink and could show that expansion of the linear phosphoketolase pathway to the circular GATHCYC increased 3-HP titers by 109% at the end of the glucose phase. However, the GATHCYC reduced the 3-HP titers after the end of the ethanol phase compared to the phosphoketolase control.

In **Paper IV**, we further characterized the GATHCYC strains in bioreactors. Implementation of the GATHCYC in bioreactor cultures showed an increase in 3-HP titers, but only at pH 6, possibly due to less waste of energy in futile acetate transportation. Even though the non-oxidative PPP was replaced by the GATHCYC, the growth rate was only reduced by 14%. We conducted proteomics and RNAseq analysis during the glucose phase, with additional RNAseq analysis during the ethanol phase and chemostat. During the glucose phase, we observed an upregulation of genes involved in stress responses and NADPH formation. During the ethanol phase, genes within the cycle were downregulated, suspected to cause the reduced 3-HP titers of the GATHCYC during that phase. Chemostat culture with a dilution rate of 0.1 h^{-1} yielded respiro-fermentative growth with acetate as the main overflow metabolite in the GATHCYC strain. This points to a metabolic imbalance and extensive AcP hydrolysis to acetate that needs to be resolved before the GATHCYC can be utilized for acetyl-CoA supply commercially.

GATHCYC needs to be further engineered in the future before it can be efficiently used. For example, the flux through the GATHCYC could potentially be increased by increasing Fba1 activity by removing the inhibitive phosphorylation sites [186–188]. Another option is to use the Fba from cyanobacteria that catalyzes the Sba reaction in the Calvin cycle [189]. The relative Xpk, Fpk and Spk activities should be assessed and balanced for optimal activity in the GATHCYC. This could be performed using an *xfspk* mutant library in a GATHCYC strain where growth is made Xfspk-dependent. A study using *C. glutamicum* managed to increase the Fpk catalytic efficiency by 80% through growth-coupled evolution in a phosphofructokinase deficient strain [190]. Another option is to engineer substrate-specific phosphoketolases and balance their expression levels. The Spk activity of the phosphoketolase was recently demonstrated *in vivo* [132] which in the end allowed implementation of the GATHCYC. There might be additional undiscovered phosphoketolase reactions that could generate AcP from other substrates and allow new carbon-conserving pathways to be discovered. A

phosphoketolase from *Saccharomonospora marina* was discovered to be able to convert glycolaldehyde to AcP, allowing the creation of a synthetic pathway from methanol to acetyl-CoA [191].

The NOG does not generate any energy or reducing power, which restricts complete carbon-conservation to a few selected products not requiring these. To expand the portfolio of products allowing full carbon-conservation, external reducing equivalents could be provided from H_2 [120]. Another option is to balance the flux to a precursor metabolite between a carbon-conserving pathway and cofactor generating pathway to obtain a higher maximum theoretical yield [22, 68, 127]. The work in this thesis will aid the development of new and more effective NOGs to be used as carbon-conserving pathways for improved product yields. This would aid the development of biocatalysts that can allow sustainable production of industrially relevant products, while also being able to compete with processes that involve petroleum-based sources.

6 Acknowledgements

This has been a long journey and it feels great to finally approach the finish line. I'd like to end this thesis by thanking the people who made it possible.

First, I want to thank Jens Nielsen for accepting me into the Sysbio family as a PhD student and introducing me to the project about carbon-conserving cycles. You were always a great source of inspiration and thanks for giving me a lot of scientific freedom to be able to shape the project into my own, allowing me to grow as a researcher.

My deepest thanks go to my supervisor Verena Siewers for all the good advice and for very thoroughly reading all my drafts. You could always find ways to improve them, and I am not sure if I ever disagreed with your comments. Also, thank you for always finding something positive in my results, even when they were not as expected.

I'd like to thank my collaborators Alexei Godina and Olivier Vidalin for trusting me to work with their secret cycles (SPANOG and GATHCYC) during the early days of the project. Thank you for all your feedback and assistance during the monthly meetings we had during my first year as a PhD student.

A lot of thanks also goes to my co-author Alexandra Bergman for allowing me the opportunity to learn and apply the RNAseq analysis in your two projects. Achieving the required four papers without the collaboration with you would have been very hard. Thanks for providing feedback and advice regarding my own projects as well, especially for the phosphoketolase assay experiment.

Being a part of the Sysbio family has been a wondrous experience. There are so many smart and friendly people here who never hesitate to help with any problems, both work- and non-work-related. We also have a great lab maintained by our research engineers, which I'm very thankful for. Thanks to all of you at Sysbio for providing such a great work culture. I will truly miss it.

I'm thankful for all the great support I received from outside work as well. Thanks to all of you in the Stormhök gang from Stockholm and all of you from the Biotech crew in Gothenburg. Thanks to mum, dad, my sisters, and the rest of my family for always being very supportive and believing in me. Most importantly, thank you Josefin for your constant support, love, and encouragement during this tough journey. This could not have been possible without you.

7 References

1. Owusu, P. A. & Asumadu-Sarkodie, S. A review of renewable energy sources, sustainability issues and climate change mitigation. *Cogent Eng.* **3**, 1167990 (2016).

2. Yu, T., Dabirian, Y., Liu, Q., Siewers, V. & Nielsen, J. Strategies and challenges for metabolic rewiring. *Curr. Opin. Syst. Biol.* **15**, 30–38 (2019).

3. Godar, A., Kamoku, C., Nielsen, D. & Wang, X. Synthetic biology strategies to address waste CO_2 loss during biofuel production. *Curr. Opin. Environ. Sci. Heal.* **24**, 100305 (2021).

4. Barnett, J. A. A history of research on yeasts 2: Louis Pasteur and his contemporaries, 1850-1880. *Yeast* **16**, 755–771 (2000).

5. Barnett, J. A. & Lichtenthaler, F. W. A history of research on yeasts 3: Emil Fischer, Eduard Buchner and their contemporaries, 1880-1900. *Yeast* **18**, 363–388 (2001).

6. Goffeau, A. *et al.* Life with 6000 Genes. *Science* **274**, 546–567 (1996).

7. Nielsen, J. Yeast Systems Biology: Model Organism and Cell Factory. *Biotechnol. J.* **14**, 1800421 (2019).

8. Orr-Weaver, T. L., Szostak, J. W. & Rothstein, R. J. Yeast transformation: a model system for the study of recombination. *Proc. Natl. Acad. Sci.* **78**, 6354–6358 (1981).

9. Thim, L., Hansen, M. T. & Sørensen, A. R. Secretion of human insulin by a transformed yeast cell. *FEBS Lett.* **212**, 307–312 (1987).

10. Nielsen, J. & Keasling, J. D. Engineering Cellular Metabolism. *Cell* **164**, 1185–1197 (2016).

11. Nielsen, J. & Jewett, M. C. Impact of systems biology on metabolic engineering of *Saccharomyces cerevisiae*. *FEMS Yeast Res.* **8**, 122–131 (2008).

12. Barnett, J. A. A history of research on yeasts 5: the fermentation pathway. *Yeast* **20**, 509–543 (2003).

13. Kruckeberg, L. & Dickinson, J. R. Carbon metabolism. in *Metabolism and Molecular Physiology of Saccharomyces cerevisiae, 2nd edition* (eds. Dickinson, J. R. & Schweizer, M.) (CRC Press, 2004).

14. Verduyn, C., Stouthamer, A. H., Scheffers, W. A. & van Dijken, J. P. A theoretical evaluation of growth yields of yeasts. *Antonie Van Leeuwenhoek* **59**, 49–63 (1991).

15. De Deken, R. H. The Crabtree effect: a regulatory system in yeast. *J. Gen. Microbiol.* **44**, 149–156 (1966).

16. Nilsson, A. & Nielsen, J. Metabolic Trade-offs in Yeast are Caused by F1F0-ATP synthase. *Sci. Rep.* **6**, 22264 (2016).

17. Vemuri, G. N., Eiteman, M. A., McEwen, J. E., Olsson, L. & Nielsen, J. Increasing NADH oxidation reduces overflow metabolism in *Saccharomyces cerevisiae*. *Proc. Natl. Acad. Sci.* **104**, 2402–2407 (2007).

18. Sánchez, B. J. *et al.* Improving the phenotype predictions of a yeast genome-scale metabolic model by incorporating enzymatic constraints. *Mol. Syst. Biol.* **13**, 935 (2017).

19. Kunze, M., Pracharoenwattana, I., Smith, S. M. & Hartig, A. A central role for the peroxisomal membrane in glyoxylate cycle function. *Biochim. Biophys. Acta - Mol. Cell Res.* **1763**, 1441–1452 (2006).

20. Krivoruchko, A., Zhang, Y., Siewers, V., Chen, Y. & Nielsen, J. Microbial acetyl-CoA metabolism and metabolic engineering. *Metab. Eng.* **28**, 28–42 (2015).

21. Nielsen, J. Synthetic biology for engineering acetyl coenzyme a metabolism in yeast. *MBio* **5**, 14–16 (2014).

22. van Rossum, H. M., Kozak, B. U., Pronk, J. T. & van Maris, A. J. A. Engineering cytosolic acetyl-coenzyme A supply in *Saccharomyces cerevisiae*: Pathway stoichiometry, free-energy conservation and

redox-cofactor balancing. *Metab. Eng.* **36**, 99–115 (2016).

23. Zhang, Q., Zeng, W., Xu, S. & Zhou, J. Metabolism and strategies for enhanced supply of acetyl-CoA in *Saccharomyces cerevisiae*. *Bioresour. Technol.* **342**, 125978 (2021).

24. Wang, Z., Gerstein, M. & Snyder, M. RNA-Seq: a revolutionary tool for transcriptomics. *Nat. Rev. Genet.* **10**, 57–63 (2009).

25. Lowe, R., Shirley, N., Bleackley, M., Dolan, S. & Shafee, T. Transcriptomics technologies. *PLoS Comput. Biol.* **13**, (2017).

26. Black, M. B. *et al.* Comparison of microarrays and RNA-Seq for gene expression analyses of dose-response experiments. *Toxicol. Sci.* **137**, 385–403 (2014).

27. Mantione, K. J. *et al.* Comparing Bioinformatic Gene Expression Profiling Methods: Microarray and RNA-Seq. *Med. Sci. Monit. Basic Res.* **20**, 138–142 (2014).

28. Ozsolak, F. & Milos, P. M. RNA sequencing: advances, challenges and opportunities. *Nat. Rev. Genet.* **12**, 87–98 (2011).

29. Sims, D., Sudbery, I., Ilott, N. E., Heger, A. & Ponting, C. P. Sequencing depth and coverage: Key considerations in genomic analyses. *Nat. Rev. Genet.* **15**, 121–132 (2014).

30. Love, M. I., Huber, W. & Anders, S. Moderated estimation of fold change and dispersion for RNA-seq data with DESeq2. *Genome Biol.* **15**, 550 (2014).

31. Benjamini, Y. & Hochberg, Y. Controlling the False Discovery Rate: A Practical and Powerful Approach to Multiple Testing. *J. R. Stat. Soc. Ser. B* **57**, 289–300 (1995).

32. Ashburner, M. *et al.* Gene Ontology: tool for the unification of biology. *Nat. Genet.* **25**, 25–29 (2000).

33. Väremo, L., Nielsen, J. & Nookaew, I. Enriching the gene set analysis of genome-wide data by incorporating directionality of gene expression and combining statistical hypotheses and methods. *Nucleic Acids Res.* **41**, 4378–4391 (2013).

34. Baumann, L. *et al.* Transcriptomic response of *Saccharomyces cerevisiae* to octanoic acid production. *FEMS Yeast Res.* **21**, 1–9 (2021).

35. Dong, C. *et al.* Identification of novel metabolic engineering targets for S-adenosyl-L-methionine production in *Saccharomyces cerevisiae* via genome-scale engineering. *Metab. Eng.* **66**, 319–327 (2021).

36. Kim, S.-K., Jin, Y.-S., Choi, I.-G., Park, Y.-C. & Seo, J.-H. Enhanced tolerance of *Saccharomyces cerevisiae* to multiple lignocellulose-derived inhibitors through modulation of spermidine contents. *Metab. Eng.* **29**, 46–55 (2015).

37. Li, X. *et al.* Metabolic network remodelling enhances yeast's fitness on xylose using aerobic glycolysis. *Nat. Catal.* **4**, 783–796 (2021).

38. Macklin, A., Khan, S. & Kislinger, T. Recent advances in mass spectrometry based clinical proteomics: applications to cancer research. *Clin. Proteomics* **17**, 17 (2020).

39. Yu, R. *et al.* Nitrogen limitation reveals large reserves in metabolic and translational capacities of yeast. *Nat. Commun.* **11**, 1881 (2020).

40. Thompson, A. *et al.* Tandem Mass Tags: A Novel Quantification Strategy for Comparative Analysis of Complex Protein Mixtures by MS/MS. *Anal. Chem.* **75**, 1895–1904 (2003).

41. Zhu, Y. *et al.* DEqMS: A method for accurate variance estimation in differential protein expression analysis. *Mol. Cell. Proteomics* **19**, 1047–1057 (2020).

42. Pereira, F. *et al.* Model-guided development of an evolutionarily stable yeast chassis. *Mol. Syst. Biol.* **17**, 1–18 (2021).

43. Varela, C. *et al.* Systems-based approaches enable identification of gene targets which improve the flavour profile of low-ethanol wine yeast strains. *Metab. Eng.* **49**, 178–191 (2018).

44. Wronska, A. K. *et al.* Engineering oxygen-independent biotin biosynthesis in *Saccharomyces cerevisiae*. *Metab. Eng.* **67**, 88–103 (2021).

45. Rodriguez, A., Kildegaard, K. R., Li, M., Borodina, I. & Nielsen, J. Establishment of a yeast platform strain for production of p-coumaric acid through metabolic engineering of aromatic amino acid biosynthesis. *Metab. Eng.* **31**, 181–188 (2015).

46. Wegner, S. A. *et al.* Engineering acetyl-CoA supply and *ERG9* repression to enhance mevalonate production in *Saccharomyces cerevisiae*. *J. Ind. Microbiol. Biotechnol.* (2021) doi:10.1093/jimb/kuab050.

47. Shiba, Y., Paradise, E. M., Kirby, J., Ro, D.-K. & Keasling, J. D. Engineering of the pyruvate dehydrogenase bypass in *Saccharomyces cerevisiae* for high-level production of isoprenoids. *Metab. Eng.* **9**, 160–168 (2007).

48. Yee, D. A. *et al.* Engineered mitochondrial production of monoterpenes in *Saccharomyces cerevisiae*. *Metab. Eng.* **55**, 76–84 (2019).

49. Kozak, B. U. *et al.* Replacement of the *Saccharomyces cerevisiae* acetyl-CoA synthetases by alternative pathways for cytosolic acetyl-CoA synthesis. *Metab. Eng.* **21**, 46–59 (2014).

50. Kozak, B. U. *et al.* Engineering Acetyl Coenzyme A Supply: Functional Expression of a Bacterial Pyruvate Dehydrogenase Complex in the Cytosol of *Saccharomyces cerevisiae*. *MBio* **5**, e01696-14 (2014).

51. Zhang, Y., Su, M., Qin, N., Nielsen, J. & Liu, Z. Expressing a cytosolic pyruvate dehydrogenase complex to increase free fatty acid production in *Saccharomyces cerevisiae*. *Microb. Cell Fact.* **19**, 226 (2020).

52. Dai, Z., Huang, M., Chen, Y., Siewers, V. & Nielsen, J. Global rewiring of cellular metabolism renders *Saccharomyces cerevisiae* Crabtree negative. *Nat. Commun.* **9**, 3059 (2018).

53. Zhang, Y. *et al.* Functional pyruvate formate lyase pathway expressed with two different electron donors in *Saccharomyces cerevisiae* at aerobic growth. *FEMS Yeast Res.* **15**, 1–8 (2015).

54. van Rossum, H. M. *et al.* Requirements for Carnitine Shuttle-Mediated Translocation of Mitochondrial Acetyl Moieties to the Yeast Cytosol. *MBio* **7**, (2016).

55. Boulton, C. A. & Ratledge, C. Correlation of lipid accumulation in yeasts with possession of ATP:citrate lyase. *J. Gen. Microbiol.* **127**, 169–176 (1981).

56. Zhu, Z. *et al.* Multidimensional engineering of *Saccharomyces cerevisiae* for efficient synthesis of medium-chain fatty acids. *Nat. Catal.* **3**, 64–74 (2020).

57. Yu, T. *et al.* Reprogramming Yeast Metabolism from Alcoholic Fermentation to Lipogenesis. *Cell* **174**, 1549-1558.e14 (2018).

58. Lynd, L. R., Wyman, C. E. & Gerngross, T. U. Biocommodity Engineering. *Biotechnol. Prog.* **15**, 777–793 (1999).

59. Bar-Even, A., Noor, E., Lewis, N. E. & Milo, R. Design and analysis of synthetic carbon fixation pathways. *Proc. Natl. Acad. Sci.* **107**, 8889–8894 (2010).

60. Guadalupe-Medina, V. *et al.* Carbon dioxide fixation by Calvin-Cycle enzymes improves ethanol yield in yeast. *Biotechnol. Biofuels* **6**, 125 (2013).

61. Papapetridis, I. *et al.* Optimizing anaerobic growth rate and fermentation kinetics in *Saccharomyces cerevisiae* strains expressing Calvin-cycle enzymes for improved ethanol yield. *Biotechnol. Biofuels* **11**, 17 (2018).

62. Xu, G. *et al.* Semi-rational evolution of pyruvate carboxylase from *Rhizopus oryzae* for elevated fumaric

acid synthesis in *Saccharomyces cerevisiae*. *Biochem. Eng. J.* **177**, 108238 (2022).

63. Henard, C. A., Freed, E. F. & Guarnieri, M. T. Phosphoketolase pathway engineering for carbon-efficient biocatalysis. *Curr. Opin. Biotechnol.* **36**, 183–188 (2015).

64. Tittmann, K. Sweet siblings with different faces: The mechanisms of FBP and F6P aldolase, transaldolase, transketolase and phosphoketolase revisited in light of recent structural data. *Bioorg. Chem.* **57**, 263–280 (2014).

65. Flamholz, A., Noor, E., Bar-Even, A. & Milo, R. eQuilibrator - the biochemical thermodynamics calculator. *Nucleic Acids Res.* **40**, D770–D775 (2012).

66. Bergman, A., Siewers, V., Nielsen, J. & Chen, Y. Functional expression and evaluation of heterologous phosphoketolases in *Saccharomyces cerevisiae*. *AMB Express* **6**, 115 (2016).

67. Suzuki, R. *et al.* Crystal structures of phosphoketolase: thiamine diphosphate-dependent dehydration mechanism. *J. Biol. Chem.* **285**, 34279–87 (2010).

68. Meadows, A. L. *et al.* Rewriting yeast central carbon metabolism for industrial isoprenoid production. *Nature* **537**, 694–697 (2016).

69. de Jong, B. W., Shi, S., Siewers, V. & Nielsen, J. Improved production of fatty acid ethyl esters in *Saccharomyces cerevisiae* through up-regulation of the ethanol degradation pathway and expression of the heterologous phosphoketolase pathway. *Microb. Cell Fact.* **13**, 39 (2014).

70. Liu, H., Fan, J., Wang, C., Li, C. & Zhou, X. Enhanced β-Amyrin Synthesis in *Saccharomyces cerevisiae* by Coupling An Optimal Acetyl-CoA Supply Pathway. *J. Agric. Food Chem.* **67**, 3723–3732 (2019).

71. Wernig, F., Baumann, L., Boles, E. & Oreb, M. Production of octanoic acid in *Saccharomyces cerevisiae*: Investigation of new precursor supply engineering strategies and intrinsic limitations. *Biotechnol. Bioeng.* **118**, 3046–3057 (2021).

72. Kocharin, K., Siewers, V. & Nielsen, J. Improved polyhydroxybutyrate production by *Saccharomyces cerevisiae* through the use of the phosphoketolase pathway. *Biotechnol. Bioeng.* **110**, 2216–2224 (2013).

73. Qin, N. *et al.* Rewiring Central Carbon Metabolism Ensures Increased Provision of Acetyl-CoA and NADPH Required for 3-OH-Propionic Acid Production. *ACS Synth. Biol.* **9**, 3236–3244 (2020).

74. Liu, Q. *et al.* Rewiring carbon metabolism in yeast for high level production of aromatic chemicals. *Nat. Commun.* **10**, 4976 (2019).

75. Niehus, X., Crutz-Le Coq, A.-M., Sandoval, G., Nicaud, J.-M. & Ledesma-Amaro, R. Engineering *Yarrowia lipolytica* to enhance lipid production from lignocellulosic materials. *Biotechnol. Biofuels* **11**, 11 (2018).

76. Kamineni, A. *et al.* Increasing lipid yield in *Yarrowia lipolytica* through phosphoketolase and phosphotransacetylase expression in a phosphofructokinase deletion strain. *Biotechnol. Biofuels* **14**, 113 (2021).

77. Song, X. *et al.* Engineering a Central Carbon Metabolism Pathway to Increase the Intracellular Acetyl-CoA Pool in *Synechocystis* sp. PCC 6803 Grown under Photomixotrophic Conditions. *ACS Synth. Biol.* **10**, 836–846 (2021).

78. Henard, C. A., Smith, H. K. & Guarnieri, M. T. Phosphoketolase overexpression increases biomass and lipid yield from methane in an obligate methanotrophic biocatalyst. *Metab. Eng.* **41**, 152–158 (2017).

79. Evans, C. T. & Ratledge, C. Induction of xylulose-5-phosphate phosphoketolase in a variety of yeasts grown ond-xylose: the key to efficient xylose metabolism. *Arch. Microbiol.* **139**, 48–52 (1984).

80. Chen, Y., Partow, S., Scalcinati, G., Siewers, V. & Nielsen, J. Enhancing the copy number of episomal plasmids in *Saccharomyces cerevisiae* for improved protein production. *FEMS Yeast Res.* **12**, 598–607 (2012).

81. Dijken, J. P. & Scheffers, W. A. Redox balances in the metabolism of sugars by yeasts. *FEMS Microbiol. Lett.* **32**, 199–224 (1986).

82. Luli, G. W. & Strohl, W. R. Comparison of growth, acetate production, and acetate inhibition of *Escherichia coli* strains in batch and fed-batch fermentations. *Appl. Environ. Microbiol.* **56**, 1004–1011 (1990).

83. Ramos, J., Sychrová, H. & Kschischo, M. Carboxylic acids plasma membrane transporter. in *Yeast Membrane Transporter* (eds. Ramos, J., Sychrová, H. & Kschischo, M.) vol. 892 299–51 (Springer International Publishing, 2016).

84. Ullah, A., Chandrasekaran, G., Brul, S. & Smits, G. J. Yeast adaptation to weak acids prevents futile energy expenditure. *Front. Microbiol.* **4**, 1–10 (2013).

85. Heyland, J., Fu, J. & Blank, L. M. Correlation between TCA cycle flux and glucose uptake rate during respiro-fermentative growth of *Saccharomyces cerevisiae*. *Microbiology* **155**, 3827–3837 (2009).

86. Lindberg, L., Santos, A. X. S., Riezman, H., Olsson, L. & Bettiga, M. Lipidomic Profiling of *Saccharomyces cerevisiae* and *Zygosaccharomyces bailii* Reveals Critical Changes in Lipid Composition in Response to Acetic Acid Stress. *PLoS One* **8**, e73936 (2013).

87. Eglinton, J. M. *et al.* Decreasing acetic acid accumulation by a glycerol overproducing strain of *Saccharomyces cerevisiae* by deletiong the *ALD6* aldehyde dehydrogenase gene. *Yeast* **19**, 295–301 (2002).

88. Bergman, A. *et al.* Heterologous phosphoketolase expression redirects flux towards acetate, perturbs sugar phosphate pools and increases respiratory demand in *Saccharomyces cerevisiae*. *Microb. Cell Fact.* **18**, 25 (2019).

89. van den Berg, M. A. *et al.* The Two Acetyl-coenzyme A Synthetases of *Saccharomyces cerevisiae* Differ with Respect to Kinetic Properties and Transcriptional Regulation. *J. Biol. Chem.* **271**, 28953–28959 (1996).

90. Fleck, C. B. & Brock, M. Re-characterisation of *Saccharomyces cerevisiae* Ach1p: Fungal CoA-transferases are involved in acetic acid detoxification. *Fungal Genet. Biol.* **46**, 473–485 (2009).

91. Hampsey, M. A Review of Phenotypes in *Saccharomyces cerevisiae*. *Yeast* **13**, 1099–1133 (1997).

92. Raghevendran, V., Patil, K. R., Olsson, L. & Nielsen, J. Hap4 Is Not Essential for Activation of Respiration at Low Specific Growth Rates in *Saccharomyces cerevisiae*. *J. Biol. Chem.* **281**, 12308–12314 (2006).

93. Daran-Lapujade, P. *et al.* Role of transcriptional regulation in controlling fluxes in central carbon metabolism of *Saccharomyces cerevisiae*. A chemostat culture study. *J. Biol. Chem.* **279**, 9125–38 (2004).

94. Karim, A. S., Curran, K. A. & Alper, H. S. Characterization of plasmid burden and copy number in *Saccharomyces cerevisiae* for optimization of metabolic engineering applications. *FEMS Yeast Res.* **13**, 107–116 (2013).

95. Zrimec, J. *et al.* Deep learning suggests that gene expression is encoded in all parts of a co-evolving interacting gene regulatory structure. *Nat. Commun.* **11**, 6141 (2020).

96. Liu, Q., Liu, Y., Chen, Y. & Nielsen, J. Current state of aromatics production using yeast: achievements and challenges. *Curr. Opin. Biotechnol.* **65**, 65–74 (2020).

97. Suástegui, M., Guo, W., Feng, X. & Shao, Z. Investigating strain dependency in the production of aromatic compounds in *Saccharomyces cerevisiae*. *Biotechnol. Bioeng.* **113**, 2676–2685 (2016).

98. Liu, Z., Moradi, H., Shi, S. & Darvishi, F. Yeasts as microbial cell factories for sustainable production of biofuels. *Renew. Sustain. Energy Rev.* **143**, 110907 (2021).

99. Larochelle, M., Drouin, S., Robert, F. & Turcotte, B. Oxidative Stress-Activated Zinc Cluster Protein Stb5 Has Dual Activator/Repressor Functions Required for Pentose Phosphate Pathway Regulation and

NADPH Production. *Mol. Cell. Biol.* **26**, 6690–6701 (2006).

100. Shi, F., Kawai, S., Mori, S., Kono, E. & Murata, K. Identification of ATP-NADH kinase isozymes and their contribution to supply of NADP(H) in *Saccharomyces cerevisiae*. *FEBS J.* **272**, 3337–3349 (2005).

101. Rintala, E., Pitkänen, J.-P., Vehkomäki, M.-L., Penttilä, M. & Ruohonen, L. The ORF *YNL274c* (*GOR1*) codes for glyoxylate reductase in *Saccharomyces cerevisiae*. *Yeast* **24**, 129–136 (2007).

102. Bergman, A. *et al.* Effects of overexpression of *STB5* in *Saccharomyces cerevisiae* on fatty acid biosynthesis, physiology and transcriptome. *FEMS Yeast Res.* **19**, 27 (2019).

103. Partow, S., Siewers, V., Bjørn, S., Nielsen, J. & Maury, J. Characterization of different promoters for designing a new expression vector in *Saccharomyces cerevisiae*. *Yeast* **27**, 955–964 (2010).

104. Peng, B., Williams, T. C., Henry, M., Nielsen, L. K. & Vickers, C. E. Controlling heterologous gene expression in yeast cell factories on different carbon substrates and across the diauxic shift: a comparison of yeast promoter activities. *Microb. Cell Fact.* **14**, 91 (2015).

105. Hector, R. E., Bowman, M. J., Skory, C. D. & Cotta, M. A. The *Saccharomyces cerevisiae YMR315W* gene encodes an NADP(H)-specific oxidoreductase regulated by the transcription factor Stb5p in response to NADPH limitation. *N. Biotechnol.* **26**, 171–180 (2009).

106. Morano, K. A., Grant, C. M. & Moye-Rowley, W. S. The Response to Heat Shock and Oxidative Stress in *Saccharomyces cerevisiae*. *Genetics* **190**, 1157–1195 (2012).

107. Ralser, M. *et al.* Dynamic rerouting of the carbohydrate flux is key to counteracting oxidative stress. *J. Biol.* **6**, (2007).

108. Scharnewski, M., Pongdontri, P., Mora, G., Hoppert, M. & Fulda, M. Mutants of *Saccharomyces cerevisiae* deficient in acyl-CoA synthetases secrete fatty acids due to interrupted fatty acid recycling. *FEBS J.* **275**, 2765–2778 (2008).

109. Yadav, S., Mody, T. A., Sharma, A. & Bachhawat, A. K. A Genetic Screen To Identify Genes Influencing the Secondary Redox Couple NADPH/$NADP^+$ in the Yeast *Saccharomyces cerevisiae*. *G3 Genes|Genomes|Genetics* **10**, 371–378 (2020).

110. Regenberg, B. *et al.* Growth-rate regulated genes have profound impact on interpretation of transcriptome profiling in *Saccharomyces cerevisiae*. *Genome Biol.* **7**, R107 (2006).

111. Monteiro, P. T. *et al.* YEASTRACT+: a portal for cross-species comparative genomics of transcription regulation in yeasts. *Nucleic Acids Res.* **48**, D642–D649 (2020).

112. Martínez-Pastor, M. T. *et al.* The *Saccharomyces cerevisiae* zinc finger proteins Msn2p and Msn4p are required for transcriptional induction through the stress response element (STRE). *EMBO J.* **15**, 2227–2235 (1996).

113. Young, E. T., Dombek, K. M., Tachibana, C. & Ideker, T. Multiple Pathways Are Co-regulated by the Protein Kinase Snf1 and the Transcription Factors Adr1 and Cat8. *J. Biol. Chem.* **278**, 26146–26158 (2003).

114. Ouyang, L., Holland, P., Lu, H., Bergenholm, D. & Nielsen, J. Integrated analysis of the yeast NADPH-regulator Stb5 reveals distinct differences in NADPH requirements and regulation in different states of yeast metabolism. *FEMS Yeast Res.* **18**, (2018).

115. Liu, Q. *et al.* De novo biosynthesis of bioactive isoflavonoids by engineered yeast cell factories. *Nat. Commun.* **12**, 6085 (2021).

116. Schramm, M. & Racker, E. Formation of Erythrose-4-phosphate and Acetyl Phosphate by a Phosphorolytic Cleavage of Fructose-6-phosphate. *Nature* **179**, 1349–1350 (1957).

117. Schramm, M., Klybas, V. & Racker, E. Phosphorolytic Cleavage of Fructose-6-phosphate by from *Acetobacter xylinum*. *J. Biol. Chem* **233**, 1283–1288 (1958).

118. Hellgren, J., Godina, A., Nielsen, J. & Siewers, V. Promiscuous phosphoketolase and metabolic rewiring enables novel non-oxidative glycolysis in yeast for high-yield production of acetyl-CoA derived products. *Metab. Eng.* **62**, 150–160 (2020).

119. Bogorad, I. W., Lin, T.-S. & Liao, J. C. Synthetic non-oxidative glycolysis enables complete carbon conservation. *Nature* **502**, 693–7 (2013).

120. Lin, P. P. *et al.* Construction and evolution of an *Escherichia coli* strain relying on nonoxidative glycolysis for sugar catabolism. *Proc. Natl. Acad. Sci. U. S. A.* **115**, 3538–3546 (2018).

121. Yang, X. *et al.* An engineered non-oxidative glycolysis pathway for acetone production in *Escherichia coli*. *Biotechnol. Lett.* **38**, 1359–1365 (2016).

122. Sauer, M. Industrial production of acetone and butanol by fermentation—100 years later. *FEMS Microbiol. Lett.* **363**, fnw134 (2016).

123. Zhu, L., Zhang, J., Yang, J., Jiang, Y. & Yang, S. Strategies for optimizing acetyl-CoA formation from glucose in bacteria. *Trends Biotechnol.* 1–17 (2021) doi:10.1016/j.tibtech.2021.04.004.

124. Brown, G. *et al.* Structural and biochemical characterization of the type II fructose-1,6-bisphosphatase GlpX from *Escherichia coli*. *J. Biol. Chem.* **284**, 3784–92 (2009).

125. Wang, Q. *et al.* Engineering an *in vivo* EP-bifido pathway in *Escherichia coli* for high-yield acetyl-CoA generation with low CO_2 emission. *Metab. Eng.* **51**, 79–87 (2019).

126. Li, Y. *et al.* Fine tuning the glycolytic flux ratio of EP-bifido pathway for mevalonate production by enhancing glucose-6-phosphate dehydrogenase (Zwf) and CRISPRi suppressing 6-phosphofructose kinase (PfkA) in *Escherichia coli*. *Microb. Cell Fact.* **20**, 32 (2021).

127. Wang, J. *et al.* Tunable hybrid carbon metabolism coordination for the carbon-efficient biosynthesis of 1,3-butanediol in *Escherichia coli*. *Green Chem.* (2021) doi:10.1039/D1GC02867G.

128. Lee, Y., Cho, H. J., Choi, J. & Woo, H. M. Hybrid Embden–Meyerhof–Parnas Pathway for Reducing CO_2 Loss and Increasing the Acetyl-CoA Levels during Microbial Fermentation. *ACS Sustain. Chem. Eng.* **9**, 12394–12405 (2021).

129. Lin, Z. *et al.* Metabolic engineering of *Escherichia coli* for poly(3-hydroxybutyrate) production via threonine bypass. *Microb. Cell Fact.* **14**, 185 (2015).

130. Andersen, J. L., Flamm, C., Merkle, D. & Stadler, P. F. Chemical Transformation Motifs—Modelling Pathways as Integer Hyperflows. *IEEE/ACM Trans. Comput. Biol. Bioinforma.* **16**, 510–523 (2019).

131. Beck, Z. Q., Eliot, A. C., Peres, C. M. & Vaviline, D. V. Utilization of phosphoketolase in the production of mevalonate, isoprenoid precursors, and isoprene. *US Pat.* **8,993,305**, (2015).

132. Krüsemann, J. L. *et al.* Artificial pathway emergence in central metabolism from three recursive phosphoketolase reactions. *FEBS J.* **285**, 4367–4377 (2018).

133. Zhao, G. & Winkler, M. E. An *Escherichia coli* K-12 *tktA tktB* mutant deficient in transketolase activity requires pyridoxine (vitamin B6) as well as the aromatic amino acids and vitamins for growth. *J. Bacteriol.* **176**, 6134–6138 (1994).

134. Calvin, M. The Path of Carbon in Photosynthesis. *Science* **135**, 879–889 (1962).

135. Nakahigashi, K. *et al.* Systematic phenome analysis of *Escherichia coli* multiple-knockout mutants reveals hidden reactions in central carbon metabolism. *Mol. Syst. Biol.* **5**, 306 (2009).

136. Woolston, B. M., King, J. R., Reiter, M., Van Hove, B. & Stephanopoulos, G. Improving formaldehyde consumption drives methanol assimilation in engineered *E. coli*. *Nat. Commun.* **9**, 2387 (2018).

137. Stolzenberger, J., Lindner, S. N., Persicke, M., Brautaset, T. & Wendisch, V. F. Characterization of fructose 1,6-bisphosphatase and sedoheptulose 1,7-bisphosphatase from the facultative ribulose monophosphate cycle methylotroph *Bacillus methanolicus*. *J. Bacteriol.* **195**, 5112–5122 (2013).

138. Fan, L. *et al.* Transcriptome analysis reveals the roles of nitrogen metabolism and sedoheptulose bisphosphatase pathway in methanol-dependent growth of *Corynebacterium glutamicum*. *Microb. Biotechnol.* **14**, 1797–1808 (2021).

139. Clasquin, M. F. *et al.* Riboneogenesis in yeast. *Cell* **145**, 969–980 (2011).

140. Hoops, S. *et al.* COPASI-a COmplex PAthway SImulator. *Bioinformatics* **22**, 3067–3074 (2006).

141. Xu, H. *et al. PHO13* deletion-induced transcriptional activation prevents sedoheptulose accumulation during xylose metabolism in engineered *Saccharomyces cerevisiae*. *Metab. Eng.* **34**, 88–96 (2016).

142. Takahashi, K. *et al.* Crystal structure of *Bifidobacterium Longum* phosphoketolase; key enzyme for glucose metabolism in Bifidobacterium. *FEBS Lett.* **584**, 3855–3861 (2010).

143. Hu, Y. *et al.* Metabolic engineering of *Saccharomyces cerevisiae* for production of germacrene A, a precursor of beta-elemene. *J. Ind. Microbiol. Biotechnol.* **44**, 1065–1072 (2017).

144. Racker, E. Fructose-6-phosphate phosphoketolase from *Acetobacter xylinum*. *Methods Enzymol.* **5**, 276–280 (1962).

145. Senac, T. & Hahn-Hagerdal, B. Intermediary metabolite concentrations in xylulose- and glucose-fermenting *Saccharomyces cerevisiae cells*. *Appl. Environ. Microbiol.* **56**, 120–126 (1990).

146. Schaaff-Gerstenschläger, I., Mannhaupt, G., Vetter, I., Zimmermann, F. K. & Feldmann, H. *TKL2*, a second transketolase gene of *Saccharomyces cerevisiae*. *Eur. J. Biochem.* **217**, 487–492 (1993).

147. Blazeck, J., Garg, R., Reed, B. & Alper, H. S. Controlling promoter strength and regulation in *Saccharomyces cerevisiae* using synthetic hybrid promoters. *Biotechnol. Bioeng.* **109**, 2884–2895 (2012).

148. Weinhandl, K., Winkler, M., Glieder, A. & Camattari, A. Carbon source dependent promoters in yeasts. *Microb. Cell Fact.* **13**, 5 (2014).

149. de Fouchécour, F., Sánchez-Castañeda, A.-K., Saulou-Bérion, C. & Spinnler, H. É. Process engineering for microbial production of 3-hydroxypropionic acid. *Biotechnol. Adv.* **36**, 1207–1222 (2018).

150. Jiang, X., Meng, X. & Xian, M. Biosynthetic pathways for 3-hydroxypropionic acid production. *Appl. Microbiol. Biotechnol.* **82**, 995–1003 (2009).

151. Hügler, M., Menendez, C., Schägger, H. & Fuchs, G. Malonyl-coenzyme a reductase from *Chloroflexus aurantiacus*, a key enzyme of the 3-hydroxypropionate cycle for autotrophic CO_2 fixation. *J. Bacteriol.* **184**, 2404–2410 (2002).

152. Chen, Y., Bao, J., Kim, I.-K., Siewers, V. & Nielsen, J. Coupled incremental precursor and co-factor supply improves 3-hydroxypropionic acid production in *Saccharomyces cerevisiae*. *Metab. Eng.* **22**, 104–109 (2014).

153. Shi, S., Chen, Y., Siewers, V. & Nielsen, J. Improving Production of Malonyl Coenzyme A-Derived Metabolites by Abolishing Snf1-Dependent Regulation of Acc1. *MBio* **5**, (2014).

154. Liu, C. *et al.* Functional balance between enzymes in malonyl-CoA pathway for 3-hydroxypropionate biosynthesis. *Metab. Eng.* **34**, 104–111 (2016).

155. Bergman, A. Evaluation of precursor and cofactor engineering strategies influencing fatty acid metabolism in *Saccharomyces cerevisiae*. *Doctoral thesis* (Chalmers University of Technology, 2019).

156. Tolosa, L., Kostov, Y., Harms, P. & Rao, G. Noninvasive measurement of dissolved oxygen in shake flasks. *Biotechnol. Bioeng.* **80**, 594–597 (2002).

157. van Dijken, J. . *et al.* An interlaboratory comparison of physiological and genetic properties of four *Saccharomyces cerevisiae* strains. *Enzyme Microb. Technol.* **26**, 706–714 (2000).

158. Kildegaard, K. R. *et al.* Engineering and systems-level analysis of *Saccharomyces cerevisiae* for production of 3-hydroxypropionic acid via malonyl-CoA reductase-dependent pathway. *Microb. Cell*

Fact. **15**, 53 (2016).

159. Klosinska, M. M., Crutchfield, C. A., Bradley, P. H., Rabinowitz, J. D. & Broach, J. R. Yeast cells can access distinct quiescent states. *Genes Dev.* **25**, 336–349 (2011).

160. Diderich, J. A. *et al.* Glucose uptake kinetics and transcription of *HXT* genes in chemostat cultures of *Saccharomyces cerevisiae*. *J. Biol. Chem.* **274**, 15350–15359 (1999).

161. Postma, E., Verduyn, C., Scheffers, W. A. & Van Dijken, J. P. Enzymic analysis of the crabtree effect in glucose-limited chemostat cultures of *Saccharomyces cerevisiae*. *Appl. Environ. Microbiol.* **55**, 468–477 (1989).

162. Van Hoek, P., Van Dijken, J. P. & Pronk, J. T. Effect of Specific Growth Rate on Fermentative Capacity of Baker's Yeast. *Appl. Environ. Microbiol.* **64**, 4226–4233 (1998).

163. Lahtvee, P.-J., Kumar, R., Hallström, B. M. & Nielsen, J. Adaptation to different types of stress converge on mitochondrial metabolism. *Mol. Biol. Cell* **27**, 2505–2514 (2016).

164. Basso, T. O., Dario, M. G., Tonso, A., Stambuk, B. U. & Gombert, A. K. Insufficient uracil supply in fully aerobic chemostat cultures of *Saccharomyces cerevisiae* leads to respiro-fermentative metabolism and double nutrient-limitation. *Biotechnol. Lett.* **32**, 973–977 (2010).

165. Scalcinati, G. *et al.* Combined metabolic engineering of precursor and co-factor supply to increase α-santalene production by *Saccharomyces cerevisiae*. *Microb. Cell Fact.* **11**, 117 (2012).

166. Szenk, M., Dill, K. A. & de Graff, A. M. R. Why Do Fast-Growing Bacteria Enter Overflow Metabolism? Testing the Membrane Real Estate Hypothesis. *Cell Syst.* **5**, 95–104 (2017).

167. Semchyshyn, H. M., Abrat, O. B., Miedzobrodzki, J., Inoue, Y. & Lushchak, V. I. Acetate but not propionate induces oxidative stress in bakers' yeast *Saccharomyces cerevisiae*. *Redox Rep.* **16**, 15–23 (2011).

168. Guo, Z. & Olsson, L. Physiological responses to acid stress by *Saccharomyces cerevisiae* when applying high initial cell density. *FEMS Yeast Res.* **16**, fow072 (2016).

169. Aung-Htut, M. T., Ayer, A., Breitenbach, M. & Dawes, I. W. Oxidative stresses and ageing. in *Subcellular Biochemistry* (ed. Breitenbach, M.) vol. 57 13–54 (Springer, 2012).

170. Martani, F. *et al.* Different response to acetic acid stress in *Saccharomyces cerevisiae* wild-type and l -ascorbic acid-producing strains. *Yeast* **30**, 365–378 (2013).

171. HENDERSON, L. M. & CHAPPELL, J. B. Dihydrorhodamine 123: a fluorescent probe for superoxide generation? *Eur. J. Biochem.* **217**, 973–980 (1993).

172. Celton, M. *et al.* A comparative transcriptomic, fluxomic and metabolomic analysis of the response of *Saccharomyces cerevisiae* to increases in NADPH oxidation. *BMC Genomics* **13**, 317 (2012).

173. Kim, S. R. *et al.* Deletion of *PHO13*, Encoding Haloacid Dehalogenase Type IIA Phosphatase, Results in Upregulation of the Pentose Phosphate Pathway in *Saccharomyces cerevisiae*. *Appl. Environ. Microbiol.* **81**, 1601–1609 (2015).

174. Keren, L. *et al.* Promoters maintain their relative activity levels under different growth conditions. *Mol. Syst. Biol.* **9**, 701 (2013).

175. Overkamp, K. M. *et al.* In Vivo Analysis of the Mechanisms for Oxidation of Cytosolic NADH by *Saccharomyces cerevisiae* Mitochondria. *J. Bacteriol.* **182**, 2823–2830 (2000).

176. Xia, J. *et al.* Proteome allocations change linearly with specic growth rate of *Saccharomyces cerevisiae* under glucose-limitation. *PREPRINT* Version 1 (2021) doi:10.21203/rs.3.rs-464207/v1.

177. Turcotte, B., Liang, X. B., Robert, F. & Soontorngun, N. Transcriptional regulation of nonfermentable carbon utilization in budding yeast. *FEMS Yeast Res.* **10**, 2–13 (2010).

178. De Jong-Gubbels, P. *et al.* Overproduction of acetyl-coenzyme A synthetase isoenzymes in respiring *Saccharomyces cerevisiae* cells does not reduce acetate production after exposure to glucose excess. *FEMS Microbiol. Lett.* **165**, 15–20 (1998).

179. Starai, V. J., Gardner, J. G. & Escalante-semerena, J. C. Residue Leu-641 of Acetyl-CoA Synthetase is Critical for the Acetylation of Residue Lys-609 by the Protein Acetyltransferase Enzyme of *Salmonella enterica*. *J. Biol. Chem.* **280**, 26200–26205 (2005).

180. Roe, A. J., O'Byrne, C., McLaggan, D. & Booth, I. R. Inhibition of *Escherichia coli* growth by acetic acid: A problem with methionine biosynthesis and homocysteine toxicity. *Microbiology* **148**, 2215–2222 (2002).

181. Vemuri, G. N., Altman, E., Sangurdekar, D. P., Khodursky, A. B. & Eiteman, M. A. Overflow Metabolism in *Escherichia coli* during Steady-State Growth: Transcriptional Regulation and Effect of the Redox Ratio. *Appl. Environ. Microbiol.* **72**, 3653–3661 (2006).

182. Gombert, A. K., Moreira dos Santos, M., Christensen, B. & Nielsen, J. Network Identification and Flux Quantification in the Central Metabolism of *Saccharomyces cerevisiae* under Different Conditions of Glucose Repression. *J. Bacteriol.* **183**, 1441–1451 (2001).

183. Hassing, E.-J., de Groot, P. A., Marquenie, V. R., Pronk, J. T. & Daran, J.-M. G. Connecting central carbon and aromatic amino acid metabolisms to improve de novo 2-phenylethanol production in *Saccharomyces cerevisiae*. *Metab. Eng.* **56**, 165–180 (2019).

184. Guo, W. *et al.* Rewiring central carbon metabolism for tyrosol and salidroside production in *Saccharomyces cerevisiae*. *Biotechnol. Bioeng.* **117**, 2410–2419 (2020).

185. Qiao, K., Wasylenko, T. M., Zhou, K., Xu, P. & Stephanopoulos, G. Lipid production in *Yarrowia lipolytica* is maximized by engineering cytosolic redox metabolism. *Nat. Biotechnol.* **35**, 173–177 (2017).

186. Oliveira, A. P. *et al.* Regulation of yeast central metabolism by enzyme phosphorylation. *Mol. Syst. Biol.* **8**, 623 (2012).

187. Chen, Y., Wang, Y. & Nielsen, J. Systematic inference of functional phosphorylation events in yeast metabolism. *Bioinformatics* **33**, 1995–2001 (2017).

188. Chen, Y. & Nielsen, J. Flux control through protein phosphorylation in yeast. *FEMS Yeast Res.* **16**, fow096 (2016).

189. Nakahara, K., Yamamoto, H., Miyake, C. & Yokota, A. Purification and Characterization of Class-I and Class-II Fructose-1,6- bisphosphate Aldolases from the Cyanobacterium *Synechocystis* sp. PCC 6803. *Plant Cell Physiol* **44**, 326–333 (2003).

190. Dele-Osibanjo, T. *et al.* Growth-coupled evolution of phosphoketolase to improve l-glutamate production by *Corynebacterium glutamicum*. *Appl. Microbiol. Biotechnol.* **103**, 8413–8425 (2019).

191. Lu, X. *et al.* Constructing a synthetic pathway for acetyl-coenzyme A from one-carbon through enzyme design. *Nat. Commun.* **10**, 1378 (2019).